NUS
National University
of Singapore

Founded 1905

INTELLIGENT CONTROL OF ROBOTS INTERACTING WITH UNKNOWN ENVIRONMENTS

LI YANAN
(B.Eng., M.Eng.)

A THESIS SUBMITTED
FOR THE DEGREE OF DOCTOR OF PHILOSOPHY
NUS GRADUATE SCHOOL FOR INTEGRATIVE SCIENCES AND ENGINEERING (NGS)
NATIONAL UNIVERSITY OF SINGAPORE
2013

Declaration

I hereby declare that this thesis is my original work and it has been written by me in its entirety. I have duly acknowledged all the sources of information which have been used in the thesis.

This thesis has also not been submitted for any degree in any university previously.

Li Yanan 13/05/2013

Li Yanan

Acknowledgements

First of all, I would like to express my deepest gratitude to my supervisor, Professor Shuzhi Sam Ge, who has kept inspiring me to explore far beyond my own expectation. It has been a great experience to do research under Professor Ge's supervision, during which he has shared a lot of his experience. He has always taught me to strive for a single goal, and it had deep impact in my research. He has provided me with opportunities to visit local industries, attend international conferences and meet with top scientists around the world, which were invaluable experiences and broadened my vision.

I would like to express my gratitude to Professor Limsoon Wong, Associate Professor Kok Kiong Tan, and Assistant Professor John-John Cabibihan, who are my thesis advisory committee members. They have provided me invaluable advices and consistent assistance through all stages of my research study.

My sincere gratitude goes to the NUS Graduate School for Integrative Sciences and Engineering (NGS) for providing me with a great opportunity and financial support to pursue my Ph.D. degree. I specially would like to thank Associate Professor Bor Luen Tang for his inspiration and encouragement. I also want to thank Ms. Irene Christina Chuan for her help and patience on handling tedious paper work for me.

My sincere gratitude and respect go to my seniors, Keng Peng Tee, Chenguang Yang, Beibei Ren, Yaozhang Pan, Wei He, Shuang Zhang, Hongsheng He, and Qun Zhang for their advices and help through the four years of my research study. My thanks goes to my dear fellow colleagues, Zhengchen Zhang and Chen Wang. Without

them I would not have had such a vivid Ph.D. life.

At last but not least, I give my dearest gratitude to my family, especially my parents, who have given me a life to live on and the freedom to pursue my dream. I have owed them so much that I could not pay back in a lifetime.

Contents

Summary

Robots are expected to participate in and learn from intuitive, long term interaction with humans, and be safely deployed in myriad social applications ranging from elderly care, entertainment to education. They are also envisioned to collaborate and co-work with human beings in the foreseeable future for productivity, service, and operations with guaranteed quality. In all of these applications, robots which are stiff and tightly controlled in position will face problems such as saturation, instability, and physical failure, when they interact with unknown environments.

While impedance control is acknowledged to be a promising method for robots interacting with unknown environments, one critical problem is the impedance control design considering that the robot dynamics are typically poor-modeled. In the first part of this thesis, learning impedance control is proposed to cope with this problem. By employing the linear-in-parameters property, a learning mechanism is proposed which requires the knowledge of the robot structure. By employing the boundedness property, the proposed learning mechanism is further developed such that the knowledge of the robot structure is not required. It is illustrated that if the bounds of the robot dynamics are known, the learning process can be avoided but the high-gain scheme must be adopted which may cause chattering. At the end of the first part, neural networks are utilized such that neither the linear-in-parameters

property nor the boundedness property is required and model-free impedance control design is achieved.

Given a desired impedance model, the robot dynamics can be controlled to follow it by the methods developed in the first part of this thesis. But how to obtain a desired impedance model is yet to be answered in the sense that the environments are typically unknown and dynamically changing. This problem will be discussed in the second part of this thesis, and impedance learning and trajectory adaptation will be investigated. When human beings interact with an unknown environment, they have a skill to adjust their limb impedance to achieve some objective by evaluating the feedback information from the environment. It is possible to apply this learning skill to robot control. In specific, suppose that the robot dynamics are governed by an impedance model, its parameters can be adjusted such that a certain cost function is reduced iteratively. Besides impedance learning, trajectory adaptation is another human skill which can be realized by robot control. In a typical human-robot collaboration application, the robot under impedance control is guaranteed to be compliant to the force exerted by the human partner. In this way, the robot passively follows the motion of its human partner. Nevertheless, as the robot refines its motion according to the force exerted by the human partner, it will act as a load when the human partner intents to change the motion. Trajectory adaptation will be developed to resolve this problem such that zero force regulation can be achieved by updating the virtual desired trajectory of the robot. As a result, the human partner will consume much less energy to move the robot and efficient human-robot collaboration is realized.

List of Figures

List of Symbols

x and q	position/orientation in the Cartesian space (operational space) and joint space
n	number of degrees-of-the-freedom (DOF)
$J(q)$	Jacobian matrix
$M(q)$, $C(q,\dot{q})$, and $G(q)$	inertial matrix, Coriolis and Centrifugal matrix, and gravitational matrix of robot in the joint space
τ	control input in the joint space
τ_e	interaction force exerted by environment to robot in the joint space
$Y(\ddot{q},\dot{q},q)$	regression matrix or regressor
θ, $\hat{\theta}$, and $\tilde{\theta}$	physical parameter of robot, its estimate, and estimation error, i.e., $\tilde{\theta} = \theta - \hat{\theta}$
k_M, k_C, and k_G	unknown bounds of the robot dynamics
$M_R(q)$, $C_R(q,\dot{q})$, and $G_R(q)$	inertial matrix, Coriolis and Centrifugal matrix, and gravitational matrix of robot in the Cartesian space
u	control input in the Cartesian space
f	interaction force exerted by environment to robot in the Cartesian space
M_d, C_d, and G_d	desired inertia, damping, and stiffness matrices in the joint space
q_0	rest position in the joint space
e	position error in the joint space

w	defined impedance error in the joint space
k and t_f	iteration number and period
K_d, K_p, K_f, Λ, and Γ	defined matrices in impedance control design
τ_l and $\hat{\tau}_l$	filtered interaction force in the joint space and its estimate
z and $\bar{z}$	defined auxiliary variable for impedance control design and its value with force noise
τ_{ct}, τ_{fb}, and τ_{com}	computed torque control input, feedback control input, and compensation control input
$\hat{\tau}_e$ and $\tilde{\tau}_e$	measurement of τ_e and measurement noise
b_f	upper bound of interaction force noise
K and S	gain matrix in feedback control input and learning ratio
τ_0 and $\tau_{ct,0}$	control input and computed torque control input in the second impedance control design
θ_0 and $\hat{\theta}_0$	$\theta_0 = [k_M, k_C, k_G + b_f]^T$ and its estimate
$m_{ij}(q)$, $c_{ij}(q,\dot{q})$, and $g_i(q)$	elements of $M(q)$, $C(q,\dot{q})$, and $G(q)$
ϵ_{Mij}, ϵ_{Cij}, and ϵ_{Gi}	NN approximation errors
θ_{Mij}^T, θ_{Cij}^T, and θ_{Gi}^T	column vectors of NN weights
$\xi_{Mij}(q)$, $\xi_{Cij}(q,\dot{q})$, and $\xi_{Gi}(q)$	vectors of Gaussian functions
p	number of NN nodes
μ_{Ml}, μ_{Cl}, and μ_{Gl}	centers of Gaussian functions
σ_M^2, σ_C^2, and σ_G^2	variances of Gaussian functions
Θ_M, Θ_C, and Θ_G	matrices formed by $\theta_{Mij}, \theta_{Cij}$, and θ_{Gij}
$\Xi_M(q)$, $\Xi_C(q,\dot{q})$, and $\Xi_G(q)$	matrices formed by $\xi_{Mij}(q), \xi_{Cij}(q,\dot{q})$, and $\xi_{Gij}(q)$

E_M, E_C, and E_G	matrices formed by ϵ_{Mij}, ϵ_{Cij}, and ϵ_{Gij}
b_M, b_C, and b_G	upper bounds of ϵ_{Mij}, ϵ_{Cij}, and ϵ_{Gij}
$\hat{M}(q)$, $\hat{C}(q,\dot{q})$, and $\hat{G}(q)$	estimates of $M(q)$, $C(q,\dot{q})$, and $G(q)$
$\hat{\Theta}_M$, $\hat{\Theta}_C$, and $\hat{\Theta}_G$	estimates of Θ_M, Θ_C, and Θ_G
τ_{nn}, $\tau_{ct,nn}$, and	control input, computed torque control input, and compensation
$\tau^k_{com,nn}$	control input by employing NN
L	$L = [\text{sgn}(\bar{z}), \text{sgn}(\bar{z}^T\ddot{q}_r)\ddot{q}_r, \text{sgn}(\bar{z}^T\dot{q}_r)\dot{q}_r]$
B and $\hat{B}$	$B = [b_f + b_G, b_M, b_C]^T$ and its estimate
S_M, S_C, S_G, and S_B	learning ratios by employing NN
$\hat{\Theta}_M$, $\hat{\Theta}_C$, and $\hat{\Theta}_G$	estimates of Θ_M, Θ_C, and Θ_G
$\tilde{M}(q)$, $\tilde{C}(q,\dot{q})$,	$\tilde{M}(q) = M(q) - \hat{M}(q)$, $\tilde{C}(q,\dot{q}) = C(q,\dot{q}) - \hat{C}(q,\dot{q})$, and
and $\tilde{G}(q)$	$\tilde{G}(q) = G(q) - \hat{G}(q)$
$\tilde{\Theta}_M$, $\tilde{\Theta}_C$, $\tilde{\Theta}_G$,	$\tilde{\Theta}_M = \hat{\Theta}_M - \Theta_M$, $\tilde{\Theta}_C = \hat{\Theta}_C - \Theta_C$, $\tilde{\Theta}_G = \hat{\Theta}_G - \Theta_G$, and
and $\tilde{B}$	$\tilde{B} = \hat{B} - B$
$\delta\tilde{\Theta}^k_M$, $\delta\tilde{\Theta}^k_C$, $\delta\tilde{\Theta}^k_G$,	$\delta\tilde{\Theta}^k_M = \tilde{\Theta}^{k-1}_M - \tilde{\Theta}^k_M$, $\delta\tilde{\Theta}^k_C = \tilde{\Theta}^{k-1}_C - \tilde{\Theta}^k_C$, $\delta\tilde{\Theta}^k_G = \tilde{\Theta}^{k-1}_G - \tilde{\Theta}^k_G$, and
and $\delta\tilde{B}^k$	$\delta\tilde{B}^k = \tilde{B}^{k-1} - \tilde{B}^k$
M_x, C_x, and G_x	desired inertia, damping, and stiffness matrices in the Cartesian space
x_0	rest position in the Cartesian space
$\xi(t)$ and $o(t)$	state and output of linear time-varying system
$o_d(t)$	desired output of linear time-varying system
$A(t)$, $B(t)$, and $C(t)$	system matrices of linear time-varying system
K_P and K_D	proportional and derivative gains
y	$y = -\dot{e} - \mu\text{Sin}(e)$

$\Upsilon(t)$	cost function to determine the interaction behavior
e_x and e_f	position error and force error in the Cartesian space
x_E	rest position of the environment
M_E, C_E, and G_E	inertia, damping, and stiffness matrices of the environment dynamics
y	$y = -\dot{e} - \mu \text{Sin}(e)$
K_s and $\hat{K}_s$	diagonal matrix satisfying $\|K_s\| = k_M l_1 + k_C l_2^2 + k_G$ and its estimate
$\bar{y}$	$\bar{y} = [y_1 \text{sgn}(y_1), y_2 \text{sgn}(y_2), \ldots, y_n \text{sgn}(y_n)]^T$
S_1	adaptation ratio in adaptive control for the inner position loop
M_h, C_h, and K_h	mass, damping, and stiffness matrices of human limb model
x_h and $\hat{x}_h$	human motion intention and its estimate
$\delta(x, \dot{x})$	uncertainty in human limb model
r	RBFNN input
$s_i(r)$	Gaussian function in RBFNN
$\hat{w}_i$	RBFNN weight
μ_i	center of the receptive field in RBFNN
η_i	width of Gaussian function
α_i	adaptation ratio
w_x	defined impedance error in the Cartesian space
$K_{d,x}$, $K_{p,x}$, $K_{f,x}$, Λ_x, and Γ_x	defined matrices in impedance control design in the Cartesian space
f_l and $\hat{f}_l$	filtered interaction force in the Cartesian space and its estimate
z_x	defined auxiliary variable for impedance control design in the Cartesian space
u_o	control input in the operational space to improve a certain measure
$\bar{J}$	dynamically consistent Jacobian inverse
Π	measure of "human muscle effort"

K_G	joint "strength"
f'	interaction force filtered by the desired impedance function
$\hat{C}_h$	estimate of $\frac{C_h}{K_h}$
x_δ	compensation component in the rest position
x_d	virtual desired trajectory in the Cartesian space
e_1	error between actual trajectory and virtual desired trajectory in the Cartesian space

Chapter 1

Introduction

This chapter presents the background and motivation for conducting the research on intelligent control of robots interacting with unknown environments. Impedance control design, impedance learning, and trajectory adaptation will be respectively introduced. Related works, research objectives, and highlighted contributions will be discussed. The outline of the rest thesis is also presented.

1.1 Background and Motivation

With growing research interest in robotic application fields such as elderly care, health care, entertainment, etc., robots are expected to work in complex and unknown social environments [1, 2]. Social robots are fundamentally different from conventional industrial robots, in the sense that industrial robots require high accuracy and high repeatability whereas social robots focus on safety issues and social interaction with human beings. Furthermore, most industrial robots are preprogrammed to work in a fixed environment. In other words, industrial robots cannot operate properly or even

fail to operate if the perceived environment is undefined. In contrast to industrial robots, we perceive social robots as intelligent agents which can communicate and interact among themselves, with human, and the environment in a safe and comfortable manner [3]. Social robots should not be simply autonomous intelligent machines with predefined function and fixed ability. They must also be able to understand, learn, and adapt to human and environment throughout its lifetime in sociology, physiology, and psychology aspects [4]. There are many challenging fundamental problems yet to be solved, of which physical robot-environment interaction is one and it is focused on in this thesis.

Interaction control of robots has been investigated for more than three decades and it still attracts a lot of researchers' attention, due to more complex environments that the robots work in and intelligence of a higher level that people expect from the robots. For the safe and compliant interaction, the application of a conventional robot which is stiff and tightly controlled in position will face lots of challenges. Saturation, instability, and physical failure are the consequences of this type of interaction. Therefore, the interaction force must be accommodated rather than resisted [5]. In the literature, there are two approaches for assuring compliant motion of robots interacting with environments. The first is hybrid position/force control which aims at controlling force and position in a nonconflicting way [6, 7]. Under hybrid position/force control, force control is designed so that rapid rise time of force, low or zero force overshoot, and good rejection of external force disturbance can be achieved [8, 9, 10, 11, 12]. However, the same force controller typically exhibits a sluggish response in contact with softer environments, and goes unstable in contact with stiffer environments [9]. It does not even discuss the interaction stability which is dependent on both the dynamics of the robot and environment. The other approach is impedance

control which aims at developing a relationship between the contact force and position [13]. If the environment is passive, then imposing a passive impedance model to a robot will guarantee the stability of the coupled robot-environment interaction system [14]. The passivity assumption is applicable to a large set of environments and thus many results have been obtained under the passivity assumption, such as [15, 16, 17, 18, 19, 20, 21, 22, 23].

1.2 Impedance Control Design

To impose the desired impedance model on the robot, the direct approach is to design low-impedance (small inertia/mass, damping and stiffness) hardware. However, intrinsically low-impedance hardware can be difficult to create, particularly with complex geometries and large force or power outputs [24]. An alternative approach is impedance control design. Two design methods have been extensively discussed in the literature, i.e., position-based and torque-based. Because most of off-the-shelf motor control systems include position mode and velocity mode, position-based impedance control is preferred in practical implementations. Position-based impedance control includes two loops, where the output of the outer loop is the virtual desired trajectory of the inner loop and the objective of the inner loop is position tracking. This two-loop framework is shown in Fig. 1.1. Although the position-based method offers the advantage of a certain implementation simplicity, its performance is dependant on the quality of the inner position control loop and suffers from an inability to provide a very "soft" impedance (small inertia/mass, damping and stiffness) [25]. Therefore, the torque-based method draws much attention of control researchers.

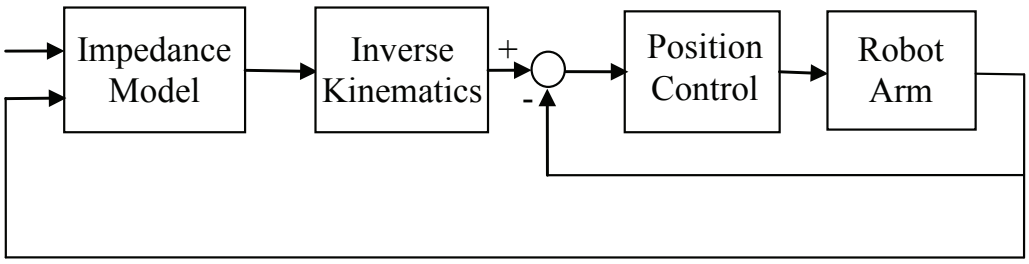

Fig. 1.1: Position-based impedance control

In the regard that the robot dynamics are typically poorly modeled and the uncertainties exist, it is essential to develop adaptive and learning methods for impedance control design. In the literature, many works have been carried out on adaptive impedance control [26]. In [27], model reference adaptive impedance control is proposed which is motivated by the model reference adaptive position control in [28]. In [29], two adaptive impedance control methods are developed and details about how to deal with the force measurement noise are discussed in [30] and [31]. In [32], adaptive impedance control is developed for flexible robot arms with parametric uncertainties. As in most adaptive control methods including [27, 29, 32], the regressor introduced in [28] is needed and thus the robot structure is required to be known for the control design. In [33], function approximation technique is employed to approximate unknown and uncertain robot dynamics, and regressor-free adaptive impedance control is developed. Other methods that do not require the robot structure can be found in [34, 35, 36, 37]. In parallel with adaptive control, there has been substantial research effort in iterative learning control [38]. The idea behind learning control is that the knowledge obtained from the previous trial is used to improve the control input for the next trial. It has been generally acknowledged that such an ability to improve performance by repeating a task is an important control strategy of the human being [39]. Despite this situation, there are few works on learning impedance control of

robots. In [40] and [41], two different iterative learning control schemes are proposed for impedance control of robots. Different from that in [40], the target impedance model in [41] unifies two phases of contact and non-contact, which avoids the switch between two phases and is thus preferred in practical implementations. However, to guarantee the results given in [41], control parameters are required to satisfy some conditions that are inconvenient to verify.

Based on the above discussion and to push the boundary of academic results further, we develop iterative learning impedance control for physical robot-environment interaction. In the first step, a straightforward framework will be proposed, which is proven to make it possible to extend existing methods in position control to impedance control. Based on this framework and Linear-In-parameters (LIP) property, learning impedance control will be developed and it requires the knowledge of the robot structure. This is similar to that in [27, 29, 32] where the regressor is used. Based on the boundedness property, learning impedance control which requires neither the robot structure nor the physical parameters is developed. As to be further discussed, if the bounds of the robot dynamics are known, the learning process is avoided while the high-gain scheme can be adopted. Although the above method is model-free and provides the design simplicity, it is found that there is chattering when the defined impedance error becomes very small. This is due to the utilization of the sign function, which is discontinuous and expected to be avoided. Therefore, Neural Networks (NN) are employed to approximate unknown robot dynamics and resolve the problem mentioned above. It will be shown that the proposed methods guarantee compliant motion when a robot arm interacts with unknown environments and smooth transition between contact-free and contact phases.

1.3 Impedance Learning

While impedance control is employed to regulate the dynamic behavior at the interaction point when the robot interacts with unknown environments, how to obtain the critical values of the desired impedance model is still an open problem due to the extreme difficulty of environment modeling [42, 43, 44, 45, 46, 47, 48]. Instead of estimating the environment parameters as in [49, 50], human beings adapt to unknown environments through repetitive learning. For example, when a person opens a door, he/she may fail at the beginning because he/she does not have the knowledge of this door, e.g., mass, inertia, friction at the hinge, etc. After he/she "tries" to open the door for several times, he/she is able to open the door to a desired position with the least effort. During the process of opening a door, this person learns a "best" set of impedance parameters of his/her limb in the sense that the target position is achieved and the control effort is minimized.

It is possible to apply human beings' learning skill discussed above to robot control [51, 52, 53]. Specifically, the robot dynamics can be governed by a target impedance model with impedance control. Then, in a similar way as human beings adjust their limb impedance, parameters of the target impedance model are adjusted through learning based on a certain criteria. This kind of learning schemes has been developed in many research studies. In [54], associative search network learning is applied to a wall-following task. In [55], a method to regulate the impedance parameters through learning of NN is proposed. However, as discussed in [56], artificial NN techniques need an expensive data preprocessing for training examples in order to learn. Instead, reinforcement learning is based on the trial-and-error method [57], which is more similar to the way of human learning. In [58], an equilibrium point control

model is employed, and the stiffness matrix is updated according to different application requirements using natural actor-critic algorithm. The basic idea in [58] is to find actions in an environment so as to maximize some notion of cumulative reward. However, the reinforcement learning methods are limited in high-dimension applications. Generally a "good" action has to be found in an extremely wide variety of candidates, so the computation complexity is a problem. In [59], a high-speed insertion problem is investigated and an internal-model-based learning scheme is developed. This method has a simple formulation but it is limited to a simple application. In this thesis, we will develop a learning method to adjust the stiffness and damping matrices simultaneously by employing gradient-following and betterment schemes. It will be shown to have a straightforward formulation and be feasible for a general class of applications. As such the desired parameters of the impedance model can be obtained and a desired interaction behavior can be achieved despite unknown and dynamically changing environments.

1.4 Trajectory Adaptation

After the desired impedance parameters are obtained, the last question is how to determine the rest position in a target impedance model. We try to give an answer by considering a typical human-robot collaboration scenario in the last part of this thesis. In human-robot collaboration, the rest position is designed so that the robot with this target impedance model is able to "actively" collaborate with its human partner. By employing impedance control, a robot is controlled to be compliant to the force exerted by the human partner. In this way, the robot passively follows the motion of its human partner, and human-robot collaboration becomes possible

[60, 61, 62]. Nevertheless, as the robot refines its motion according to the force exerted by the human partner, it will act as a load when the human partner intents to change the motion [63].

To cope with the above problem, a natural choice is to make the robot understand and observe the human partner's motion intention [64]. As a matter of fact, understanding the motion intention of the other party is essential in human-human collaboration [65, 66]. Both parties in human-human collaboration usually keep communicating with each other through kinds of medias. In a typical physical human-robot collaboration, force and position sensors are available and they represent the communication medias between a robot arm and a human limb. There has been much effort made to investigate how to estimate the motion intention of the human partner from available sensory information [67, 68]. In [69], the motion characteristics of the human limb is investigated. It is utilized and applied to generate a point-to-point cooperative movement in [70]. In [71], under the assumption that the momentum is preserved during an interaction task, the motion intention of the human partner is represented by the change of the interaction force, which is estimated by the change of the control effort. Under this scheme, if the magnitude of the filtered-control-force vector exceeds a defined threshold for a defined continuous duration, the impedance control mode is switched to the interactive control mode, in which the estimated motion intention is integrated. The above illustration indicates that there is an inherent delay from the intention estimation to the beginning of the interactive control mode. In [72], the motion intention state is deemed as a stochastic process and it is estimated by employing the Hidden Markov Model (HMM). In this method, parameters of the human limb model are estimated online, and two intention states (active and passive) are defined to indicate that the human partner leads and follows, respectively. In [73],

a crane robot is designed to aid the walking of the elderly and handicapped, and the user's intentional walking direction is estimated using the Kalman filter. However, human motion intention is typically a time-varying trajectory, which cannot be represented by only several states as in [72] or motion directions as in [73]. In this regard, we employ the human limb model as in [45, 46], and define the desired trajectory in this model as the motion intention of the human partner in this thesis. Related work can be found in [74], in which the desired trajectory in the human limb model is calculated with unknown parameters of the human limb as design parameters. Considering nonlinear and time-varying properties of the human limb model, we estimate the desired trajectory in this model based on NN, which are acknowledged to possess excellent universal approximation ability [75]. Interaction force, position, and velocity at the interaction port are used as the inputs of the developed NN. An updating law is developed to online adjust the NN weights, so that the estimation accuracy is guaranteed even when human motion intention changes. Thereafter, the estimated motion intention is integrated into impedance control as the rest position of a given target impedance model. As a result, the robot "actively" moves towards its human partner's intended position rather than "passively" complies to the interaction force, and the collaboration efficiency is increased.

As discussed above, the human partner and the robot are considered to be two subsystems and the performance of the whole coupled collaboration system has not been analyzed. In this regard, force control and impedance control with adaptive rest position can be another choice for human-robot collaboration. More importantly, the environment dynamics have been taken into account under the framework of force control and impedance control, and subsequently, the performance of the whole coupled system can be evaluated. By employing force control, the robot will move

along a trajectory to make the interaction force between the human partner and the robot track a zero force, and this will indirectly make the robot's motion synchronize with the human partner's [76]. However, the robustness of force control is questionable considering that the dynamics of the human limb are highly nonlinear and subject-dependent. By adopting force control, there also exist switchings between free motion and constrained motion phases, which causes problems such as bouncing [77]. Impedance control is proved by previous studies and illustrated in the above to be able to provide better robustness and avoid phase switching. However, as the interaction force is indirectly controlled with impedance control, zero interaction force and thus efficient human-robot collaboration cannot be achieved in a straightforward way. To deal with this issue, much effort has been made to achieve force regulation under the framework of impedance control [78, 79, 80, 81, 82]. In [78], two adaptive schemes are proposed to achieve force regulation by adjusting the rest position in the impedance model. In [80], an impedance model with zero stiffness is adopted, and the force error is eliminated by an adaptive scheme subject to uncertainty and little knowledge of both robot and environment dynamics. Instead of adjusting the rest position in the impedance model, the stiffness parameter in the impedance model is adjusted to achieve a small force regulation error in [81]. In the above works, the environment is described by a damping-stiffness model where the rest position is a constant. Nevertheless, in the case of the human-robot collaboration, where the human limb is the environment to the robot arm, its dynamics cannot be simply described by such a model with a constant rest position. Instead, the human limb dynamics are usually described by a general mass-damping-stiffness model as mentioned above [45, 46], with the desired trajectory (instead of the rest position) planned in the Central Nervous System (CNS). This desired trajectory is generally time-varying and uncertain due to the modeling error and external disturbance. In the last part of this thesis,

we employ impedance control and develop force regulation control to achieve human-robot collaboration, subject to uncertain human limb dynamics. Adaptive control is proposed to deal with the point-to-point movement, and learning control and NN control are developed to generate periodic and non-periodic trajectories, respectively. The stability and tracking performance of the whole coupled system are discussed through the rigorous analysis.

1.5 Contribution and Thesis Organization

In summary, intelligent control is developed for robots which interact with unknown environments in this thesis. Three problems will be respectively resolved, i.e., impedance control design, impedance learning, and trajectory adaptation. Based on the discussion in the above sections, we highlight the main contributions of this thesis as follows:

(i) Iterative learning impedance control is proposed to guarantee the robot dynamics governed by a target impedance model. An auxiliary impedance error is defined to make it possible to extend existing methods in position control to impedance control. Based on the LIP property, learning control is developed which requires the knowledge of robot structure. The boundedness property is considered so that the knowledge of the robot structure is not required. NN method is further developed so that neither the LIP property nor the boundedness property is not needed and thus the corresponding problems are avoided.

(ii) The environment is described as a time-varying system in the state-space form, and impedance learning is proposed to iteratively adjust the impedance parameters of the robot arm. As a result, the target impedance model which guarantees

the desired interaction behavior is obtained despite unknown and dynamically changing environments.

(iii) The motion intention of the human partner is defined as the desired trajectory in the human limb model. It is online estimated and integrated into impedance control, so that the robot "actively" moves towards its human partner's intended position. Human limb dynamics are taken into consideration in the system performance analysis, and it is rigorously proved that zero force regulation is guaranteed subject to uncertain human limb dynamics. Adaptive control is proposed to deal with the point-to-point movement, and learning control and NN control are developed to generate periodic and non-periodic trajectories, respectively.

The rest of this thesis is organized as follows. In Chapter 2, the proposed learning impedance control is introduced, the rigorous analysis of the control performance is presented, and the extensive simulation studies are carried out to verify the validity of the proposed method. In Chapter 3, NN are employed to approximate unknown and uncertain robot dynamics, so that neither the LIP property nor the boundedness property in Chapter 2 is needed. As impedance control is guaranteed by the methods in Chapters 2 and 3, impedance learning and trajectory adaptation are respectively discussed in Chapters 4 and 5-6. In Chapter 4, gradient following and betterment scheme are adopted to develop impedance learning so that the robot is able to adjust its stiffness and damping parameters through iterative learning. Simulation and experiment studies are carried out to show the effectiveness of the proposed method. In Chapter 5, human motion intention is estimated and integrated to impedance control, so that the robot is able to "actively" collaborate with its human partner. In Chapter 6, by taking the human limb dynamics into account, it is rigorously proved that the

proposed trajectory adaptation makes the interaction force go to zero. Simulation and experiment results are also presented in Chapters 5 and 6 to show that the efficient human-robot collaboration is achieved with the proposed methods. This thesis is concluded in Chapter 7, where the achievement and future work are discussed.

Part I

Impedance Control Design

Chapter 2

Learning Impedance Control

In this chapter, a learning control framework is proposed which guarantees that the robot dynamics follow a target impedance model. In particular, an auxiliary impedance error is defined which makes it possible to extend existing methods in position control to impedance control. The performance and robustness of the proposed learning impedance control are discussed in details through the rigorous analysis. The validity of the proposed method is verified by simulation studies.

The rest of this chapter is organized as follows. In Section 2.1, the robot kinematics and dynamics are presented, and the control objective of impedance control is introduced. In Section 2.2, learning impedance control based on the LIP property is introduced and the rigorous proof follows immediately. In Section 2.3, learning impedance control based on the boundedness property is developed with further discussion. In Section 2.4, intensive simulation studies are used to show the validity and effectiveness of the proposed method. Concluding remarks are given in Section 2.5.

2.1 Problem Statement

We consider a system in which a rigid robot arm is physically interacting with unknown environments. In what follows, the coordinates of the robot arm are expressed relative to a common reference frame unless otherwise stated. Besides, the dependence of the system parameters and signals in time is implied unless otherwise specified.

2.1.1 Robot Kinematics and Dynamics

The robot kinematics are given by

$$x(t) = \phi(q), \tag{2.1}$$

where ϕ, $x(t)$, $q \in \mathbb{R}^n$, and n are forward kinematics, positions/orientations in the Cartesian space (operational space), joint coordinates, and number of Degrees-Of-the-Freedom (DOF), respectively.

Differentiating (2.1) with respect to time results in

$$\dot{x}(t) = J(q)\dot{q}, \tag{2.2}$$

where $J(q) \in \mathbb{R}^{n \times n}$ is the Jacobian matrix which is assumed to be nonsingular in a finite work space.

Further differentiating (2.2) with respect to time results in

$$\ddot{x}(t) = \dot{J}(q)\dot{q} + J(q)\ddot{q}. \tag{2.3}$$

(2.1)-(2.3) represent the kinematic constraints of the robot.

The robot dynamics are described as

$$M(q)\ddot{q} + C(q,\dot{q})\dot{q} + G(q) = \tau - \tau_e, \tag{2.4}$$

where $M(q) \in \mathbb{R}^{n\times n}$ is the symmetric bounded positive definite inertia matrix; $C(q,\dot{q})\dot{q} \in \mathbb{R}^n$ denotes the Coriolis and Centrifugal force; $G(q) \in \mathbb{R}^n$ is the gravitational force; $\tau \in \mathbb{R}^n$ is the vector of control input; and $\tau_e \in \mathbb{R}^n$ denotes the vector of constraint force exerted by the environment, which is 0 when there is no interaction between the robot and environment.

Property 1. *[83] Matrix $M(q)$ is symmetric and positive definite.*

Property 2. *[83] Matrix $2C(q,\dot{q}) - \dot{M}(q)$ is a skew-symmetric matrix.*

Property 3. *[83] $M(q)$, $C(q,\dot{q})$, and $G(q)$ are linear in terms of a suitable selected set of physical parameters of the robot, i.e.,*

$$M(q)\ddot{q} + C(q,\dot{q})\dot{q} + G(q) = Y(\ddot{q},\dot{q},q)\theta, \tag{2.5}$$

where $\theta \in \mathbb{R}^{n_\theta}$ is a vector of physical parameters of the robot; n_θ is a positive integer denoting the number of these parameters; and $Y(\ddot{q},\dot{q},q) \in \mathbb{R}^{n\times n_\theta}$ is the regression matrix which is independent of physical parameters.

Remark 1. *The above property is the LIP property which is employed in many adaptive control designs for position control of the robot [28, 84, 85, 86].*

Property 4. *[87] $\|M(q)\| \le k_M$, $\|C(q,\dot{q})\| \le k_C\|\dot{q}\|$, and $\|G(q)\| \le k_G$, where k_M, k_C, and k_G are unknown positive scalars, and $\|*\|$ denotes any norm of $*$.*

Remark 2. *It is shown in [88] that not all robots possess the above property. In particular, the class of serial robots with bounded inertia matrix is referred to as class* BD *and it includes the robots with all revolute joints and the robots with all prismatic joints. The complete description of the* BD *robots can be found in [88]. In this regard, the method that is developed based on the above property will not be valid for the robots out of the* BD *class.*

Since there are many tasks that are defined in the operational space, it is necessary to transfer the above dynamics in (2.6) to the operational space in these tasks. Considering the kinematic constraints in (2.1)-(2.3) and dynamics in (2.6), we obtain the robot dynamics in the operational space as below

$$M_R(q)\ddot{x} + C_R(q,\dot{q})\dot{x} + G_R(q) = u - f, \tag{2.6}$$

where

$$\begin{aligned} M_R(q) &= J^{-T}(q)M(q)J^{-1}(q), \\ C_R(q,\dot{q}) &= J^{-T}(q)(C(q,\dot{q}) - M(q)J^{-1}(q)\dot{J}(q))J^{-1}(q), \\ G_R(q) &= J^{-T}(q)G(q), \\ u &= J^{-T}(q)\tau, \\ f &= J^{-T}(q)\tau_e. \end{aligned} \tag{2.7}$$

Remark 3. *In this chapter and Chapter 3, the impedance control design is only discussed in the joint space. It can be similarly developed in the Cartesian space based on the transformation as mentioned above.*

2.1.2 Control Objective

As discussed in Chapter 1, impedance control can be employed for a robot interacting with unknown environments. The stability of the coupled interaction system is guaranteed if the environments are passive.

Suppose that there is a desired impedance model given in the joint space

$$M_d\ddot{e} + C_d\dot{e} + G_d e = -\tau_e, \tag{2.8}$$

where $e = q - q_0$ with q_0 as the rest position of the robot, and M_d, C_d, and G_d are the desired inertia, damping and stiffness matrices, respectively. The selection of M_d, C_d, and G_d depends on different applications for different objectives. For example, in the grinding task, to smooth the surface down to the commanded trajectory, we usually require a large stiffness value in the direction perpendicular to the work surface with a small stiffness value in the direction along the surface.

Remark 4. *The desired impedance model (2.8) specifies a desired dynamic relationship between the position error and the interaction force. In the special case of non-contact task where the contact force τ_e is zero, the actual position q will converge to the rest position q_0 considering (2.8) is stable. As a result, impedance control unifies two modes of contact and non-contact, and it implies no transition between the free motion and contact motion. This is important because transition between two modes may cause chattering and even destroy the system stability in practice.*

The control objective of the impedance control design is to find a sequence of control torques such that the impedance of the whole system tracks the given desired impedance model (2.8). The first step is to construct an error signal between the real system and a virtual system with the specified desired impedance model (2.8). The

following impedance error in [40] is used

$$w = M_d\ddot{e} + C_d\dot{e} + G_d e + \tau_e. \tag{2.9}$$

By repeating the action for $t \in [0,\ t_f]$ at each iteration, the learning impedance control design is to develop an iterative learning law such that the following objective is achieved

$$\lim_{k\to\infty} w^k(t) = 0,\ \forall t \in [0, t_f], \tag{2.10}$$

where k is the iteration number and t_f is the iteration period.

Remark 5. *The problem under study is very difficult to solve by conventional control methods because we do not have complete knowledge of the robot arm. The situation becomes even more difficult when the unknown system parameters are time-varying due to payload changes, mechanical wear, etc. To overcome this difficulty, iterative learning control is proposed in the following, which searches for a desired control input through a sequence of repetitive operations with pre-specified operating conditions.*

For the convenience of the following analysis, we define an augmented impedance error as below

$$\bar{w}^k = K_f w^k = \ddot{e}^k + K_d\dot{e}^k + K_p e^k + K_f\tau_e^k, \tag{2.11}$$

where $K_d = M_d^{-1}C_d$, $K_p = M_d^{-1}G_d$, and $K_f = M_d^{-1}$.

Remark 6. *In (2.11), M_d is assumed to be nonsingular, which is usually attainable and has to be kept in mind when selecting the impedance model parameters.*

By choosing two positive definite matrices Λ and Γ such that

$$\Lambda + \Gamma = K_d \text{ and } \dot{\Lambda} + \Gamma\Lambda = K_p, \tag{2.12}$$

we further rewrite (2.11) as

$$\bar{w}^k = \ddot{e}^k + (\Lambda + \Gamma)\dot{e}^k + (\dot{\Lambda} + \Gamma\Lambda)e^k + \dot{\tau}_l^k + \Gamma\tau_l^k, \tag{2.13}$$

where τ_l^k satisfies

$$\dot{\tau}_l^k + \Gamma\tau_l^k = K_f\tau_e^k. \tag{2.14}$$

By defining

$$z^k = \dot{e}^k + \Lambda e^k + \tau_l^k, \tag{2.15}$$

we obtain

$$\bar{w}^k = \dot{z}^k + \Gamma z^k. \tag{2.16}$$

Suppose that $\lim_{k\to\infty} \dot{z}^k$ exists, $\lim_{k\to\infty} z^k = 0$ will lead to $\lim_{k\to\infty} \dot{z}^k = 0$. Based on this fact, the control objective (2.10) finally becomes

$$\lim_{k\to\infty} z^k(t) = 0, \ \forall t \in [0, t_f]. \tag{2.17}$$

Remark 7. *The above derivation is important in the sense that we define an auxiliary variable z, with which the following analysis becomes more convenient. The following control design and performance analysis will show that z in impedance control is*

"equivalent" to the position error in position control. Therefore, it becomes possible to extend some existing methods in position control to impedance control, although it is not straightforward.

2.2 Control Design Based on Property 3

In this section, we are ready to give details of the learning control design based on the LIP property. We propose to compute the control input as follows

$$\tau^k = \tau_{ct}^k + \tau_{fb}^k + \tau_{com}^k + \hat{\tau}_e^k, \tag{2.18}$$

where τ_{ct}^k, τ_{fb}^k, and τ_{com}^k are the computed torque vector, feedback torque vector, and compensation torque vector, respectively, and $\hat{\tau}_e^k$ is the measurement of τ_e^k.

Remark 8. *To relax the restriction on the results to be achieved, we consider the case where the accurate force measurement is not attainable, i.e., there exists force measurement noise* $\tilde{\tau}_e^k = \hat{\tau}_e^k - \tau_e^k \neq 0$.

Assumption 1. *The force measurement noise is assumed to be bounded by* b_f*, i.e.,* $\|\tilde{\tau}_e^k\| \leq b_f$.

In particular, the computed torque vector τ_{ct}^k is given by

$$\tau_{ct}^k = -Y(\ddot{q}_r^k, \dot{q}_r^k, \dot{q}^k, q^k)\hat{\theta}^k, \tag{2.19}$$

where $\hat{\theta}$ is the estimate of θ and

$$\begin{aligned} \dot{q}_r^k &= \dot{q}_0 - \Lambda e^k - \hat{\tau}_l^k, \\ \ddot{q}_r^k &= \ddot{q}_0 - \Lambda \dot{e}^k - \dot{\hat{\tau}}_l^k \end{aligned} \tag{2.20}$$

with $\hat{\tau}_l^k$ satisfying

$$\dot{\hat{\tau}}_l^k + \Gamma \hat{\tau}_l^k = K_f \hat{\tau}^k. \tag{2.21}$$

The feedback torque vector is given by

$$\tau_{fb}^k = -K\bar{z}^k, \tag{2.22}$$

where K is a symmetric positive definite matrix and

$$\bar{z}^k = \dot{e}^k + \Lambda e^k + \hat{\tau}_l^k = z^k + \tilde{\tau}_l^k \tag{2.23}$$

with $\tilde{\tau}_l^k = \hat{\tau}_l^k - \tau_l^k$.

The compensation torque is given by

$$\tau_{com}^k = -b_f \mathrm{sgn}(\bar{z}^k), \tag{2.24}$$

where $\mathrm{sgn}(*)$ is the vector/matrix obtained by applying the sign function to all elements of $*$.

Remark 9. *The analysis in the following will show that τ_{com}^k is used to compensate for the error caused by the inaccurate force measurement.*

Integrating the above control input (2.19) into the robot dynamics (2.4) gives the closed-loop dynamics

$$M(q^k)\dot{\bar{z}}^k + C(q^k, \dot{q}^k)\bar{z}^k + K\bar{z}^k = Y(\ddot{q}_r^k, \dot{q}_r^k, \dot{q}^k, q^k)\tilde{\theta}^k - (b_f \mathrm{sgn}(\bar{z}^k) - \hat{\tau}_e^k), \quad (2.25)$$

where $\tilde{\theta}^k = \theta^k - \hat{\theta}^k$.

In the following, for the convenience, we use Y^k instead of $Y^k(\ddot{q}_r^k, \dot{q}_r^k, \dot{q}^k, q^k)$ where it does not result in any confusion.

We develop the following learning law to update $\hat{\theta}$

$$\hat{\theta}^k = \hat{\theta}^{k-1} + S^{-1}Y^{k^T}(\ddot{q}_r^k, \dot{q}_r^k, \dot{q}^k, q^k)\bar{z}^k, \quad (2.26)$$

where S is a symmetric positive definite matrix.

Theorem 1. *Considering the system described by (2.4), we use the control input (2.19) with the learning law (2.26) to achieve the following results:*

(i) $\lim_{k\to\infty} w^k(t)$ *is bounded by* $\|M_d\Gamma\|b_f$ *for all* $t \in [0, t_f]$, *i.e.,* $\lim_{k\to\infty} \|w^k(t)\| \leq \|M_d\Gamma\|b_f$. *When the force measurement is accurate,* $b_f = 0$ *indicates* $\lim_{k\to\infty} w^k(t) = 0$.

(ii) all the signals in the closed-loop system are bounded for all $t \geq 0$.

Proof. Consider the following Lyapunov function candidate

$$W^k(t) = V^k(t) + U^k(t), \quad (2.27)$$

where

$$\begin{aligned} V^k(t) &= \frac{1}{2}\bar{z}^{k^T} M(q)\bar{z}^k, \\ U^k(t) &= \frac{1}{2}\int_0^t \tilde{\theta}^{k^T} S\tilde{\theta}^k dv. \end{aligned} \tag{2.28}$$

Considering the robot dynamics (2.4) and control input (2.19), we obtain

$$\begin{aligned} V^k(t) &= V^k(0) + \int_0^t (\bar{z}^{k^T} M(q)\dot{\bar{z}}^k + \frac{1}{2}\bar{z}^{k^T}\dot{M}(q)\bar{z}^k)dv \\ &= V^k(0) + \int_0^t (\bar{z}^{k^T} M(q)\dot{\bar{z}}^k + \bar{z}^{k^T} C(q,\dot{q})\bar{z}^k)dv \\ &= V^k(0) + \int_0^t \bar{z}^{k^T}(-M(q)\ddot{q}_r^k - C(q,\dot{q})\dot{q}_r^k - G(q) + \tau^k - \tau_e^k)dv \\ &= V^k(0) + \int_0^t \bar{z}^{k^T}(Y^k\theta - Y^k\hat{\theta}^k - K\bar{z}^k + \tilde{\tau}_e^k - b_f \mathrm{sgn}(\bar{z}^k))dv \\ &\leq V^k(0) + \int_0^t \bar{z}^{k^T}(Y^k\tilde{\theta}^k - K\bar{z}^k + b_f\mathrm{sgn}(\bar{z}^k) - b_f\mathrm{sgn}(\bar{z}^k))dv \\ &= V^k(0) + \int_0^t \bar{z}^{k^T}(Y^k\tilde{\theta}^k - K\bar{z}^k)dv, \end{aligned} \tag{2.29}$$

where we have used Property 2 in the second equality.

Suppose that $\dot{q}_0(0) = \dot{q}(0)$, $q_0(0) = q(0)$, and $\hat{\tau}_e(0) = 0$. Then, we have $V^k(0) = 0$ and

$$V^k(t) \leq \int_0^t \bar{z}^{k^T}(Y^k\tilde{\theta}^k - K\bar{z}^k)dv. \tag{2.30}$$

On the other hand, by defining

$$\delta\tilde{\theta}^k = \tilde{\theta}^{k-1} - \tilde{\theta}^k, \tag{2.31}$$

we have $\delta\tilde{\theta}^k = S^{-1}Y^{k^T}\bar{z}^k$ and

$$\begin{aligned} U^k(t) - U^{k-1}(t) &= -\frac{1}{2}\int_0^t (\delta\tilde{\theta}^{k^T} S\delta\tilde{\theta}^k + 2\delta\tilde{\theta}^{k^T} S\tilde{\theta}^k)dv \\ &= -\frac{1}{2}\int_0^t \bar{z}^{k^T} Y^k S^{-1} Y^{k^T}\bar{z}^k dv - \int_0^t \bar{z}^{k^T} Y^k \tilde{\theta}^k dv. \end{aligned} \tag{2.32}$$

According to (2.27), (2.30), and (2.32), we have the following result

$$\begin{aligned} \Delta W^k(t) &= W^k(t) - W^{k-1}(t) \\ &= (V^k(t) - V^{k-1}(t)) + (U^k(t) - U^{k-1}(t)) \\ &\leq -V^{k-1}(t) - \int_0^t \bar{z}^{k^T} K\bar{z}^k dv - \frac{1}{2}\int_0^t \bar{z}^{k^T} Y^k S^{-1} Y^{k^T}\bar{z}^k dv \\ &\leq 0. \end{aligned} \tag{2.33}$$

Since $\bar{z}^0$ and $\tilde{\theta}^0$ are bounded, $W^0(t)$ is bounded for all $t \in [0, t_f]$. With (2.33), it is indicated that the monotonically decreasing nonnegative sequence W^k converges to a nonnegative fixed value, thus we have $\Delta W^k \to 0$ as $k \to \infty$.

From (2.33), we have

$$\Delta W^k \leq -\int_0^t \bar{z}^{k^T} K\bar{z}^k dv \leq 0. \tag{2.34}$$

Taking the limit of the above equation, we obtain

$$\lim_{k\to\infty} \int_0^t \bar{z}^{k^T} K\bar{z}^k dv = 0, \tag{2.35}$$

which indicates $\lim_{k\to\infty} \bar{z}^k = 0$.

Furthermore, with the definitions of z^k in (2.15) and $\bar{z}^k$ in (2.23), we have

$$\bar{z}^k = z^k + \tilde{\tau}_l^k, \tag{2.36}$$

where $\tilde{\tau}_l^k = \hat{\tau}_l^k - \tau_l^k$, and thus $\lim_{k\to\infty} \bar{z}^k = 0$ leads to

$$\lim_{k\to\infty} z^k = \lim_{k\to\infty} \tilde{\tau}_l^k. \tag{2.37}$$

Together with the above equation, (2.11) and (2.16) result in

$$\lim_{k\to\infty} w^k(t) = M_d\Gamma \lim_{k\to\infty} \tilde{\tau}_e^k, \text{ for all } t \in [0, t_f]. \tag{2.38}$$

And finally, we obtain the following result

$$\lim_{k\to\infty} \|w^k(t)\| \leq \|M_d\Gamma\| b_f, \text{ for all } t \in [0, t_f], \tag{2.39}$$

which completes the proof. □

Remark 10. *Since no time-invariance condition is imposed on the unknown system parameters, the learning control design applies equally well to uncertain time-varying parametric systems as long as the parameter and tracking errors are restricted in stable region at the first iteration.*

Remark 11. *In the above proof, we have used the resetting condition, i.e.,* $\dot{q}_0(0) = \dot{q}^k(0)$ *and* $q_0(0) = q^k(0)$*, to obtain (2.30). However, it is well-known that this condition is very difficult to satisfy in practical implementation, considering the system has to be set to the same initial position in each iteration. In fact, the resetting condition can be replaced by the alignment condition as in [89]. In details, the alignment condition is:* $\dot{q}^k(0) = \dot{q}^{k-1}(t_f)$, $q^k(0) = q^{k-1}(t_f)$, $\dot{q}_0(0) = \dot{q}_0(t_f)$, *and* $q_0(0) = q_0(t_f)$,

which means that we can start the system at the k-th iteration from where it stops at the $(k-1)th$ iteration.

The above discussion is summarized by the following Lemma:

Lemma 1. *The results achieved in Theorem 1 are guaranteed under the alignment condition*

$$\dot{q}^k(0) = \dot{q}^{k-1}(t_f),\ q^k(0) = q^{k-1}(t_f),\ \dot{q}_0(0) = \dot{q}_0(t_f),\ q_0(0) = q_0(t_f). \tag{2.40}$$

Proof. Under the alignment condition (2.40), we have the following result

$$V^k(t) \leq V^k(0) + \int_0^t \bar{z}^{k^T}(Y_0^k\tilde{\theta}_0^k - K\bar{z}^k)dv. \tag{2.41}$$

According to (2.27), (2.32), and (2.41), we obtain

$$\Delta W_0^k(t) \leq V^k(0) - V^{k-1}(t) - \int_0^t \bar{z}^{k^T} K\bar{z}^k dv - \frac{1}{2}\int_0^t \bar{z}^{k^T} Y_0^k S_0^{-1} Y_0^{k^T}\bar{z}^k dv. \tag{2.42}$$

For $t = t_f$, we have

$$\Delta W_0^k(t_f) \leq V^k(0) - V^{k-1}(t_f) - \int_0^{t_f} \bar{z}^{k^T} K\bar{z}^k dv - \frac{1}{2}\int_0^{t_f} \bar{z}^{k^T} Y_0^k S_0^{-1} Y_0^{k^T}\bar{z}^k dv. \tag{2.43}$$

Considering the definition (2.23) and alignment condition (2.40), we have $\bar{z}^{k-1}(t_f) = \bar{z}^k(0)$ and thus $V^k(0) = V^{k-1}(t_f)$. Substituting it into the above equation leads to

$$\Delta W_0^k(t_f) \leq -\int_0^{t_f} \bar{z}^{k^T} K\bar{z}^k dv - \frac{1}{2}\int_0^{t_f} \bar{z}^{k^T} Y_0^k S_0^{-1} Y_0^{k^T}\bar{z}^k dv \leq 0. \tag{2.44}$$

The rest is similar to the proof of Theorem 1 and is thus omitted. □

In this section, learning impedance control has been developed for the robot. It has been proven that the robot dynamics follow a target impedance model with the proposed method. However, as Property 3 has been utilized in this method, the knowledge of the robot structure is required by the proposed method. This problem will be resolved in the following section.

2.3 Control Design Based on Property 4

Following the previous section, learning impedance control is further developed for robots interacting with unknown environments. While the problem formulation and control objective are the same as that in the previous section, the method developed in this section employs Property 4 and does not require the knowledge of the robot structure.

We propose to compute the control input as follows

$$\tau_0^k = \tau_{ct,0}^k + \tau_{fb}^k + \hat{\tau}_e^k, \tag{2.45}$$

where τ_{fb}^k and $\hat{\tau}_e^k$ are the same as that in (2.19), while τ_0^k and $\tau_{ct,0}^k$ have different expressions as τ^k and τ_{ct}^k in (2.45). In the following, the subscript "0" is used to distinguish variables with the same meanings but different expressions.

The computed torque vector $\tau_{ct,0}^k$ is given by

$$\tau_{ct,0}^k = -Y_0^k(\ddot{q}_r^k, \dot{q}_r^k, \dot{q}^k, q^k)\hat{\theta}_0^k, \tag{2.46}$$

where $\hat{\theta}_0^k$ is the estimate of $\theta_0 = [k_M, k_C, k_G + b_f]^T$ and

$$Y_0^k(\ddot{q}_r^k, \dot{q}_r^k, \dot{q}^k, q^k) = [\|\ddot{q}_r^k\|\text{sgn}(\bar{z}^k), \|\dot{q}^k\|\|\dot{q}_r^k\|\text{sgn}(\bar{z}^k), \text{sgn}(\bar{z}^k)]. \tag{2.47}$$

To obtain $\hat{\theta}_0^k$, we develop the following learning law

$$\hat{\theta}_0^k = \hat{\theta}_0^{k-1} + S_0^{-1} Y_0^{k^T} \bar{z}^k, \tag{2.48}$$

where S_0 is a diagonal positive definite matrix.

Theorem 2. *Considering the system described by (2.4), we use the control input (2.45) with the learning law (2.48) to achieve the following results:*

(i) $\lim_{k\to\infty} w^k(t)$ *is bounded by* $\|M_d\Gamma\|b_f$ *for all* $t \in [0, t_f]$, *i.e.,* $\lim_{k\to\infty} \|w^k(t)\| \leq \|M_d\Gamma\|b_f$. *When the force measurement is accurate,* $b_f = 0$ *indicates* $\lim_{k\to\infty} w^k(t) = 0$.

(ii) all the signals in the closed-loop system are bounded for all $t \geq 0$.

Proof. Consider the following Lyapunov function candidate

$$W_0^k(t) = V^k(t) + U_0^k(t), \tag{2.49}$$

where

$$\begin{aligned} V^k(t) &= \frac{1}{2}\bar{z}^{k^T} M(q)\bar{z}^k, \\ U_0^k(t) &= \frac{1}{2}\int_0^t \tilde{\theta}_0^{k^T} S_0^T \tilde{\theta}_0^k dv \end{aligned} \tag{2.50}$$

with $\tilde{\theta}_0^k(t) = \theta_0(t) - \hat{\theta}_0^k(t)$.

According to Property 4 and the definitions of Y_0^k and θ_0, we have

$$\begin{aligned}
&-\bar{z}^{k^T}(M(q)\ddot{q}_r^k + C(q,\dot{q})\dot{q}_r^k + G(q) - \tilde{\tau}_e) \\
&\leq \|\bar{z}^k\|(\|M(q)\ddot{q}_r^k\| + \|C(q,\dot{q})\dot{q}_r^k\| + \|G(q)\| - \tilde{\tau}_e) \\
&\leq \|\bar{z}^k\|(\|M(q)\|\|\ddot{q}_r^k\| + \|C(q,\dot{q})\|\|\dot{q}_r^k\| + \|G(q)\| - \tilde{\tau}_e) \\
&\leq \|\bar{z}^k\|(k_M\|\ddot{q}_r^k\| + k_C\|\dot{q}^k\|\|\dot{q}_r^k\| + k_G + k_\delta) \\
&= \bar{z}^{k^T}\mathrm{sgn}(\bar{z}^k)(k_M\|\ddot{q}_r^k\| + k_C\|\dot{q}^k\|\|\dot{q}_r^k\| + k_G + b_f) \\
&= \bar{z}^{k^T}Y_0^k\theta_0. \qquad (2.51)
\end{aligned}$$

Then, by considering the robot dynamics (2.4) and control (2.45), we obtain

$$\begin{aligned}
V_0^k(t) &= V_0^k(0) + \int_0^t (\bar{z}^{k^T}M(q)\dot{\bar{z}}^k + \frac{1}{2}\bar{z}^{k^T}\dot{M}(q)\bar{z}^k)dv \\
&= V_0^k(0) + \int_0^t (\bar{z}^{k^T}M(q)\dot{\bar{z}}^k + \bar{z}^{k^T}C(q,\dot{q})\bar{z}^k)dv \\
&= V_0^k(0) + \int_0^t \bar{z}^{k^T}(-M(q)\ddot{q}_r^k - C(q,\dot{q})\dot{q}_r^k - G(q) + \tau^k - \tau_e^k)dv \\
&\leq V_0^k(0) + \int_0^t \bar{z}^{k^T}(Y_0^k\theta_0 - Y_0^k\hat{\theta}_0^k - K\bar{z}^k)dv \\
&= V_0^k(0) + \int_0^t \bar{z}^{k^T}(Y_0^k\tilde{\theta}_0^k - K\bar{z}^k)dv. \qquad (2.52)
\end{aligned}$$

The following is the same as that in the proof of Theorem 1, and thus omitted. □

Remark 12. *From the above proof, we can find that in the computed torque vector, the learning scheme is employed to deal with unknown bounds k_M, k_C and k_G. Therefore, if we have limited knowledge of k_M, k_C and k_G, it is possible to develop a "learning-free" method and make the control design simpler. Instead of Property 4, we have the following assumption:*

Assumption 2. $\|M(q)\| \leq k_M$, $\|C(q,\dot{q})\| \leq k_C\|\dot{q}\|$, *and* $\|G(q)\| \leq k_G$, *where* k_M, k_C,

and k_G are known positive scalars.

We propose to compute the control input as the same as in (2.45)

$$\tau_0 = \tau_{ct,0} + \tau_{fb} + \hat{\tau}_e \tag{2.53}$$

with the same τ_{fb}, $\hat{\tau}_e$, and

$$\tau_{ct,0} = -(K_1\|\ddot{q}_r\| + K_2\|\dot{q}\|\|\dot{q}_r\| + K_3)sgn(\bar{z}), \tag{2.54}$$

where K_1, K_2, and K_3 are definite positive diagonal matrices of which the elements are large enough so that

$$k_{1,i} \geq k_M,\ k_{2,i} \geq k_C,\ k_{3,i} \geq (k_G + b_f),\ \textit{for } i = 1, 2, \ldots, n. \tag{2.55}$$

Then we obtain the following results similar to Theorem 2:

Theorem 3. *Considering the robot dynamics described by (2.4), under Assumption 2, the control design (2.45) guarantees the following results:*

(i) $\lim_{t\to\infty} w(t)$ *is bounded by* $\|M_d\Gamma\|b_f$, *i.e.,* $\|\lim_{t\to\infty} w(t)\| \leq \|M_d\Gamma\|b_f$. *When the force measurement is accurate,* $b_f = 0$ *indicates* $\lim_{t\to\infty} w(t) = 0$.

(ii) all the signals in the closed-loop are bounded.

Proof. Consider the following Lyapunov function candidate

$$V(t) = \frac{1}{2}\bar{z}^T M(q)\bar{z}. \tag{2.56}$$

Taking the derivative of (2.49) leads to

$$\begin{aligned}
\dot{V}(t) &= \bar{z}^T M(q)\dot{\bar{z}} + \frac{1}{2}\bar{z}^T \dot{M}(q)\bar{z} \\
&= \bar{z}^T M(q)\dot{\bar{z}} + \bar{z}^T C(q,\dot{q})\bar{z} \\
&= \bar{z}^T M(q)(\ddot{q} - \ddot{q}_r) + \bar{z}^T C(q,\dot{q})(\dot{q} - \dot{q}_r) \\
&= \bar{z}^T((M(q)\ddot{q} + C(q,\dot{q})\dot{q} + G(q)) - (M(q)\ddot{q}_r + C(q,\dot{q})\dot{q}_r + G(q))) \\
&= \bar{z}^T(-K\bar{z} - (K_1\|\ddot{q}_r\| + K_2\|\dot{q}\|\|\dot{q}_r\| + K_3)\mathrm{sgn}(\bar{z}) \\
&\quad +\tilde{\tau}_e - (M(q)\ddot{q}_r + C(q,\dot{q})\dot{q}_r + G(q))), \qquad (2.57)
\end{aligned}$$

where we have used Property 1 and Property 2 in the first equality.

Taking Assumption 2 into consideration, we have

$$\begin{aligned}
& -\bar{z}^T(M(q)\ddot{q}_r + C(q,\dot{q})\dot{q}_r + G(q) - \tilde{\tau}_e) \\
\leq\ & \|\bar{z}\|(\|M(q)\ddot{q}_r\| + \|C(q,\dot{q})\dot{q}_r\| + \|G(q)\| - \tilde{\tau}_e) \\
\leq\ & \|\bar{z}\|(\|M(q)\|\|\ddot{q}_r\| + \|C(q,\dot{q})\|\|\dot{q}_r\| + \|G(q)\| - \tilde{\tau}_e) \\
\leq\ & \|\bar{z}\|(k_M\|\ddot{q}_r\| + k_C\|\dot{q}\|\|\dot{q}_r\| + k_G + b_f) \\
=\ & \bar{z}^T\mathrm{sgn}(\bar{z})(k_M\|\ddot{q}_r\| + k_C\|\dot{q}\|\|\dot{q}_r\| + k_G + b_f). \qquad (2.58)
\end{aligned}$$

Substituting (2.58) into (2.57) results in

$$\begin{aligned}
\dot{V}(t) &\leq \bar{z}^T(-K\bar{z} - (K_1\|\ddot{q}_r\| + K_2\|\dot{q}\|\|\dot{q}_r\| + K_3)\mathrm{sgn}(\bar{z})) \\
&\quad + b_f\bar{z}^T\mathrm{sgn}(\bar{z}) + \bar{z}^T(k_M\|\ddot{q}_r\| + k_C\|\dot{q}\|\|\dot{q}_r\| + k_G)\mathrm{sgn}(\bar{z}) \\
&= -K\bar{z}^T\bar{z} - \bar{z}^T((K_1 - k_M I_n)\|\ddot{q}_r\| + (K_2 - k_C I_n)\|\dot{q}\|\|\dot{q}_r\| \\
&\quad + (K_3 - k_G I_n - b_f I_n))\mathrm{sgn}(\bar{z}) \\
&= -K\bar{z}^T\bar{z} - (K_1 - k_M I_n)\|\ddot{q}_r\|\bar{z}^T\mathrm{sgn}(\bar{z}) - (K_2 - k_C I_n)\|\dot{q}\|\|\dot{q}_r\|\bar{z}^T\mathrm{sgn}(\bar{z}) \\
&\quad - (K_3 - k_G I_n - b_f I_n)\bar{z}^T\mathrm{sgn}(\bar{z}) \leq 0, \qquad (2.59)
\end{aligned}$$

where I_n denotes a n-dimension identity matrix. (2.59) indicates that W is monotonically decreasing. Besides, suppose that $\bar{z}(0)$ is bounded, which comes from the assumption that $e(0) = 0$ and $\hat{\tau}_e(0) = 0$, then $V(0)$ is bounded since $\|M(q)\|$ is bounded. Therefore, V will converge to a nonnegative fixed value, and thus we have $\lim_{t\to\infty} \dot{V} = 0$. Immediately, we have the following inequality

$$\dot{V} \leq -\bar{z}^T K\bar{z} \leq 0, \qquad (2.60)$$

which leads to $\lim_{t\to\infty} \bar{z} = 0$. The rest of the proof is similar to that in the proof of Theorem 1 and is thus omitted. □

Remark 13. *The control design in (2.53) indicates that the robot dynamics are mainly compensated by the high gain scheme, which makes the control design easy to apply in the practical implementation. In some situations where the high gain method is not suitable due to the instability concern, the learning method in (2.45) is more favorable. Besides, under the learning scheme, it is not necessary to know k_M, k_C, k_G and b_f. Therefore, a good choice between the high gain and learning*

methods is to be considered by evaluating the practical concern.

2.4 Simulation Studies

2.4.1 System Description

To verify the validity of the proposed method, we consider a scenario where a 2-DOF robot arm with two revolute joints interacting with the environment in the $X-Y$ plane as shown in Fig. 2.1. The simulation is conducted with the Robotics Toolbox introduced in [90].

The robot arm parameters are: $m_1 = m_2 = 1.0$kg, $l_1 = l_2 = 0.2$m, $i_1 = i_2 = 0.003$kgm^2, and $l_{c1} = l_{c2} = 0.1$m, where m_j, l_j, i_j, and l_{cj} $(j = 1, 2)$ represent the mass, the length, the inertia about the Z-axis that comes out of the page passing through the center of mass, and the distance from the previous joint to the center of mass of link j, respectively. Note that these parameters are only used for the simulation and they will not be used in the control design. The initial positions of the robot arm are $q_1 = \pi/6$ and $q_2 = \pi/6$.

For the convenience, the following abbreviation is employed

$$\begin{aligned} s_{12} &= \sin(q_1+q_2), c_{12} = \cos(q_1+q_2),\ c_1 = \cos(q_1), \\ s_1 &= \sin(q_1),\ s_2 = \sin(q_2),\ c_2 = \cos(q_2). \end{aligned} \tag{2.61}$$

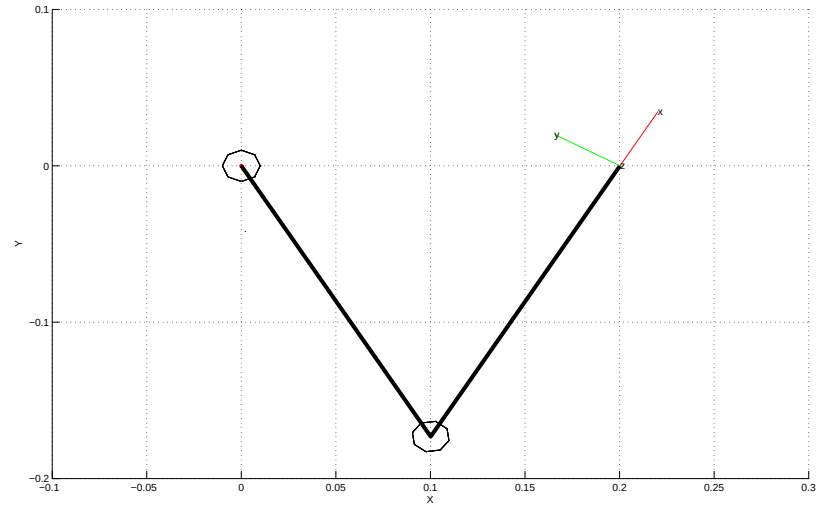

(a) plane view

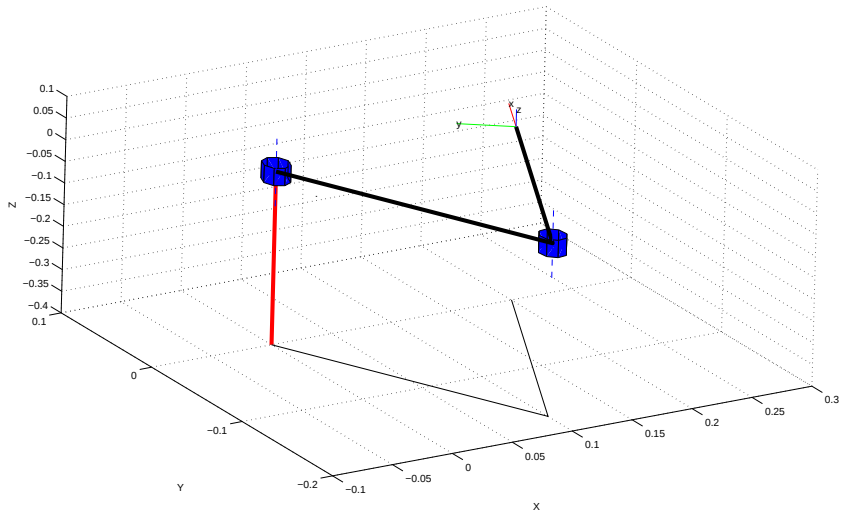

(b) stereo view

Fig. 2.1: Simulation scenario: a 2-DOF robot arm interacts with an unknown environment

The dynamics of the robot arm in the joint space is given as (2.4) with $G(q) = 0$ and

$$M(q) = \begin{bmatrix} M_{11} & M_{12} \\ M_{21} & M_{22} \end{bmatrix},\ C(q, \dot{q}) = \begin{bmatrix} C_{11} & C_{12} \\ C_{21} & C_{22} \end{bmatrix}, \tag{2.62}$$

where

$$\begin{aligned} M_{11} &= m_1 l_{c1}^2 + m_2(l_1^2 + l_{c2}^2 + 2l_1 l_{c2} c_2) + i_1 + i_2, \\ M_{12} &= M_{21} = m_2(l_{c2}^2 + l_1 l_{c2} c_2) + I_2,\ M_{22} = m_2 l_{c2}^2 + i_2, \\ C_{11} &= -m_2 l_1 l_{c2} s_2 \dot{q}_2,\ C_{12} = -m_2 l_1 l_{c2} s_2 (\dot{q}_1 + \dot{q}_2), \\ C_{21} &= m_2 l_1 l_{c2} s_2 \dot{q}_1,\ C_{22} = 0. \end{aligned} \tag{2.63}$$

The rest position of the robot arm is a minimum jerk motion, which is specified in the Cartesian space as

$$x_0(t) = [1 + 0.5(6t^5 - 15t^4 + 10t^3), 0]^T,\ \text{for } t \in [0, t_f], \tag{2.64}$$

where $t_f = 1s$.

The rest position q_0 is obtained by $q_0 = \int_0^t J(q)^{-1} x_0(v) dv$ with

$$J(q) = \begin{bmatrix} -(l_1 s_1 + l_2 s_{12}) & -l_2 s_{12} \\ l_1 c_1 + l_2 c_{12} & l_2 c_{12} \end{bmatrix}. \tag{2.65}$$

The parameters of the target impedance model (2.8) are

$$M_d = 0.1 I_2,\ C_d = 8 I_2,\ G_d = 0.1 I_2. \tag{2.66}$$

Then, Γ and Λ are obtained immediately according to (2.12). Signals $\bar{z}^k$, $\dot{q}_r^k$, and $\hat{\tau}_l^k$ in control (2.45) can be obtained based on the measured signals q^k and $\hat{\tau}^k$.

With $\theta^0 = 0$, the parameters in control (2.45) and learning law (2.48) are given as

$$K = 50I_2, \ S_0 = 0.05I_2. \tag{2.67}$$

Compared with the methods in [40, 41], the proposed control design has a simpler structure and fewer open parameters to be set by the designers, so it is more feasible in practical implementations. Other choices of K and S_0 different from those given by (2.67) can be also applied as long as K and S_0 are positive definite.

2.4.2 Simulation Results

When there is no contact between the environment and the robot arm, impedance control will reduce to position control, i.e., the control objective will become trajectory tracking. In the first case, the interaction force τ_e is set as zero to investigate the tracking performance of the robot arm with the proposed impedance method.

The defined impedance error w, tracking error e, and estimated parameter $\hat{\theta}_0$ for $k = 1$, $k = 20$, $k = 60$, and $k = 80$ are shown in Figs. 2.2, 2.3, 2.4, and 2.5, respectively. It is easy to find that the impedance error w becomes smaller when k becomes larger. When $k = 80$, w converges to around zero, which indicates that the robot arm dynamics are governed by the target impedance model. Besides, because there is no force exerted to the robot arm, the tracking error e also converges to zero when $k = 80$, which confirms the fact that impedance control reduces to position control when $\tau_e = 0$. The estimated parameter $\hat{\theta}_0^k$ is shown to visualize the convergence rate of the developed learning law (2.26), where $\hat{\theta}_1$, $\hat{\theta}_2$, and $\hat{\theta}_3$ are three

components of $\hat{\theta}_0$. According to Theorem 2, $w \to 0$ when $k \to \infty$, which means that the learning process is supposed to be stopped when $k \to \infty$. However, this is not realizable in practice. Usually we only require that w converges to a pre-defined bound set and then the learning process is stopped. From Figs. 2.4 and 2.5, it is found that $\hat{\theta}_0^{60}$ and $\hat{\theta}_0^{80}$ are almost the same, which indicates that the convergence is almost achieved, so the learning process is stopped at $k = 80$. Furthermore, the convergence rate can be modulated by choosing different S_0 in (2.26). Particularly, larger S_0^{-1} will lead to faster convergence but more control effort will be required.

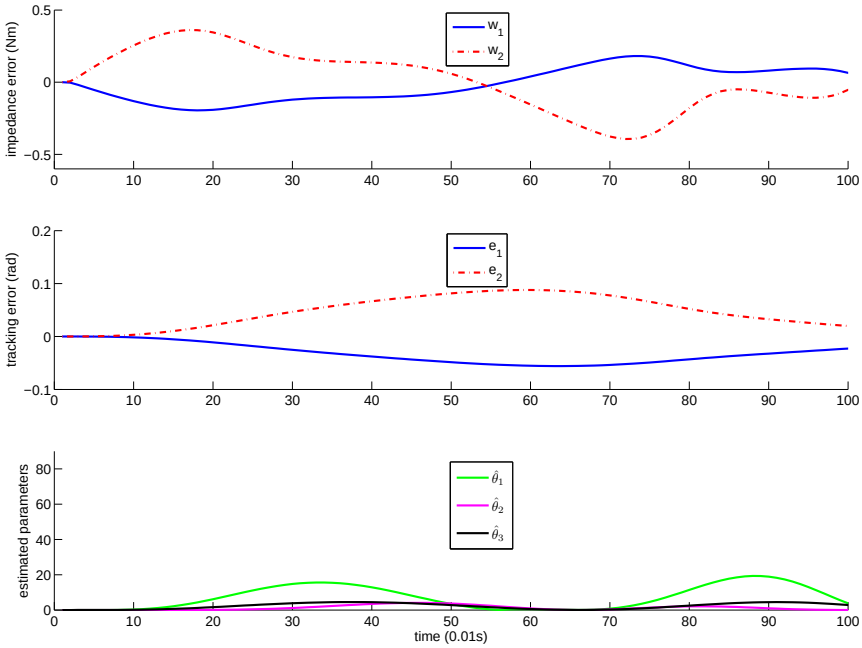

Fig. 2.2: The first case: k=1

In the second case, we assume that there is an interaction force exerted to the robot arm by the environment. The interaction force is with a constant value of 0.1. It is measured by torque sensors mounted on two joints. The force measurement noise is a uniform-random-number signal with amplitude of 0.01.

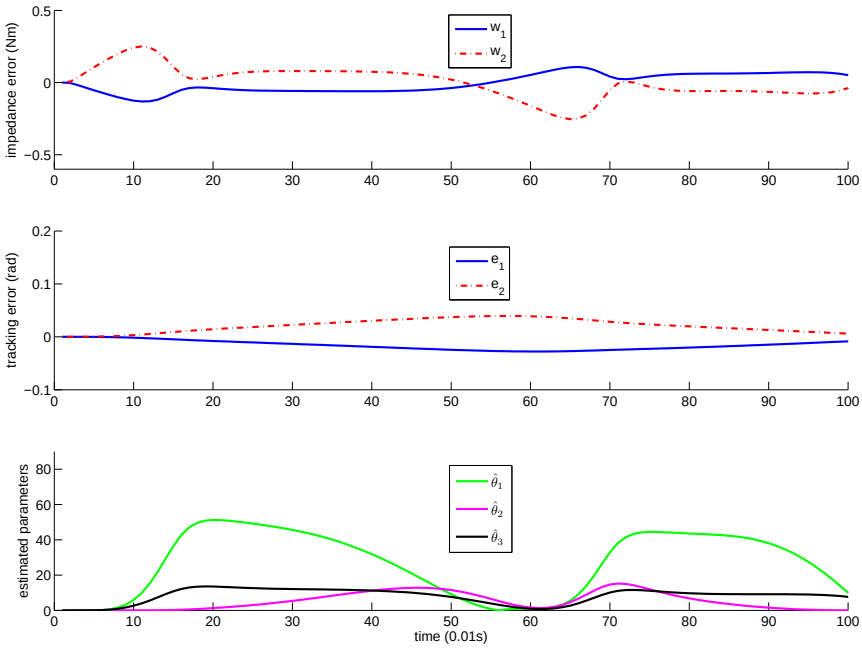

Fig. 2.3: The first case: k=20

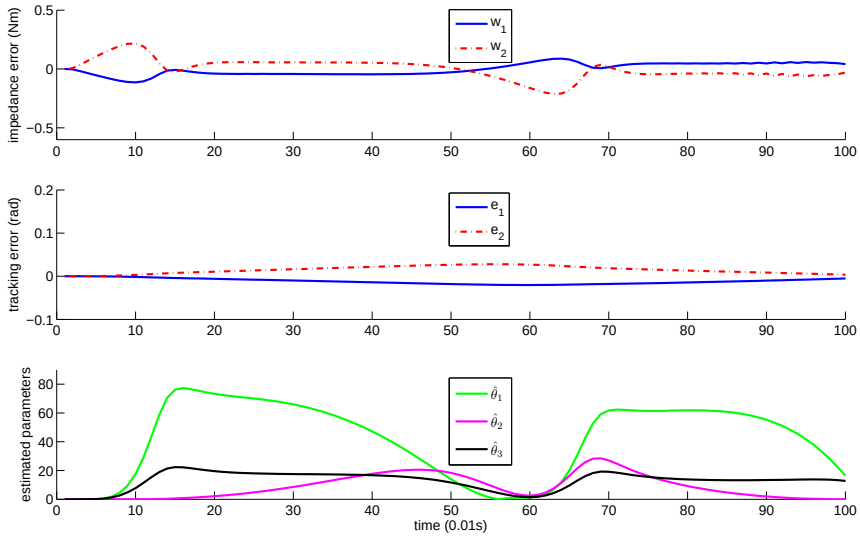

Fig. 2.4: The first case: k=60

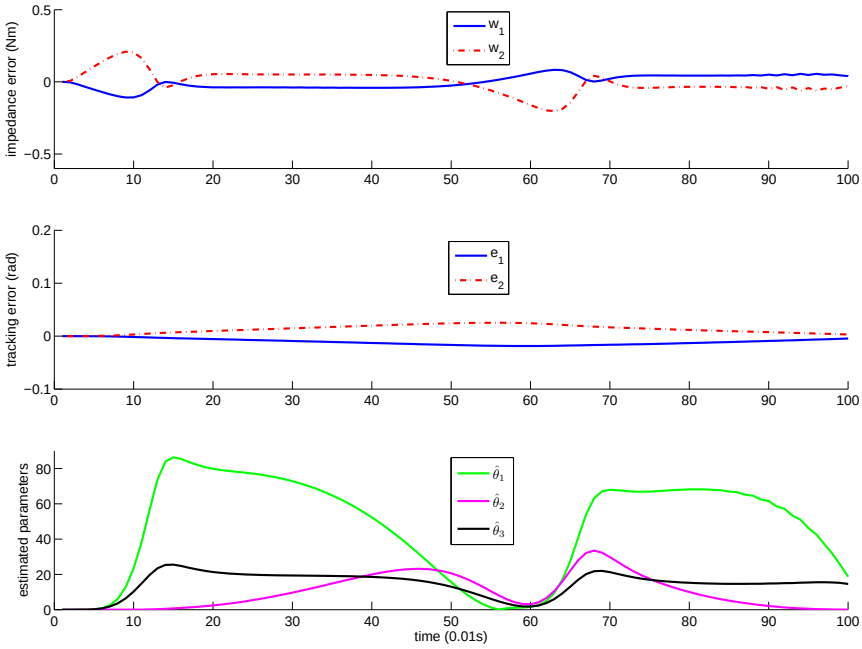

Fig. 2.5: The first case: k=80

The results for $k = 1$, $k = 10$, and $k = 20$ are shown in Figs. 2.6, 2.7, and 2.8, respectively. The results of the impedance error shown in Figs. 2.6, 2.7, and 2.8 are similar to that in Figs. 2.2, 2.3, 2.4, and 2.5, which further verify that the robot arm dynamics are governed by the target impedance model. The results of the tracking error in Figs. 2.6, 2.7, and 2.8 clearly show the compliant behavior of the robot arm. In particular, it is found that the tracking error is larger than that in Figs. 2.2, 2.3, and 2.4, which means that the robot arm drifts away from the rest position q_0 due to the effect of the interaction force.

The results in the above two cases illustrate that impedance control unifies both the contact and non-contact cases. Note that in the contact case, the interaction force is assumed to be with a constant value, which indicates that the environment dynamics have not been taken into consideration. As it is well-known that the system may

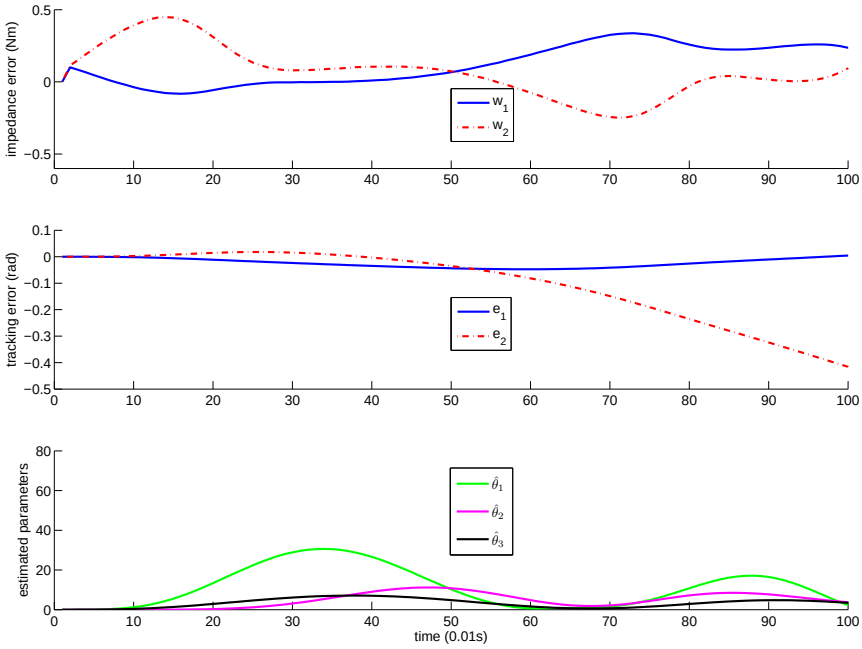

Fig. 2.6: The second case: k=1

become unstable when the robot arm interacts with an dynamic environment, further verification of the proposed method in the dynamic environment case is needed. Besides, the target impedance model (2.8) is given as a priori knowledge. But in many applications, it is actually very difficult to find a desired impedance model, especially when the environments are dynamically changing. These problems will be investigated in Chapters 4, 5, and 6. Furthermore, in the real-world implementation, practical issues such as system resetting (as discussed in Section 2.2) and computation complexity will be carefully dealt with.

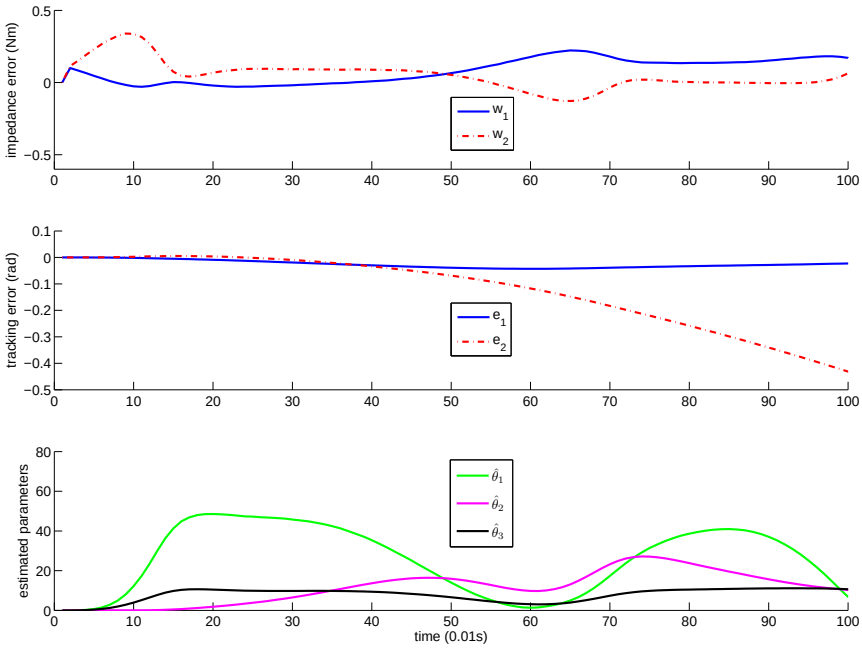

Fig. 2.7: The second case: k=10

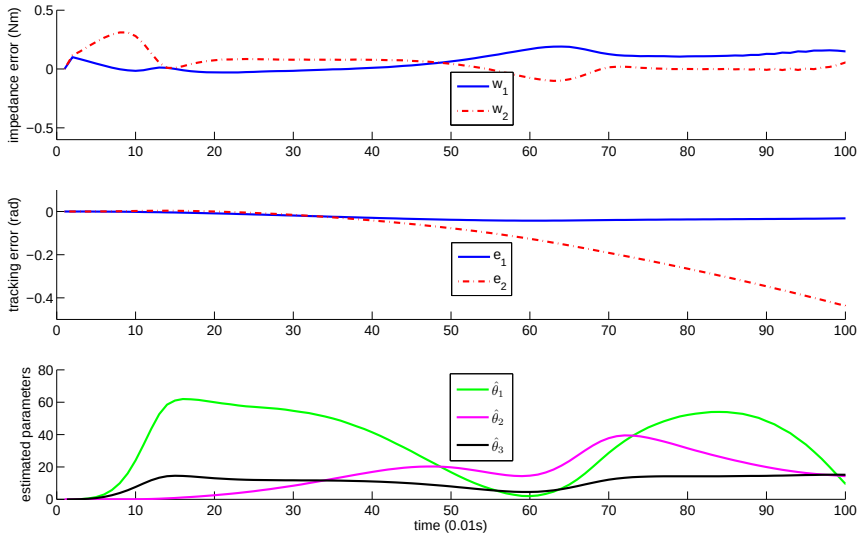

Fig. 2.8: The second case: k=20

2.5 Conclusion

In this chapter, an auxiliary error variable has been introduced such that it is possible to extend existing methods in position control to impedance control. Based on the LIP property, learning impedance control has been developed but it requires the knowledge of the robot structure. Based on the boundedness property, learning impedance control which requires neither the knowledge of the robot structure nor that of physical parameters has been developed. As further discussed, if the bounds of the robot dynamics are known, the learning process is avoided while the high-gain scheme can be adopted. Both methods have been proven to be able to guarantee the robot dynamics to follow a target impedance model. The control performance has been discussed through the rigorous proof and remarking arguments. The simulation results have shown the validity of the proposed methods.

Although the second method that is based on the boundedness property provides the design simplicity, it is found that there is chattering when the defined impedance error becomes very small. This is due to the utilization of sign function, which is discontinuous and expected to be avoided. Therefore, in the following chapter, we will utilize function approximators to solve this problem.

Chapter 3

NN Impedance Control

In this chapter, we consider the same system under study in the previous chapter, in which a rigid robot arm is physically interacting with unknown environments. The method to be discussed in this chapter is based on the learning mechanism as proposed in the previous chapter, while NN are employed to cope with the problem of unknown robot dynamics. It has been demonstrated that NN control is particularly suitable for controlling highly uncertain, nonlinear, and complex systems, due to the excellent universal approximation ability of NN to unknown complicated nonlinearities [75, 91, 92, 93]. The method using NN to approximate robot dynamics has been studied in the literature [94], which motivates the control design in this chapter. While the robot dynamics are not required in the learning impedance control to be developed in this chapter, the adoption of the boundedness property in the previous chapter is also avoided. Then the chattering problem which is inherently along with the method in the previous chapter can be resolved. This will be illustrated in details through rigorous analysis and comparative simulation studies.

The rest of this chapter is organized as follows. In Section 3.1, the robot dynamics

are approximated by NN. In Section 3.2, the details of the proposed learning control are presented, followed by the rigorous analysis. In Section 3.3, the validity of the proposed method is verified by simulation studies. Concluding remarks are given in Section 3.4.

3.1 NN Approximation of Robot Dynamics

As discussed in [94], the robot dynamics can be appoximated by NN. Denote the elements of $M(q)$, $C(q,\dot{q})$, and $G(q)$ as $m_{ij}(q)$, $c_{ij}(q,\dot{q})$, and $g_i(q)$ for $i = 1, 2, \ldots, n, j = 1, 2, \ldots, n$, respectively. Then, they are represented by

$$\begin{aligned} m_{ij}(q) &= \theta_{Mij}^T \xi_{Mij}(q) + \epsilon_{Mij}, \\ c_{ij}(q,\dot{q}) &= \theta_{Cij}^T \xi_{Cij}(q,\dot{q}) + \epsilon_{Cij}, \\ g_i(q) &= \theta_{Gi}^T \xi_{Gi}(q) + \epsilon_{Gi}, \end{aligned} \tag{3.1}$$

where $\epsilon_{Mij}, \epsilon_{Cij}$, and ϵ_{Gi} are the bounded approximation errors, θ_{Mij}^T, θ_{Cij}^T, and θ_{Gi}^T are the column vectors of the NN weights, $\xi_{Mij}(q)$, $\xi_{Cij}(q,\dot{q})$, and $\xi_{Gi}(q)$ are the vectors of Gaussian functions with elements

$$\begin{aligned} \xi_{Mijl}(q) &= \exp\left(\frac{-(q-\mu_{Ml})^T(q-\mu_{Ml})}{\sigma_M^2}\right), \\ \xi_{Cijl}(q) &= \exp\left(\frac{-(\eta-\mu_{Cl})^T(\eta-\mu_{Cl})}{\sigma_C^2}\right), \\ \xi_{Gil}(q) &= \exp\left(\frac{-(q-\mu_{Gl})^T(q-\mu_{Gl})}{\sigma_G^2}\right), \end{aligned} \tag{3.2}$$

where $l = 1, 2, \ldots, p$ and p is the number of NN nodes, μ_{Ml}, μ_{Cl}, and μ_{Gl} are the centers of the functions, and σ_M^2, σ_C^2, and σ_G^2 are the variances, and $\eta = [q^T, \dot{q}^T]^T$.

Remark 14. (GL matrices and operation [83]) *As the complexity and nonlinearity of individual entries of a matrix (vector) are different, to achieve roughly the same level of approximation accuracy, the sizes of the corresponding NN should also be different. The introduction of General-Leeway/Ge-Lee (GL) matrices* $\{*\}$ *and operation "*$\bullet$*" makes convenient expression and efficient computation possible for any general matrices/vectors in a manner with extra flexibility and leeway.*

Suppose that there are three matrices $A = [a_{ij}]$, $B = [b_{ij}]$, and $C = [c_{ij}]$, where the elements a_{ij} and b_{ij} are column vectors, and c_{ij} are scalars. The corresponding GL matrices have the following properties:

$$\{A\}^T = [a_{ij}^T],\ \{A\}^T \bullet \{B\} = [a_{ij}^T b_{ij}],\ \{A\} \bullet C = [c_{ij} a_{ij}]. \tag{3.3}$$

Note that a_{ij} and b_{ij} may have different sizes for different i and j, which increases the design freedom and analysis efficiency [83].

By employing NN and GL denotation, the robot dynamics are described as

$$\begin{aligned} M(q) &= \{\Theta_M\}^T \bullet \{\Xi_M(q)\} + E_M, \\ C(q,\dot{q}) &= \{\Theta_C\}^T \bullet \{\Xi_C(q,\dot{q})\} + E_C, \\ G(q) &= \{\Theta_G\}^T \bullet \{\Xi_G(q)\} + E_G, \end{aligned} \tag{3.4}$$

where Θ_M, Θ_C, and Θ_G are matrices formed by θ_{Mij}, θ_{Cij}, and θ_{Gij}, respectively, $\Xi_M(q)$, $\Xi_C(q,\dot{q})$, and $\Xi_G(q)$ are matrices formed by $\xi_{Mij}(q)$, $\xi_{Cij}(q,\dot{q})$, and $\xi_{Gij}(q)$, respectively, and E_M, E_C, and E_G are matrices formed by ϵ_{Mij}, ϵ_{Cij}, and ϵ_{Gij}, respectively. Because E_M, E_C, and E_G are bounded, we denote their upper bounds are b_M,

b_C, and b_G, respectively. Equivalently, we have

$$\|E_M\| \leq b_M,\ \|E_C\| \leq b_C,\ \|E_G\| \leq b_G. \tag{3.5}$$

Note that b_M, b_C, and b_G are unknown.

3.2 Control Design

In this section, NN learning impedance control is developed to achieve the same control objective discussed in Section 2.1.

Let the estimates of $M(q)$, $C(q,\dot{q})$, and $G(q)$ be $\hat{M}(q)$, $\hat{C}(q,\dot{q})$, and $\hat{G}(q)$, respectively, and they are defined as

$$\begin{aligned} \hat{M}(q) &= \{\hat{\Theta}_M\}^T \bullet \{\Xi_M(q)\}, \\ \hat{C}(q,\dot{q}) &= \{\hat{\Theta}_C\}^T \bullet \{\Xi_C(q,\dot{q})\}, \\ \hat{G}(q) &= \{\hat{\Theta}_G\}^T \bullet \{\Xi_G(q)\}, \end{aligned} \tag{3.6}$$

where $\hat{\Theta}_M$, $\hat{\Theta}_C$, and $\hat{\Theta}_G$ are the estimates of Θ_M, Θ_C, and Θ_G, respectively.

The control input is proposed as

$$\tau_{nn}^k = \tau_{ct,nn}^k + \tau_{fb}^k + \tau_{com,nn}^k + \hat{\tau}_e^k, \tag{3.7}$$

where $\tau_{ct,nn}^k$, τ_{fb}^k, and $\tau_{com,nn}^k$ are the computed torque vector, feedback torque vector, and compensation torque vector, respectively. τ_{fb}^k is the same as that in Section 2.2.

In specific, the computed torque vector is given by

$$\tau_{ct,nn}^k = \hat{M}^k(q)\ddot{q}_r^k + \hat{C}^k(q,\dot{q})\dot{q}_r^k + \hat{G}^k(q). \tag{3.8}$$

The compensation torque vector is given by

$$\tau_{com,nn}^k = -L^k\hat{B}^k, \tag{3.9}$$

where $L^k = [\mathrm{sgn}(\bar{z}^k), \mathrm{sgn}(\bar{z}^k)\|\ddot{q}_r^k\|, \mathrm{sgn}(\bar{z}^k)\|\dot{q}_r^k\|]$ and $\hat{B}$ is the estimate of $B = [b_f + b_G, b_M, b_C]^T$.

Remark 15. *The following analysis will show that the compensation torque vector (3.9) will compensate for not only the inaccurate force measurement, but also the NN estimation error.*

To obtain $\hat{M}(q)^k$, $\hat{C}^k(q,\dot{q})$, and $\hat{G}^k(q)$ in (3.8) and $\hat{B}^k$ in (3.9), we develop the following learning law

$$\begin{aligned}
\hat{\Theta}_M^k &= \hat{\Theta}_M^{k-1} - S_M^{-1} \bullet \{\Xi_M(q)\}\bar{z}^k\ddot{q}_r^{k^T}, \\
\hat{\Theta}_C^k &= \hat{\Theta}_C^{k-1} - S_C^{-1} \bullet \{\Xi_C(q,\dot{q})\}\bar{z}^k\dot{q}_r^{k^T}, \\
\hat{\Theta}_G^k &= \hat{\Theta}_G^{k-1} - S_G^{-1}\{\Xi_G(q)\} \bullet \bar{z}^k, \\
\hat{B}^k &= \hat{B}^{k-1} + S_B^{-1}L^{k^T}\bar{z}^k,
\end{aligned} \tag{3.10}$$

where S_M, S_C, S_G, and S_B are symmetric positive definite matrices, and $\hat{\Theta}_M^k$, $\hat{\Theta}_C^k$, and $\hat{\Theta}_G^k$ are the estimates of Θ_M^k, Θ_C^k, and Θ_G^k, respectively.

Substituting the control input (3.7) into the dynamics (2.4), we obtain the closed-loop system

$$\begin{aligned} & M^k(q)\dot{\bar{z}}^k + C^k(q,\dot{q})\bar{z}^k \\ & = -(\tilde{M}^k(q)\ddot{q}_r^k + \tilde{C}^k(q,\dot{q})\dot{q}_r^k + \tilde{G}^k(q) + K\bar{z}^k + L^k\hat{B}^k + \tilde{\tau}_e^k), \end{aligned} \tag{3.11}$$

where $\tilde{M}^k(q) = M^k(q) - \hat{M}^k(q)$, $\tilde{C}^k(q,\dot{q}) = C^k(q,\dot{q}) - \hat{C}^k(q,\dot{q})$, and $\tilde{G}^k(q) = G^k(q) - \hat{G}^k(q)$. Note that we have the following equations

$$\begin{aligned} \tilde{M}^k(q) &= \{\tilde{\Theta}_M^k\}^T \bullet \{\Xi_M^k(q)\} + E_M^k, \\ \tilde{C}^k(q,\dot{q}) &= \{\tilde{\Theta}_C^k\}^T \bullet \{\Xi_C^k(q,\dot{q})\} + E_C^k, \\ \tilde{G}^k(q) &= \{\tilde{\Theta}_G^k\}^T \bullet \{\Xi_G^k(q)\} + E_G^k, \end{aligned} \tag{3.12}$$

where $\tilde{\Theta}_M^k = \hat{\Theta}_M^k - \Theta_M$, $\tilde{\Theta}_C^k = \hat{\Theta}_C^k - \Theta_C$, $\tilde{\Theta}_G^k = \hat{\Theta}_G^k - \Theta_G$, and $\tilde{B}^k = \hat{B}^k - B$.

Theorem 4. *Considering the system described by (2.4) under Assumption 1, with the control input (3.7) and the learning law (3.10), we have the following results:*

(i) $\lim_{k\to\infty} w^k(t)$ *is bounded by* $\|M_d\Gamma\|b_f$ *for all* $t \in [0, t_f]$, *i.e.,* $\|\lim_{k\to\infty} w^k(t)\| \leq b_f$. *When the force measurement is accurate,* $b_f = 0$ *indicates* $\lim_{k\to\infty} w^k(t) = 0$.

(ii) all the signals in the closed-loop are bounded for all $t \geq 0$.

Proof. Consider the following Lyapunov function candidate

$$\Omega^k(t) = U^k(t) + V^k(t) + W^k(t), \tag{3.13}$$

where

$$\begin{aligned} U^k(t) &= \frac{1}{2}\bar{z}^{k^T} M^k \bar{z}^k, \\ V^k(t) &= \frac{1}{2}\int_0^t [\mathrm{tr}(\tilde{\Theta}_M^{k^T} S_M^T \tilde{\Theta}_M^k + \tilde{\Theta}_C^{k^T} S_C^T \tilde{\Theta}_C^k) + \tilde{\Theta}_G^{k^T} S_G^T \tilde{\Theta}_G^k] dv, \\ W^k(t) &= \frac{1}{2}\int_0^t \tilde{B}^{k^T} S_B^T \tilde{B}^k dv, \end{aligned} \tag{3.14}$$

where $\mathrm{tr}(\cdot)$ denotes the matrix trace.

According to Property 2 and closed-loop dynamics (3.11), we have

$$\begin{aligned} U^k(t) &= U^k(0) + \int_0^t [\bar{z}^{k^T} M^k(q)\dot{\bar{z}}^k + \frac{1}{2}\bar{z}^{k^T}\dot{M}^k(q)\bar{z}^k] dv \\ &= U^k(0) + \int_0^t \bar{z}^{k^T}[M^k(q)\dot{\bar{z}}^k + C^k(q,\dot{q})\bar{z}^k] dv \\ &= U^k(0) - \int_0^t \bar{z}^{k^T}[\tilde{M}^k(q)\ddot{q}_r^k + \tilde{C}^k(q,\dot{q})\dot{q}_r^k + \tilde{G}^k(q) + K\bar{z}^k + L^k\hat{B}^k + \tilde{\tau}_e^k] dv \\ &= -\int_0^t \bar{z}^{k^T}[\tilde{M}^k(q)\ddot{q}_r^k + \tilde{C}^k(q,\dot{q})\dot{q}_r^k + \tilde{G}^k(q) + K\bar{z}^k + L^k\hat{B}^k + \tilde{\tau}_e^k] dv, \end{aligned} \tag{3.15}$$

where we use the assumption that $U^k(0) = 0$. This is obtained by assuming that $\dot{q}^k(0) = \dot{q}_d(0)$, $q^k(0) = q_d(0)$, and $\hat{\tau}_e^k(0) = 0$, which are known as the resetting condition [89].

Besides, we consider

$$\begin{aligned} & V^k(t) - V^{k-1}(t) \\ = & -\int_0^t [\mathrm{tr}(\frac{1}{2}\delta\tilde{\Theta}_M^{k^T} S_M \delta\tilde{\Theta}_M^k + \tilde{\Theta}_M^{k^T} S_M \delta\tilde{\Theta}_M^k + \frac{1}{2}\delta\tilde{\Theta}_C^{k^T} S_C \delta\tilde{\Theta}_C^k + \tilde{\Theta}_C^{k^T} S_C \delta\tilde{\Theta}_C^k) \\ & + \frac{1}{2}\delta\tilde{\Theta}_G^{k^T} S_G \delta\tilde{\Theta}_G^k + \tilde{\Theta}_G^{k^T} S_G \delta\tilde{\Theta}_G^k] dv \\ \leq & -\int_0^t [\mathrm{tr}(\tilde{\Theta}_M^{k^T} S_M \delta\tilde{\Theta}_M^k + \tilde{\Theta}_C^{k^T} S_C \delta\tilde{\Theta}_C^k) + \tilde{\Theta}_G^{k^T} S_G \delta\tilde{\Theta}_G^k] dv. \end{aligned} \tag{3.16}$$

By defining $\delta\tilde{\Theta}_M^k = \tilde{\Theta}_M^{k-1} - \tilde{\Theta}_M^k$, $\delta\tilde{\Theta}_C^k = \tilde{\Theta}_C^{k-1} - \tilde{\Theta}_C^k$, and $\delta\tilde{\Theta}_G^k = \tilde{\Theta}_G^{k-1} - \tilde{\Theta}_G^k$, we obtain the following equations from (3.10)

$$\begin{aligned}
\delta\tilde{\Theta}_M^k &= -S_M^{-1} \bullet \{\Xi_M(q)\}\bar{z}^k \ddot{q}_r^{k^T}, \\
\delta\tilde{\Theta}_C^k &= -S_C^{-1} \bullet \{\Xi_C(q,\dot{q})\}\bar{z}^k \dot{q}_r^{k^T}, \\
\delta\tilde{\Theta}_G^k &= -S_G^{-1}\{\Xi_G(q)\} \bullet \bar{z}^k.
\end{aligned} \tag{3.17}$$

Based on the above results, we have

$$\begin{aligned}
& -\int_0^t [\mathrm{tr}(\tilde{\Theta}_M^{k^T} S_M \delta\tilde{\Theta}_M^k + \tilde{\Theta}_C^{k^T} S_C \delta\tilde{\Theta}_C^k) + \tilde{\Theta}_G^{k^T} S_G \delta\tilde{\Theta}_G^k] dv \\
= & \int_0^t [\mathrm{tr}[(\{\tilde{\Theta}_M^k\}^T \bullet \{\Xi_M(q)\})(\bar{z}^k \ddot{q}_r^{k^T}) + (\{\tilde{\Theta}_C^k\}^T \bullet \{\Xi_C(q,\dot{q})\})(\bar{z}^k \dot{q}_r^{k^T})] \\
& + \tilde{\Theta}_G^{k^T}(\{\Xi_G(q)\} \bullet \bar{z}^k)] dv \\
= & \int_0^t [\mathrm{tr}[(\ddot{q}_r^k \bar{z}^{k^T})(\{\tilde{\Theta}_M^k\}^T \bullet \{\Xi_M(q)\}) + (\dot{q}_r^k \bar{z}^{k^T})(\{\tilde{\Theta}_C^k\}^T \bullet \{\Xi_C(q,\dot{q})\})] \\
& + \bar{z}^{k^T}(\{\tilde{\Theta}_G^k\}^T \bullet \{\Xi_G(q)\})] dv \\
= & \int_0^t [\mathrm{tr}[\ddot{q}_r^k \bar{z}^{k^T}(\tilde{M}^k(q) - E_M^k) + \dot{q}_r^k \bar{z}^{k^T}(\tilde{C}^k(q,\dot{q}) - E_C^k)] \\
& + \bar{z}^{k^T}(\tilde{G}^k(q) - E_G^k)] dv.
\end{aligned} \tag{3.18}$$

Considering the following fact

$$\begin{aligned}
\mathrm{tr}[\ddot{q}_r^k \bar{z}^{k^T}(\tilde{M}^k(q) - E_M^k)] &= \bar{z}^{k^T}(\tilde{M}^k(q) - E_M^k)\ddot{q}_r^k, \\
\mathrm{tr}[\dot{q}_r^k \bar{z}^{k^T}(\tilde{C}^k(q,\dot{q}) - E_C^k)] &= \bar{z}^{k^T}(\tilde{C}^k(q,\dot{q}) - E_C^k)\dot{q}_r^k,
\end{aligned} \tag{3.19}$$

we have

$$\begin{aligned}
& \int_0^t [\mathrm{tr}[\ddot{q}_r^k \bar{z}^{k^T}(\tilde{M}^k(q) - E_M^k) + \dot{q}_r^k \bar{z}^{k^T}(\tilde{C}^k(q,\dot{q}) - E_C^k)] \\
& + \bar{z}^{k^T}(\tilde{G}^k(q) - E_G^k)]dv \\
= & \int_0^t \bar{z}^{k^T}[(\tilde{M}^k(q) - E_M^k)\ddot{q}_r^k + (\tilde{C}^k(q,\dot{q}) - E_C^k)\dot{q}_r^k \\
& + (\tilde{G}^k(q) - E_G^k)]dv \\
= & \int_0^t \bar{z}^{k^T}(\tilde{M}^k(q)\ddot{q}_r^k + \tilde{C}^k(q,\dot{q})\dot{q}_r^k + \tilde{G}^k(q))dv \\
& - \int_0^t \bar{z}^{k^T}(E_M^k \ddot{q}_r^k + E_C^k \dot{q}_r^k + E_G^k)dv. \qquad (3.20)
\end{aligned}$$

Considering (3.16), (3.18) and (3.20), we obtain

$$\begin{aligned}
& V^k(t) - V^{k-1}(t) \\
\leq & \int_0^t \bar{z}^{k^T}(\tilde{M}^k(q)\ddot{q}_r^k + \tilde{C}^k(q,\dot{q})\dot{q}_r^k + \tilde{G}^k(q))dv \\
& - \int_0^t \bar{z}^{k^T}(E_M^k \ddot{q}_r^k + E_C^k \dot{q}_r^k + E_G^k)dv. \qquad (3.21)
\end{aligned}$$

Furthermore, by defining $\delta\tilde{B}^k = \tilde{B}^{k-1} - \tilde{B}^k$, we have $\delta\tilde{B}^k = -S_B^{-1}L^{k^T}\bar{z}^k$, and

$$\begin{aligned}
& W^k(t) - W^{k-1}(t) \\
= & \int_0^t (\frac{1}{2}\tilde{B}^{k^T} S_B^T \tilde{B}^k - \tilde{B}^{k-1^T} S_B^T \tilde{B}^{k-1})dv \\
= & -\int_0^t (\delta\tilde{B}^{k^T} S_B^T \tilde{B}^k + \frac{1}{2}\delta\tilde{B}^{k^T} S_B^T \delta\tilde{B}^k)dv \\
\leq & -\int_0^t \delta\tilde{B}^{k^T} S_B^T \tilde{B}^k dv = \int_0^t \bar{z}^{k^T} L^k \tilde{B}^k dv. \qquad (3.22)
\end{aligned}$$

According to (3.13), (3.15), (3.21), and (3.22), we have the following result

$$\begin{aligned}
\Delta\Omega^k(t) &= \Omega^k(t) - \Omega^{k-1}(t) \\
&= (U^k(t) - U^{k-1}(t)) + (V^k(t) - V^{k-1}(t)) + (W^k(t) - W^{k-1}(t)) \\
&\leq -\int_0^t (\bar{z}^{k^T}(K\bar{z}^k + L^k\hat{B}^k + \tilde{\tau}_e^k))dv \\
&\quad -\int_0^t \bar{z}^{k^T}(E_M^k\ddot{q}_r^k + E_C^k\dot{q}_r^k + E_G^k)dv + \int_0^t \bar{z}^{k^T}L^k\tilde{B}^k dv \\
&\leq -\int_0^t \bar{z}^{k^T}K\bar{z}^k dv - \int_0^t (\bar{z}^{k^T}(L^kB - L^kB))dv \\
&= -\int_0^t \bar{z}^{k^T}K\bar{z}^k dv. \qquad (3.23)
\end{aligned}$$

In the above derivations, the following result is used

$$\begin{aligned}
& -\bar{z}^{k^T}(\tilde{\tau}_e^k + E_M^k\ddot{q}_r^k + E_C^k\dot{q}_r^k + E_G^k) \\
\leq\ & \|\bar{z}^k\|(\|\tilde{\tau}_e^k\| + \|E_M^k\ddot{q}_r^k\| + \|E_C^k\dot{q}_r^k\| + \|E_G^k\|) \\
\leq\ & \|\bar{z}^k\|(\|\tilde{\tau}_e^k\| + \|E_M^k\|\|\ddot{q}_r^k\| + \|E_C^k\|\|\dot{q}_r^k\| + \|E_G^k\|) \\
\leq\ & \|\bar{z}^k\|(b_f + b_M\|\ddot{q}_r^k\| + b_C\|\dot{q}_r^k\| + b_G) \\
=\ & \bar{z}^{k^T}\mathrm{sgn}(\bar{z}^k)(b_f + b_M\|\ddot{q}_r^k\| + b_C\|\dot{q}_r^k\| + b_G) \\
=\ & \bar{z}^{k^T}L^kB^T. \qquad (3.24)
\end{aligned}$$

Assuming that Ω^0 is bounded for all $t \in [0, t_f]$, (3.23) indicates that the monotonically decreasing nonnegative sequence Ω^k converges to a nonnegative fixed value, thus we have $\Delta\Omega^k \to 0$ as $k \to \infty$.

Considering that

$$\Delta\Omega^k \leq -\bar{z}^{k^T}K\bar{z}^k \leq 0, \qquad (3.25)$$

we obtain

$$\lim_{k\to\infty} \bar{z}^k = 0. \tag{3.26}$$

Considering the definition of $\bar{z}$ in (2.23), we obtain

$$\lim_{k\to\infty} z^k = \lim_{k\to\infty} \tilde{\tau}_l^k. \tag{3.27}$$

It follows from (2.11), (2.16), and the above equation that

$$\lim_{k\to\infty} w^k(t) = \lim_{k\to\infty} \tilde{\tau}_e^k(t), \tag{3.28}$$

which immediately leads to

$$\| \lim_{k\to\infty} w^k(t)\| \leq b_f. \tag{3.29}$$

It completes the proof. □

Remark 16. *As discussed in the previous chapter, Property 3 is considered in most adaptive/learning methods, and the regressor $Y(\ddot{q}, \dot{q}, q)$ is used in the control design. However, the usage of the regressor indicates a requirement that the robot structure is known as a priori knowledge. The computation of the regressor is quite tedious especially when the robot arm has a high DOF. In this regard, it is interesting to look for a method without using the regressor. In the second method developed in the previous chapter, this problem has been investigated by employing Property 4. It has indicated the boundedness of the robot dynamics and the learning mechanism was developed to "learn" unknown bounds k_M, k_C, and k_G. It has also been shown that if the bounds k_M, k_C, and k_G are known, the learning process can be further*

avoided by employing the high-gain scheme. In the proposed methods in the previous chapter, the high-gain feedback is required and the chattering exists when the defined impedance error becomes very small. This is due to the employment of the boundedness property and the use of sign function. Even if the sign function can be replaced by a smooth threshold function, the high-gain feedback is still needed. By employing NN, the unknown robot dynamics instead of the unknown bounds are estimated in this chapter, and thus the usage of the sign function and high-gain feedback is avoided in the computed torque component.

Remark 17. *Although NN are employed in the control design discussed in this section, it can be replaced by other linearly parameterized function approximators such as fuzzy systems [95], polynomials, splines, etc.*

3.3 Simulation Studies

As in the previous chapter, we conduct the simulation using the Robotics Toolbox introduced in [90]. A two-DOF robot arm with two revolute joints moves in the $X-Y$ plane, as shown in Fig. 2.1. The robot arm repeats its motion to track the desired trajectory in each iteration, and is repositioned to its initial position at the beginning of each iteration. We set $m_1 = m_2 = 1.0$kg, $l_1 = l_2 = 0.2$m, $i_1 = i_2 = 0.01$kgm^2, and $l_{c1} = l_{c2} = 0.1$m. The initial position of the robot arm at the kth iteration is $q^k(0) = [-\frac{\pi}{3}, \frac{2\pi}{3}]^T$.

The desired trajectory of the robot arm in the Cartesian space is specified by

$$x_d(t) = 0.2 + 0.1(6t^5 - 15t^4 + 10t^3),\ y_d(t) = 0, \tag{3.30}$$

where $t \in [0, t_f]$ and $t_f = 1$s.

The desired impedance model is specified by (2.8) with

$$M_d = 0.1I_2,\ C_d = 8I_2,\ G_d = 8I_2. \tag{3.31}$$

Consider the control input (3.7) with each component (3.8), (3.9), and (2.22), and the updating law (3.10). In (3.8), we choose $\mu_{Ml} = 0.1$, $\mu_{Cl} = 0.1$, $\mu_{Gl} = 0.1$, $\delta_M = 1$, $\delta_C = 1$, and $\delta_G = 1$, for $l = 1, 2, \ldots, 10$. In (2.22), we choose $K = I_2$. In (3.10), we choose $S_M = 0.33I_2$, $S_C = 0.25I_2$, $S_G = 0.33I_2$, and $S_B = 0.67I_2$ to obtain $\hat{\Theta}_M^k$, $\hat{\Theta}_C^k$, $\hat{\Theta}_G^k$, and $\hat{B}^k$. Similarly as the method in the previous chapter, no dynamics information is needed so the control design is straightforward and simple. While the above parameters do not guarantee the best control performance, it is feasible to change them with other values.

In the first case of this simulation, the robot arm is considered to be contact-free, which indicates that there is no external force exerted by the environment. The defined impedance error in the joint space and positions in X and Y directions are shown in Figs. 3.1, 3.3, and 3.5, which illustrate the results at $k = 1$, $k = 10$, and $k = 30$ respectively. It is easy to find that the impedance error becomes smaller as the iteration number increases. At $k = 30$, the impedance errors at two directions almost go to zero, as shown in Fig. 3.5, which indicates that the dynamics of the robot arm are governed by the desired impedance model. As there is no external force from the environment, the actual position converges to the desired trajectory, which can be found in the last two sub-figures of Figs. 3.1, 3.3, and 3.5. The estimated parameters at $k = 1$, $k = 10$, and $k = 30$ are shown in Figs. 3.2, 3.4, and 3.6, respectively. Note that these estimated parameters do not necessarily converge to their true values but

their boundedness is guaranteed. To show the convergence of the learning process more clearly, the norms of the estimated parameters with respect to iterations are shown in Fig. 3.7. While the norms almost converge to certain values at $k = 30$, the learning process still continues. Theoretically, the learning process will not stop till $k \to \infty$. However, in the practical implementations, the learning process can be manually stopped when the impedance error falls into a pre-defined small set.

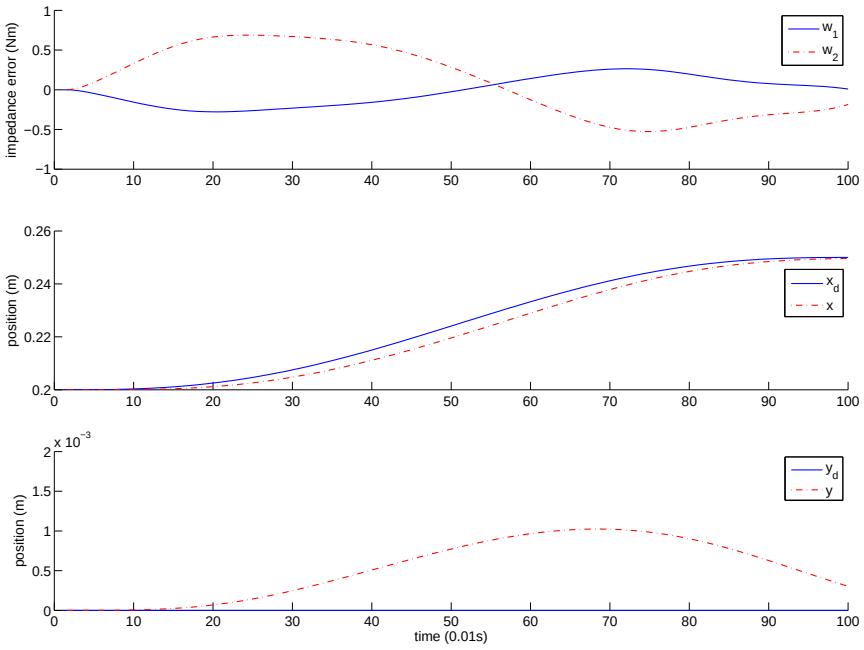

Fig. 3.1: The first case: impedance error, actual trajectory, and desired trajectory at k=1

In the second case, it is considered that there is an external force $\tau_e = 0.02$Nm, and the force measurement noise is a uniform-random-number signal with amplitude of 0.01. The defined impedance error and positions in X and Y directions at $k = 1$, $k = 10$, and $k = 30$ are shown in Figs. 3.8, 3.9, and 3.10, respectively. It is found that the positions in X and Y directions drift away from the desired trajectories due to the effect of the external force, which is different from that in the first case.

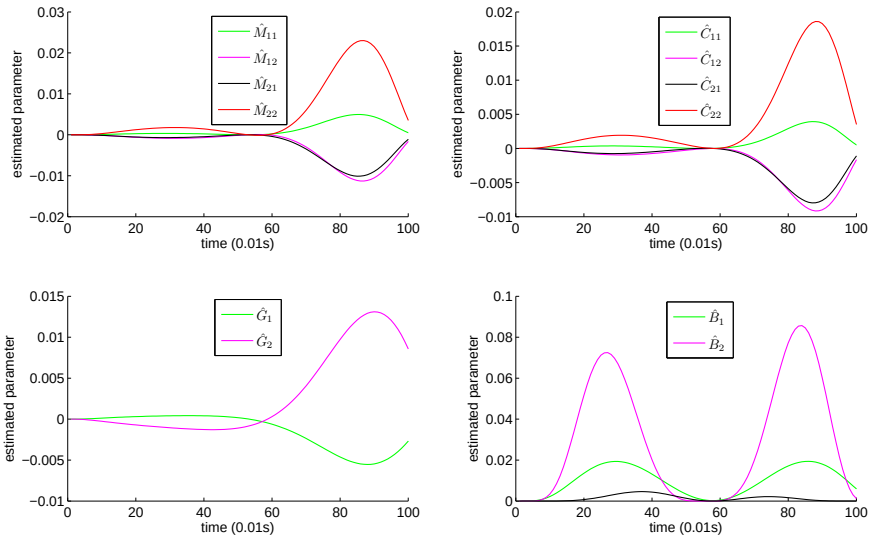

Fig. 3.2: The first case: estimated parameters at k=1

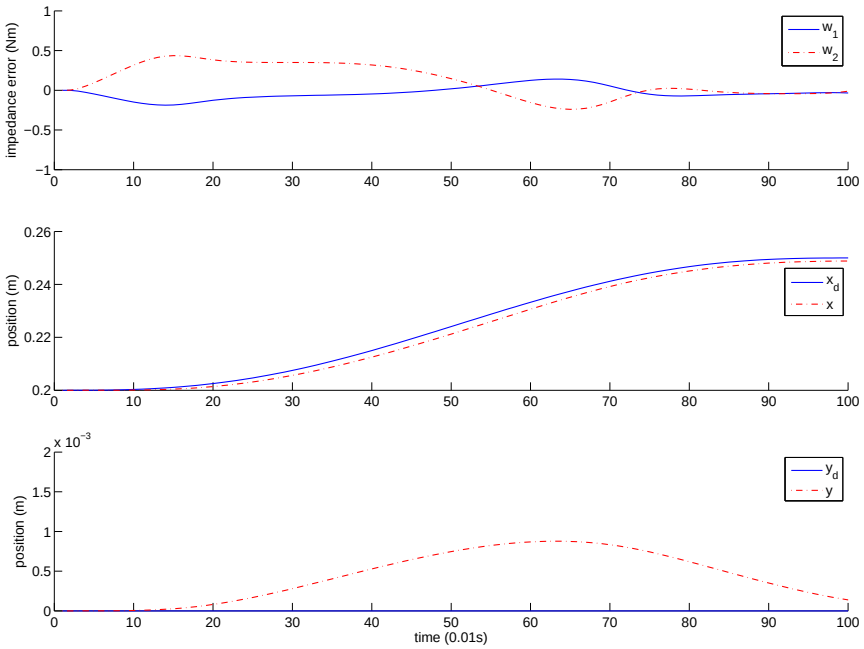

Fig. 3.3: The first case: impedance error, actual trajectory, and desired trajectory at k=10

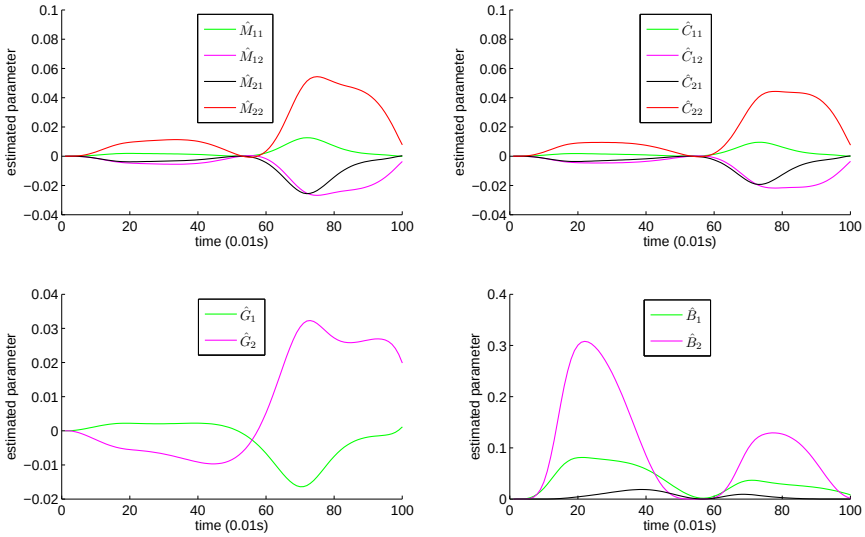

Fig. 3.4: The first case: estimated parameters at k=10

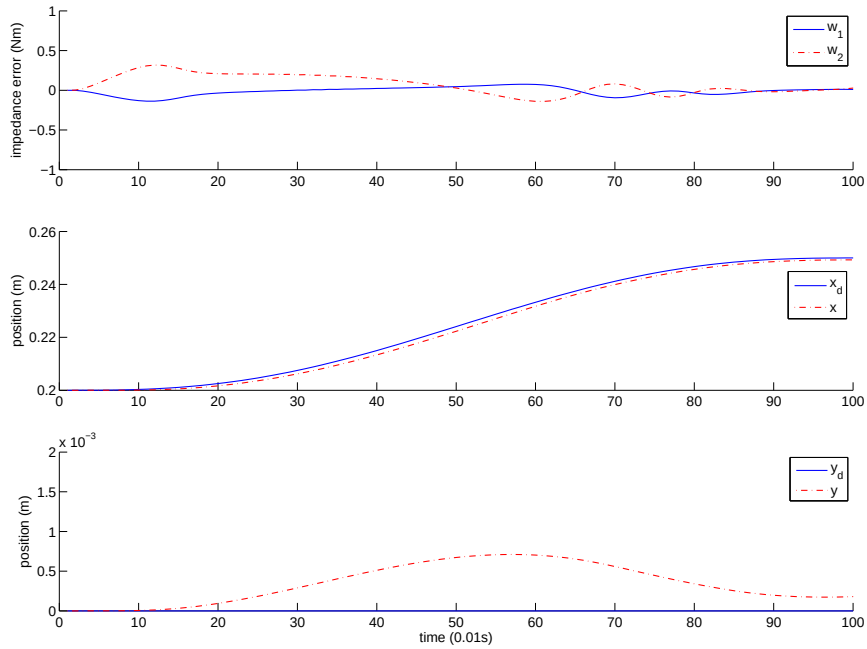

Fig. 3.5: The first case: impedance error, actual trajectory, and desired trajectory at k=30

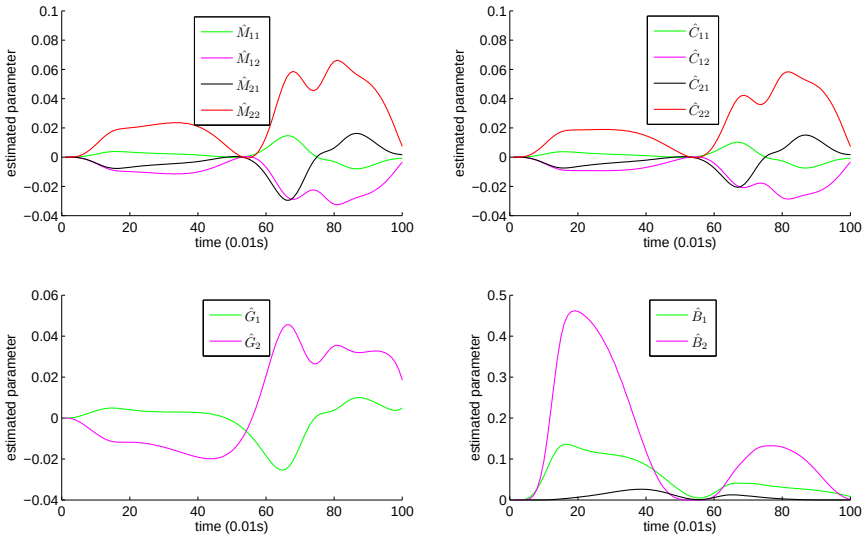

Fig. 3.6: The first case: estimated parameters at k=30

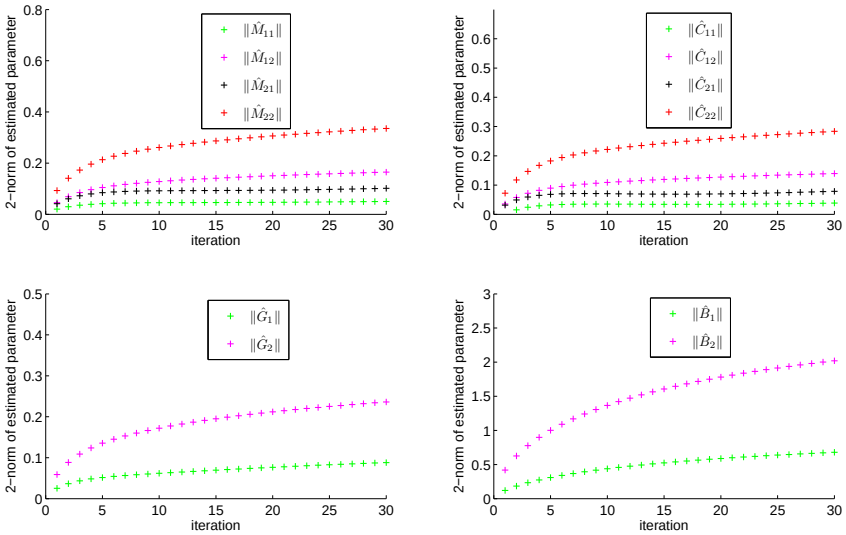

Fig. 3.7: The first case: norms of estimated parameters with respect to iterations

Nevertheless, as the iteration number increases, the impedance error becomes smaller and converges to zero as the iteration number becomes very large. This is similar to that in the first case and indicates that the proposed method guarantees the robot dynamics governed by the desired impedance model in both contact-free and contact cases. The results of estimated parameters are similar to that in the first case and are thus omitted.

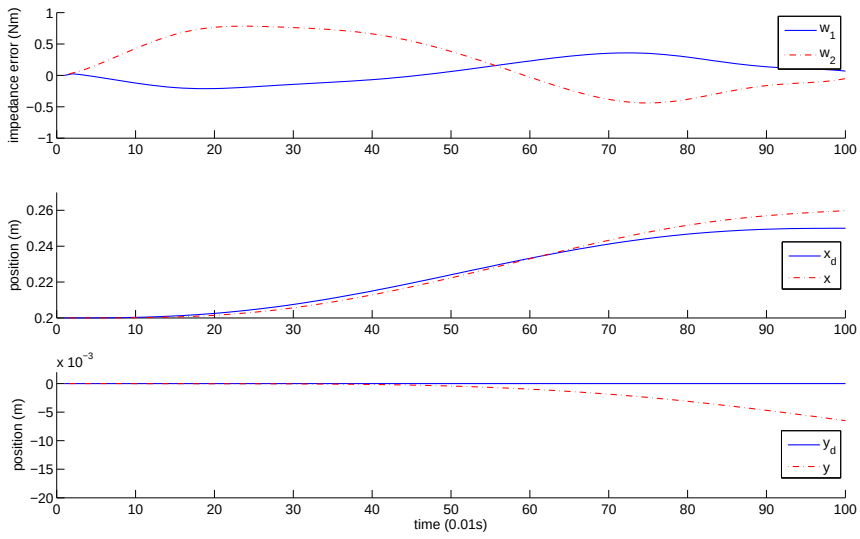

Fig. 3.8: The second case: impedance error, actual trajectory, and desired trajectory at k=1

Furthermore, the above results may be achieved by learning control in the previous chapter which is based on a property that the robot dynamics are bounded and the high-gain feedback is required in the computed torque component. In Figs. 3.11 and 3.12, the results with learning control in the previous chapter in two cases of contact-free and contact are shown, respectively. The learning rate of the method in the previous chapter is $S_0 = 0.04I_2$ and other parameters are the same as in above simulation studies. Compared to that in Figs. 3.5 and 3.10, similar results of impedance error and trajectory tracking are found in Figs. 3.11 and 3.12 but there

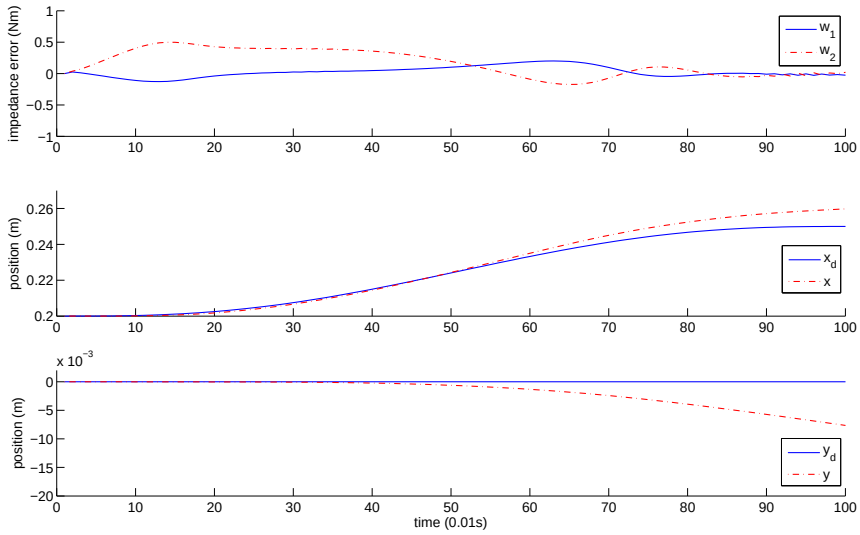

Fig. 3.9: The second case: impedance error, actual trajectory, and desired trajectory at k=10

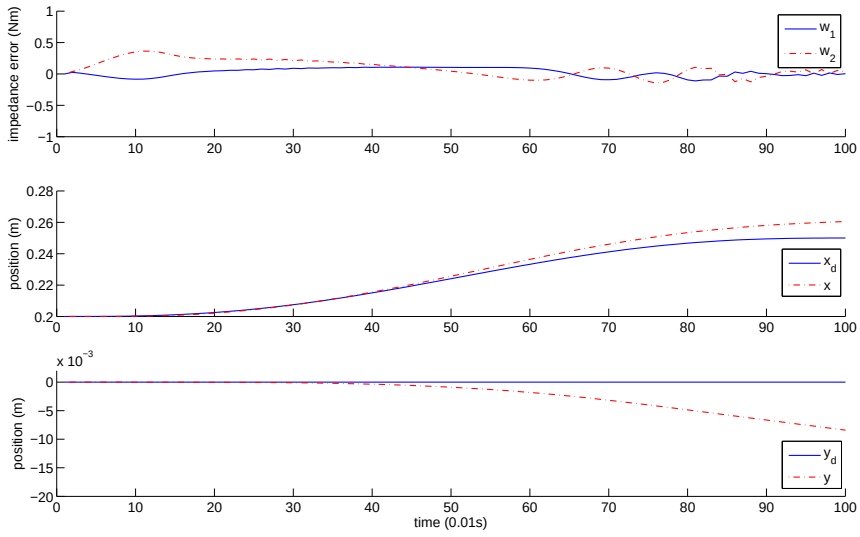

Fig. 3.10: The second case: impedance error, actual trajectory, and desired trajectory at k=30

exists an obvious chattering phenomenon in both figures. In this regard, NN based method proposed in this chapter is preferred.

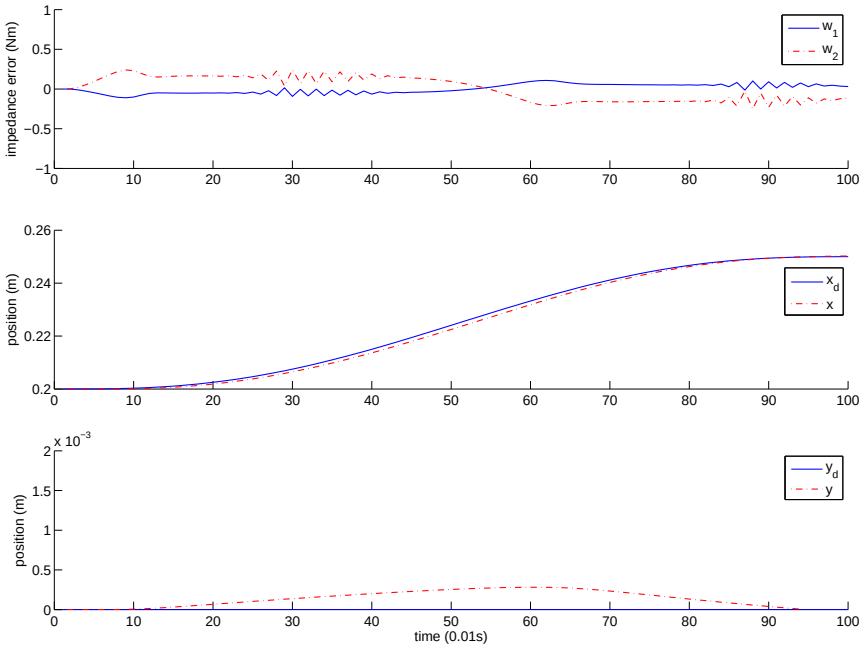

Fig. 3.11: The first case: impedance error, actual trajectory, and desired trajectory at k=30 with the method in the previous chapter

3.4 Conclusion

In this chapter, learning control has been further developed to make the robot dynamics follow a given target impedance model. By adopting the NN, neither the LIP property nor the boundedness property was needed. The control performance has been discussed through rigorous proof and remarking arguments. The simulation results have shown the validity of the proposed method and superiority over the existing methods.

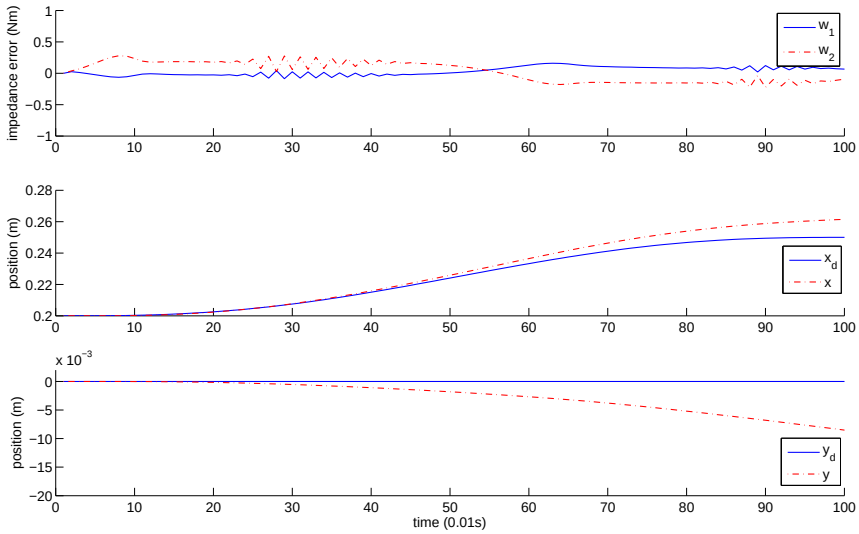

Fig. 3.12: The second case: impedance error, actual trajectory, and desired trajectory at k=30 with the method in the previous chapter

In Part I, we have achieved impedance control design, i.e., the robot dynamics can be controlled to follow a given impedance model. However, how to find a desired impedance model in the case of unknown and dynamically changing environment is yet to be answered. This will be investigated in Part II of this thesis.

Part II

Impedance Learning and Trajectory Adaptation

Chapter 4

Impedance Learning

In this chapter, impedance learning is investigated to obtain the desired impedance parameters subject to unknown environments. The gradient-following and betterment schemes are employed, and the robot with the resulted learning law is able to adjust the stiffness and damping matrices simultaneously. This learning law has a straightforward formulation and is feasible for a general class of applications. Simulation and experiment with different control objectives are carried out to show the feasibility of the proposed method.

The rest of this chapter is organized as follows. In Section 4.1, the problem of a robot interacting with unknown environments is formulated. In Section 4.2, the details of the proposed learning law are presented. In Sections 4.3 and 4.4, simulation and experiment with different control objectives are conducted to verify the feasibility of the proposed method. Concluding remarks are given in Section 4.5.

4.1 Problem Statement

4.1.1 Problem Formulation

As discussed in Part I, impedance control is employed for the robot interacting with environments. To be specific, the robot dynamics (2.4) are governed by a target impedance model as below

$$M_x(\ddot{x}_0 - \ddot{x}) + C_x(\dot{x}_0 - \dot{x}) + G_x(x_0 - x) = f, \tag{4.1}$$

where M_x, C_x, and G_x are the desired inertia, damping and stiffness matrices, respectively, and x_0 is the rest position in the Cartesian space. Note that the above impedance model is given in the Cartesian space instead of the joint space as in Part I, for the analysis convenience for tasks defined in the Cartesian space. The transformations between the joint space and Cartesian space require the forward and inverse kinematics as discussed in Remark 3.

In order to obtain M_x, C_x, and G_x to achieve the desired interaction performance, the environment dynamics have to be taken into consideration. However, previous studies have shown that it is extremely difficult to obtain an exact model of the environment (e.g., human limb) in many situations. In this regard, we aim to develop an iterative learning law, which is able to find M_x, C_x, and G_x during the repetitive interaction. When M_x, C_x, and G_x are obtained through learning, impedance control is employed to govern the dynamics of the robot arm to follow the obtained desired impedance model.

4.1.2 Preliminaries

For the development of the learning law in Section 4.2, we introduce the following lemma about the betterment scheme proposed in [96].

Lemma 2. *[96] Consider the following linear time-varying systems described by*

$$\begin{aligned} \dot{\xi}(t) &= A(t)\xi(t) + B(t)u(t), \\ o(t) &= C(t)\xi(t),\ \xi \in R^m,\ u, o \in R^r. \end{aligned} \tag{4.2}$$

The control input $u(t)$ is iteratively updated as

$$u^k(t) = u^{k-1}(t) + \alpha[\dot{o}_d(t) - \dot{o}^k(t)], \tag{4.3}$$

where k is the iteration number, $o_d(t)$ is the desired output, and α satisfies the following inequality

$$\|I - \alpha B(t)C(t)\|_\infty < 1 \tag{4.4}$$

with I as the unit matrix of a proper dimension.

If $C(t)B(t)$ is nonsingular and $o^k(0) = o_d(0)$, then the betterment process for system (4.2) is convergent in the sense that $o^k(t) \to o_d(t)$ uniformly in $t \in [0, t_f]$ as $k \to \infty$, where t_f is the iteration period.

For the trajectory tracking control of (2.4), we consider the PD-like control as in [85, 86]

$$\tau = K_P \mathrm{Sin}(e) + K_D\dot{e} + J^T(q)f, \tag{4.5}$$

where K_P and K_D are diagonal matrices with positive entries. $\mathrm{Sin}(e)$ is defined as

$$\mathrm{Sin}(e) = [\mathrm{Sin}(e_1), \mathrm{Sin}(e_2), \ldots, \mathrm{Sin}(e_n)]^T, \tag{4.6}$$

where $e_i,\ i = 1, 2, \ldots, n$ are the components of e, and $\mathrm{Sin}(e_i)$ is defined as

$$\mathrm{Sin}(e_i) = \begin{cases} 1, & e_i \geq \frac{\pi}{2}; \\ \sin(e_i), & |e_i| < \frac{\pi}{2}; \\ -1, & e_i \leq -\frac{\pi}{2}. \end{cases} \tag{4.7}$$

It has been proven that the residual robot dynamics with above PD-like control are passive [85, 86]. Equivalently, we have the following lemma.

Lemma 3. *[85, 86] Denoting an auxiliary variable*

$$y = -\dot{e} - \mu Sin(e) \tag{4.8}$$

with $\mu > 0$, we have the following inequality

$$\begin{aligned} &\{[M(q)\ddot{e} + C(q,\dot{q})\dot{e} - K_P Sin(e) - K_D\dot{e}] + [M(q) - M(q_d)]\ddot{q}_d \\ &+[C(q,\dot{q}) - C(q_d,\dot{q}_d)]\dot{q}_d + [G(q) - G(q_d)]\}^T y \geq V(e,\dot{e}) + \frac{d}{dt}(W(e,\dot{e})), \end{aligned} \tag{4.9}$$

where

$$\begin{aligned} W(e,\dot{e}) &= \frac{1}{2}\dot{e}^T M(q)\dot{e} + \sum_{i=1}^{n} p_i(1 - Cos(\dot{q}_i)) + \mu Sin^T(e)M(q)\dot{e}, \\ V(e,\dot{e}) &= \dot{e}^T\{K_D - c_1 I - \alpha[M(q) + (c_2 + c_3)I]\}\dot{e} \\ &\quad + Sin^T(e)(\mu K_P - c_4 I)Sin(e) \end{aligned} \tag{4.10}$$

with $p_i, i = 1, 2, \ldots, n$ *as the diagonal entries of* K_P, $q_i, i = 1, 2, \ldots, n$ *as the components of* q, $c_j, j = 1, 2, 3, 4$ *as some constants, and* $Cos(\dot{q}_i)$ *defined as*

$$Cos(\dot{q}_i) = \begin{cases} -\dot{q}_i + \frac{\pi}{2}, & \dot{q}_i \geq \frac{\pi}{2}; \\ cos(\dot{q}_i), & |\dot{q}_i| < \frac{\pi}{2}; \\ \dot{q}_i + \frac{\pi}{2}, & \dot{q}_i \leq -\frac{\pi}{2}. \end{cases} \tag{4.11}$$

$V(e, \dot{e})$ *and* $W(e, \dot{e})$ *are positive definite in* e *and* $\dot{e}$ *if* $\mu > 0$.

Remark 18. *The above lemma is essential in the sense that the passivity concept is introduced for the trajectory tracking control of robot arm. Several control methods based on this idea and further discussion may be found in [85, 86, 97, 98, 99].*

Lemma 4. *According to Property 4, the following inequality holds*

$$[-M(q_d)\ddot{q}_d - C(q_d, \dot{q}_d)\dot{q}_d - G(q_d) - K_s sgn(y)]^T y \leq 0, \tag{4.12}$$

where $K_s = diag(k_{s1}, k_{s2}, \ldots, k_{sn})$ *and* $\|K_s\| = k_M l_1 + k_C l_2^2 + k_G$, *with* l_1, l_2 *as the upper bounds of* $\|\ddot{q}_d\|, \|\dot{q}_d\|$, *respectively,* $sgn(y) = [sgn(y_1), sgn(y_2), \ldots, sgn(y_n))]^T$ *with* $y_1, y_2, \ldots, y_n$ *as the components of* y, *and* $sgn(\cdot)$ *denotes the sign function.*

Proof.

$$\begin{aligned} & [-M(q_d)\ddot{q}_d - C(q_d, \dot{q}_d)\dot{q}_d - G(q_d) - K_s \mathrm{sgn}(y)]^T y \\ \leq\ & [\|M(q_d)\ddot{q}_d\| + \|C(q_d, \dot{q}_d)\dot{q}_d\| + \|G(q_d)\|]\|y\| - \|K_s y\| \\ \leq\ & [\|M(q_d)\|\|\ddot{q}_d\| + \|C(q_d, \dot{q}_d)\|\|\dot{q}_d\| + \|G(q_d)\|]\|y\| - \|K_s y\| \\ \leq\ & (k_M\|\ddot{q}_d\| + k_C\|\dot{q}_d\|\|\dot{q}_d\| + k_G)\|y\| - \|K_s\|\|y\| \leq 0. \end{aligned} \tag{4.13}$$

□

4.2 Impedance Learning Design

This section is dedicated to present the details of the proposed impedance learning law. Because arbitrary selection of M_x may cause instability [47], it is fixed to equal to the apparent endpoint inertia and only C_x and G_x are updated.

First, a cost function to measure the interaction performance is denoted as $\Upsilon(t)$, which will be defined later. To gradually decrease this cost function by updating C_x and G_x, gradient-following scheme is employed and the following learning law is proposed

$$\begin{aligned} C_x^k(t) &= C_x^{k-1}(t) - \beta_C(\frac{\partial \Upsilon^k(t)}{\partial C_x^k(t)})^T = C_x^{k-1}(t) - \beta_C(\frac{\partial f^k(t)}{\partial C_x^k(t)})^T(\frac{\partial \Upsilon^k(t)}{\partial f^k(t)})^T, \\ G_x^k(t) &= G_x^{k-1}(t) - \beta_G(\frac{\partial \Upsilon^k(t)}{\partial G_x^k(t)})^T = G_x^{k-1}(t) - \beta_G(\frac{\partial f^k(t)}{\partial G_x^k(t)})^T(\frac{\partial \Upsilon^k(t)}{\partial f^k(t)})^T, \end{aligned} \quad (4.14)$$

where positive scalars β_C and β_G represent the learning rates. They can be chosen by considering the tradeoff between stability and learning rate, i.e., a large β_C/β_G will lead to a fast learning but the system may become unstable, while a small β_C/β_G will lead to a slow learning but the system stability is guaranteed.

According to (4.1), we have

$$\begin{aligned} \frac{\partial f^k(t)}{\partial C_x^k(t)} &= \dot{e}_x^{k^T}(t), \\ \frac{\partial f^k(t)}{\partial G_x^k(t)} &= e_x^{k^T}(t), \end{aligned} \quad (4.15)$$

where $e_x^k(t) = x_0(t) - x^k(t)$.

Because the environment dynamics are unknown, the gradient of reinforcement $\frac{\partial \Upsilon^k(t)}{\partial f^k(t)}$ is not available. To solve this problem, various estimation methods have been

proposed. In [59], $\frac{\partial \Upsilon^k(t)}{\partial f^k(t)}$ is estimated based on an internal model which is identified from the data collection of input $f^k(t)$ and output $\Upsilon^k(t)$. Suppose that the internal model is obtained as $\hat{\Upsilon}^k(t) = \rho^T f^k(t)$, then the gradient of reinforcement is estimated as $\frac{\partial \hat{\Upsilon}^k(t)}{\partial f^k(t)} = \rho^T$. In this section, however, we employ the betterment scheme as stated in Lemma 2. Under the betterment scheme, a time series of input signal to a plant is iteratively updated using an error signal between the output signal and the target signal such that the output signal at the next iteration approaches the target signal [55]. The details will be explained by investigating the environment dynamics.

Suppose that the environment dynamics are described by the following mass-damping-spring model [7]

$$M_E\ddot{x} + C_E\dot{x} + G_E(x - x_E) = f, \tag{4.16}$$

where x_E is the rest position of the environment, and M_E, C_E, and G_E are inertia, damping and stiffness matrices of the environment dynamics, respectively. Note that M_E, C_E, and G_E are unknown and they are only used for the analysis convenience.

Suppose that $x_E = 0$, then (4.16) is rewritten as

$$M_E\ddot{x} + C_E\dot{x} + G_E x = f. \tag{4.17}$$

Choosing states $x_1 = x$, $x_2 = \dot{x}$, and $x_3 = \int_0^t f(v)dv$, we rewrite (4.16) in the state-space form

$$\begin{bmatrix} \dot{x}_1 \\ \dot{x}_2 \\ \dot{x}_3 \end{bmatrix} = \begin{bmatrix} 0 & I_n & 0 \\ -M_E^{-1}G_E & -M_E^{-1}C_E & 0 \\ 0 & 0 & 0 \end{bmatrix} \begin{bmatrix} x_1 \\ x_2 \\ x_3 \end{bmatrix} + \begin{bmatrix} 0 \\ -M_E^{-1} \\ I_n \end{bmatrix} f. \tag{4.18}$$

In the above formulation, we assume that $f(0) = 0$ such that $\dot{x}_3(t) = f(t) - f(0) = f(t)$. By denoting

$$\xi = \begin{bmatrix} x_1 \\ x_2 \\ x_3 \end{bmatrix}, \; A = \begin{bmatrix} 0 & I_n & 0 \\ -M_E^{-1}G_E & -M_E^{-1}C_E & 0 \\ 0 & 0 & 0 \end{bmatrix}, \; B = \begin{bmatrix} 0 \\ -M_E^{-1} \\ I_n \end{bmatrix}, \tag{4.19}$$

we further write the above equation into a more compact form

$$\dot{\xi}(t) = A(t)\xi(t) + B(t)f(t). \tag{4.20}$$

To be coherent with the denotation in Lemma 2, we have

$$o(t) = C(t)\xi(t), \tag{4.21}$$

where $C(t)$ defines the relationship between the states (i.e., position, velocity, and integral of interaction force) and the output $o(t)$.

As indicated by Lemma 2, if we take the interaction force f as the "control input" to the environment dynamics (4.20), it will be updated as

$$f^k(t) = f^{k-1}(t) + \alpha'(\dot{o}_d(t) - \dot{o}^k(t)) = f^{k-1}(t) - \alpha'(\dot{o}(t) - \dot{o}_d(t)), \tag{4.22}$$

where α' satisfies the inequality (4.4), such that $o^k(t) \to o_d(t)$ as $k \to \infty$. In other words, the "control input" f is iteratively updated to decrease the error between $o^k(t)$ and $o_d(t)$. Approximately, we measure this error by the cost function $\Upsilon(t) =$

$\|o(t) - o_d(t)\|_2$ where $\|\cdot\|_2$ denotes 2-norm, and we have

$$f^k(t) = f^{k-1}(t) - \beta(\frac{\partial \Upsilon^k(t)}{\partial f^k(t)})^T. \tag{4.23}$$

Remark 19. *The definition of the cost function $\Upsilon(t)$ indicates that the aim of impedance learning in this chapter can be trajectory tracking, integral force tracking or the combination/compromise of these two, by choosing different $C(t)$. For example, if the control objective is integral force tracking, we may choose $C(t) = [0, 0, c]^T$, where c is a constant. Note that the defined cost function includes position, velocity and integral interaction force which are different quantities with different units of measurements. Therefore, in practical implementations, partial knowledge of both the robot and environment and trial and error may be needed to define a proper cost function. This is the same as in the well-known linear quadratic regulator [100], where a typical cost function includes position, velocity and control torque and it is nontrivial to determine their weights.*

Remark 20. *The cost function based method has been employed in most works of impedance learning in the literature, such as wall following [54], ball inserting [59], door opening and ball catching [58], and explosive movement tasks [101].*

Comparing (4.22) and (4.23), we obtain

$$\frac{\partial \Upsilon^k(t)}{\partial f^k(t)} = \alpha(\dot{o}(t) - \dot{o}_d(t))^T, \tag{4.24}$$

where it is noted that β has been absorbed by α as $\alpha = \frac{\alpha'}{\beta}$.

Substituting (4.15) and (4.24) to (4.14), we obtain the learning law

$$\begin{aligned} C_x^k(t) &= C_x^{k-1}(t) - \alpha\beta_C \dot{e}_x^k(t)(\dot{o}(t) - \dot{o}_d(t))^T, \\ G_x^k(t) &= G_x^{k-1}(t) - \alpha\beta_G e_x^k(t)(\dot{o}(t) - \dot{o}_d(t))^T. \end{aligned} \tag{4.25}$$

Remark 21. *It is found that the above learning law has a simple formulation, which is developed based on the sensory feedback from the environment instead of the environment model. The sensory feedback includes the position and velocity errors $e_x(t)$ and $\dot{e}_x(t)$, which are respectively used to update $G_x(t)$ and $C_x(t)$. It may also include the force error $e_f(t) = f_d(t) - f(t)$, which is introduced by the defined cost function $\Upsilon(t)$.*

After C_x and G_x are obtained through learning, we design impedance control to make the robot dynamics follow the desired impedance model. Instead of employing the impedance control design discussed in Chapters 2 and 3, we adopt the two-loop impedance control framework as shown in Fig. 4.1 in this chapter. In this framework, the virtual desired trajectory q_d is obtained according to $q_d = \int_0^t J^{-1}(q(v))\dot{x}(v)dv$, where x is obtained from (4.1). The following adaptive control is to make $\lim_{t\to\infty} q(t) = q_d(t)$.

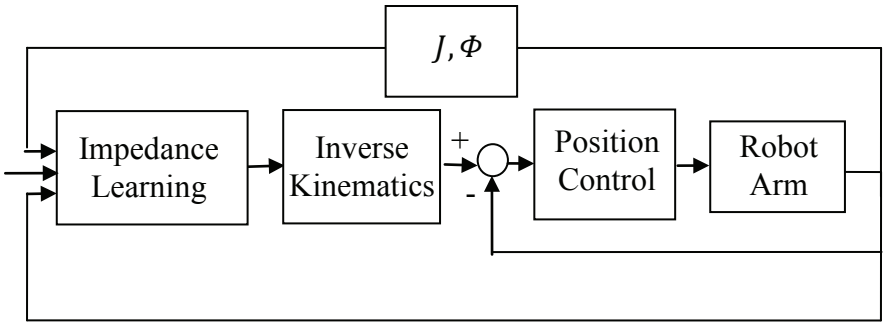

Fig. 4.1: Impedance learning and its implementation

The control input for the inner position control loop is proposed as

$$\tau = K_P \text{Sin}(e) + K_D \dot{e} - \hat{K}_s \text{sgn}(y) + J^T(q) f(t), \tag{4.26}$$

where $\hat{K}_s$ is a diagonal matrix with elements $\hat{k}_i,\ i = 1, 2, \ldots, n$. For the analysis convenience, we denote

$$k = [k_{s1}, k_{s2}, \ldots, k_{sn}]^T,\ \hat{k} = [\hat{k}_{s1}, \hat{k}_{s2}, \ldots, \hat{k}_{sn}]^T, \tag{4.27}$$

and thus $K_s = \text{diag}(k)$ and $\hat{K}_s = \text{diag}(\hat{k})$.

The updating law for $\hat{k}$ is developed as

$$\dot{\hat{k}} = S_1^{-1} \bar{y}, \tag{4.28}$$

where S_1 is a positive definite matrix and $\bar{y} = [y_1 \text{sgn}(y_1), y_2 \text{sgn}(y_2), \ldots, y_n \text{sgn}(y_n)]^T$. Note that after $\hat{k}$ is obtained from (4.28), $\hat{K}_s$ in (4.26) is obtained as $\hat{K}_s = \text{diag}(\hat{k})$.

Considering (2.4) and the control input (4.26), the closed-loop system dynamics are given by

$$M(q)\ddot{q} + C(q, \dot{q})\dot{q} + G(q) - K_P \text{Sin}(e) - K_D \dot{e} + \hat{K}_s \text{sgn}(y) = 0. \tag{4.29}$$

Theorem 5. *Given the dynamics (2.4), with the developed control (4.26) and updating law (4.28), trajectory tracking of the robot arm is achieved, i.e.,*

$$\lim_{t \to \infty} e(t) = 0. \tag{4.30}$$

Besides, all the signals in the closed-loop system (4.29) are bounded.

Proof. Rewrite the closed-loop dynamics (4.29) as

$$\begin{aligned}
& M(q)\ddot{q} + C(q,\dot{q})\dot{q} + G(q) - K_p\mathrm{Sin}(e) - K_d\dot{e} + \hat{K}_s\mathrm{sgn}(y) \\
= \; & [M(q)\ddot{e} + C(q,\dot{q})\dot{e} - K_p\mathrm{Sin}(e) - K_d\dot{e}] + [M(q)\ddot{q}_d + C(q,\dot{q})\dot{q}_d + G(q)] \\
& + \hat{K}_s\mathrm{sgn}(y) \\
= \; & [M(q)\ddot{e} + C(q,\dot{q})\dot{e} - K_p\mathrm{Sin}(e) - K_d\dot{e}] + \{[M(q) - M(q_d)]\ddot{q}_d \\
& + [C(q,\dot{q}) - C(q_d,\dot{q}_d)]\dot{q}_d + [G(q) - G(q_d)]\} + [M(q_d)\ddot{q}_d + C(q_d,\dot{q}_d)\dot{q}_d + G(q_d)] \\
& + \hat{K}_s\mathrm{sgn}(y) \\
= \; & [M(q)\ddot{e} + C(q,\dot{q})\dot{e} - K_p\mathrm{Sin}(e) - K_d\dot{e}] + \{[M(q) - M(q_d)]\ddot{q}_d \\
& + [C(q,\dot{q}) - C(q_d,\dot{q}_d)]\dot{q}_d + [G(q) - G(q_d)]\} + [M(q_d)\ddot{q}_d + C(q_d,\dot{q}_d)\dot{q}_d + G(q_d)] \\
& + [K_s\mathrm{sgn}(y) + \tilde{K}_s\mathrm{sgn}(y)] = 0, \qquad (4.31)
\end{aligned}$$

where $\tilde{K}_s = \hat{K}_s - K_s$. From the above equation, we obtain

$$\begin{aligned}
& M(q)\ddot{e} + C(q,\dot{q})\dot{e} - K_p\mathrm{Sin}(e) - K_d\dot{e} + \{[M(q) - M(q_d)]\ddot{q}_d \\
& + [C(q,\dot{q}) - C(q_d,\dot{q}_d)]\dot{q}_d + [G(q) - G(q_d)]\} + \tilde{K}_s\mathrm{sgn}(y) \\
= \; & -M(q_d)\ddot{q}_d - C(q_d,\dot{q}_d)\dot{q}_d - G(q_d) - K_s\mathrm{sgn}(y). \qquad (4.32)
\end{aligned}$$

According to Lemma 3, we have

$$\begin{aligned}
& \{[M(q)\ddot{e} + C(q,\dot{q})\dot{e} - K_p\mathrm{Sin}(e) - K_d\dot{e}] + [M(q) - M(q_d)]\ddot{q}_d \\
& + [C(q,\dot{q}) - C(q_d,\dot{q}_d)]\dot{q}_d + [G(q) - G(q_d)]\}^T y \geq V(e,\dot{e}) + \frac{d}{dt}[W(e,\dot{e})]. \qquad (4.33)
\end{aligned}$$

Besides, we have the following result according to the updating law (4.28)

$$\frac{d}{dt}(\frac{1}{2}\tilde{k}^T S\tilde{k}) = \tilde{k}^T S\dot{\tilde{k}} = \tilde{k}^T S\dot{\hat{k}} = \tilde{k}^T \bar{y} = \tilde{K}_s \text{sgn}(y) y^T. \tag{4.34}$$

Substituting the above equation into (4.33), we have

$$\begin{aligned} & \{[M(q)\ddot{e} + C(q,\dot{q})\dot{e} - K_p \text{Sin}(e) - K_d\dot{e}] + [M(q) - M(q_d)]\ddot{q}_d \\ & +[C(q,\dot{q}) - C(q_d,\dot{q}_d)]\dot{q}_d + [G(q) - G(q_d)]\}^T y + \tilde{K}_s y^T \text{sgn}(y) \\ \geq \; & V(e,\dot{e}) + \frac{d}{dt}[W(e,\dot{e}) + \frac{1}{2}\tilde{k}S\tilde{k}], \end{aligned} \tag{4.35}$$

which leads to

$$\begin{aligned} & [-M(q_d)\ddot{q}_d - C(q_d,\dot{q}_d)\dot{q}_d - G(q_d) - K_s \text{sgn}(y)]^T y \\ \geq \; & V(e,\dot{e}) + \frac{d}{dt}[W(e,\dot{e}) + \frac{1}{2}\tilde{k}S\tilde{k}]. \end{aligned} \tag{4.36}$$

According to Lemma 4, we obtain

$$V(e,\dot{e}) + \frac{d}{dt}[W(e,\dot{e}) + \frac{1}{2}\tilde{k}S\tilde{k}] \leq 0, \tag{4.37}$$

and thus

$$\frac{d}{dt}[W(e,\dot{e}) + \frac{1}{2}\tilde{k}S\tilde{k}] \leq -V(e,\dot{e}). \tag{4.38}$$

Taking the integral of both sides of the above equation, we have

$$\begin{aligned} & W(e(t),\dot{e}(t)) + \frac{1}{2}\tilde{k}(t)S\tilde{k}(t) - W(e(0),\dot{e}(0)) - \frac{1}{2}\tilde{k}(0)S\tilde{k}(0) \\ \leq \; & -\int_0^t V(e(v),\dot{e}(v))dv \leq 0. \end{aligned} \tag{4.39}$$

The above inequality indicates that $W(e(t),\dot{e}(t)) + \frac{1}{2}\tilde{k}(t)S\tilde{k}(t) \leq W(e(0),\dot{e}(0)) + \frac{1}{2}\tilde{k}(0)S\tilde{k}(0)$ and thus $W(e(t),\dot{e}(t)) + \frac{1}{2}\tilde{k}(t)S\tilde{k}(t)$ is bounded suppose $W(e(0),\dot{e}(0))$ and $\frac{1}{2}\tilde{k}(0)S\tilde{k}(0)$ are bounded. According to Lemma 3, $W(e(t),\dot{e}(t))$ is positive definite in $e(t)$ and $\dot{e}(t)$, thus $W(e(t),\dot{e}(t))$ and $\tilde{k}(t)S\tilde{k}(t)$ are bounded, and immediately we obtain $e(t) \in L_\infty$, $\dot{e}(t) \in L_\infty$, and $\tilde{k}(t) \in L_\infty$. Besides, it is found from the above inequality that $\int_0^t V(e(v),\dot{e}(v))dv$ is bounded, and thus we have $e(t) \in L_2$ as $V(e(t),\dot{e}(t))$ is positive definite in $e(t)$ and $\dot{e}(t)$. $\dot{e}(t) \in L_\infty$ and $e(t) \in L_2$ lead to

$$\lim_{t\to\infty} e(t) = 0, \tag{4.40}$$

which completes the proof. □

Remark 22. *Compared to the methods in [28, 84, 86], $\ddot{q}_d$ is not used in above adaptive control while the trajectory tracking is still guaranteed. This may help in some applications where $\ddot{q}_d$ is not available.*

4.3 Simulation Studies

In this section, we verify the validity of the proposed impedance learning and adaptive control through simulation studies. A 6-DOF PUMA560 robot is considered and this simulation is implemented with the robotics toolbox introduced in [90].

The initial position of the robot arm in the joint space is $q(0) = [0,0,0,0,0,0]^T$. The desired trajectory of the robot arm for each joint is given by $12(\frac{t}{t_f})^5 - 30(\frac{t}{t_f})^4 + 20(\frac{t}{t_f})^3$, where $t_f = 5$. The environment dynamics are described by (4.16) with $M_E = 0.01(\sin\pi t)^2 I$, $C_E = 0.1(\sin\pi t)^2 I$, and $G_E = 20(\sin\pi t)^2 I$, which are time-varying and unknown to the designer. To show the robustness of the proposed impedance learning,

the discontinuity of the environment dynamics has also been considered during the simulation. In particular, the interaction force is considered to suddenly drop to 0 at $t = 1$s, i.e., $M_E = 0$, $C_E = 0$, and $G_E = 0$ for $t > 1$s. The control parameters in (4.26) and (4.28) are $K_P = \text{diag}\,[1000, 100, 100, 10, 10, 10]$, $K_D = \text{diag}\,[50, 10, 10, 1, 1, 1]$, and $S_1 = \text{diag}\,[0.2, 0.02, 0.04, 0.2, 0.2, 0.2]$. M_d is fixed to equal to the apparent inertia and the initial values of C_d and G_d in the first iteration ($k = 0$) are $C_d^0(t) = 10I_6$ and $G_d^0(t) = 10I_6$. The parameters in (4.25) are $\alpha\beta_C = 20$ and $\alpha\beta_G = 20$, which can be adjusted to modulate the convergence rate of the learning process. As discussed in Section 4.2, the control objective can be trajectory tracking, integral force tracking and the combination/compromise of these two with the proposed impedance learning, by choosing different cost functions.

In the first case, we choose $C(t) = [50, 0, 1]^T$, $f_d = 0$, and thus the cost function is $\Upsilon(t) = \|50e_x(t) - \int_0^t e_f(v)dv\|_2$. The simulation results are shown in Figs. 4.2, 4.3, and 4.4. Note that tracking errors and interaction forces in Fig. 4.3 are the simulation results of Joint 1. The results of other joints are similar and thus not shown in this simulation. From Fig. 4.2, it is found that the cost function becomes smaller when the iteration number increases. This is followed by the result that the tracking error becomes smaller while the interaction force from 0s to 1s becomes larger when the iteration number increases, as shown in Fig. 4.3. Correspondingly, impedance parameters from 0s to 1s become larger when the iteration number increases, as shown in Fig. 4.4. Observing the impedance parameters of the environment dynamics with respect to time, the impedance parameters of the robot arm in Fig. 4.4 are updated correspondingly. For example, the peak of the interaction force appears at around 0.6s when the impedance parameters of the environment dynamics become the largest, and the impedance parameters of the robot arm also become the largest. Besides,

the interaction force is set to suddenly drop to 0 at $t = 1$s, and there is discontinuity at this point. As a result, an overshoot appears after $t = 1$s in Fig. 4.4. Nonetheless, the robot arm moves smoothly which can be observed by the tracking error in Fig. 4.3. The above results have indicated that the robot arm increases its impedance parameters iteratively to resist the interference from the environment, while it keeps its impedance parameters when there is no interference. These results are similar to that in [52] and in accord with the human motor control performance.

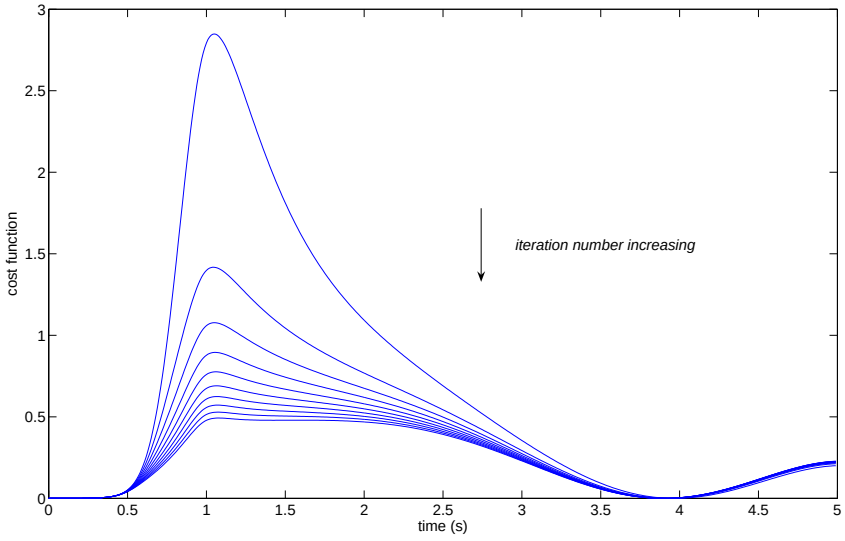

Fig. 4.2: Cost functions in the first case

In the first case, the weight of the tracking error in the cost function is 50 while the weight of the integral interaction force is 1, which indicates that trajectory tracking is more important than zero force tracking. Therefore, impedance parameters become larger such that the robot arm stiffen up to resist the interference from the environment. Subsequently, the tracking error becomes smaller and the interaction force becomes larger. In the second case, we change $C(t)$ to $C(t) = [3, 0, 1]^T$, and thus the cost function becomes $\Upsilon(t) = \|3e_x(t) - \int_0^t e_f(v)dv\|_2$. As the weight of the

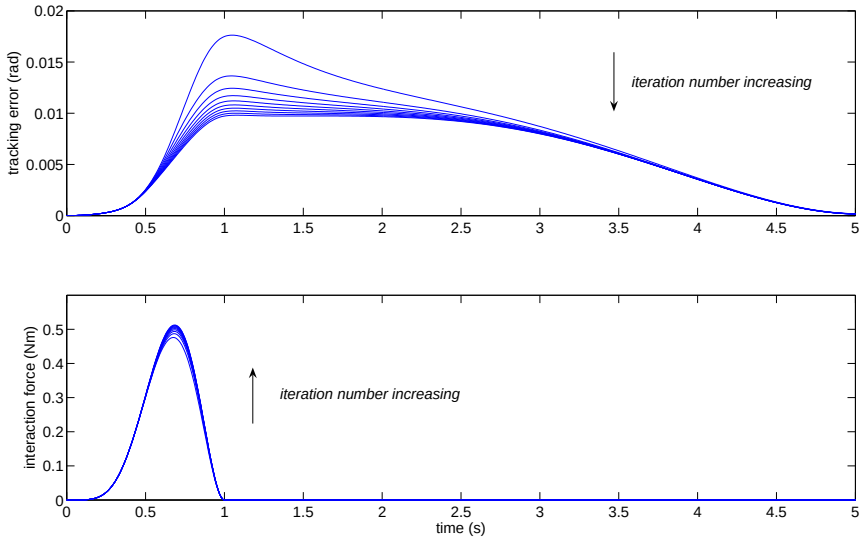

Fig. 4.3: Tracking errors and interaction forces in the first case

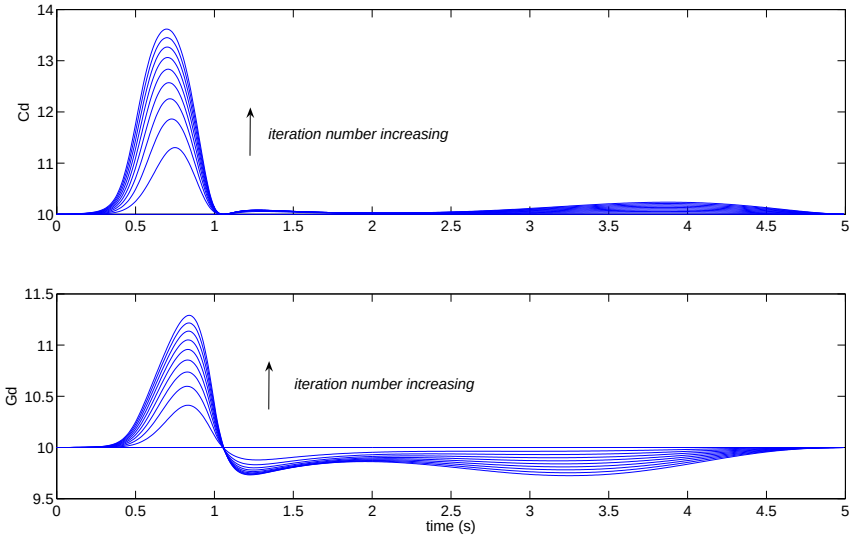

Fig. 4.4: Damping and stiffness parameters in the first case

tracking error in this case is smaller than that in the first case, it is expected that the robot arm becomes more compliant. The simulation results are shown in Figs. 4.5, 4.6, and 4.7. In particular, the impedance parameters shown in Fig. 4.7 indeed become smaller from 0s to 1s. Accordingly, in Fig. 4.6 it is shown that the interaction force becomes smaller while the tracking error becomes larger. In Fig. 4.5, the cost function still becomes smaller as the iteration number increases, although the performance is very different from that in Fig. 4.2. Similarly as in Fig. 4.4, there is also an overshoot in Fig. 4.7 due to the existence of discontinuity in the environment dynamics, but it does not have an obvious effect on the control performance of the robot arm.

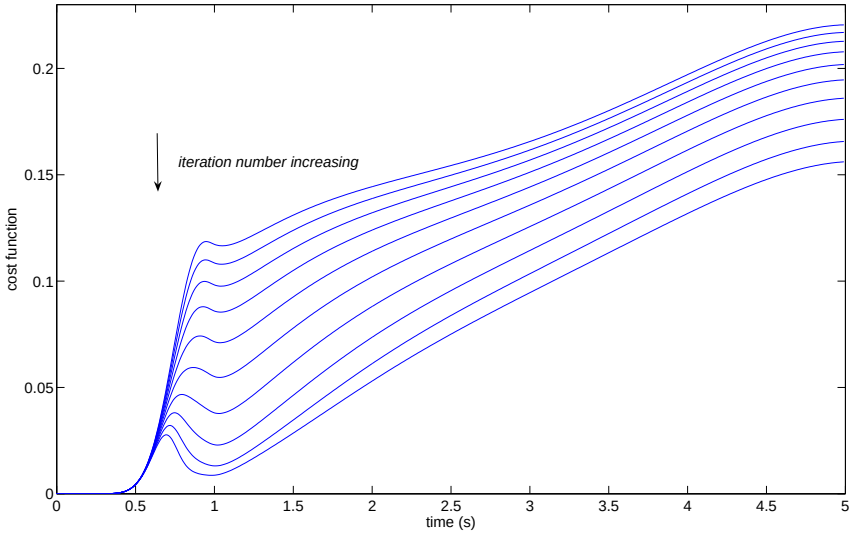

Fig. 4.5: Cost functions in the second case

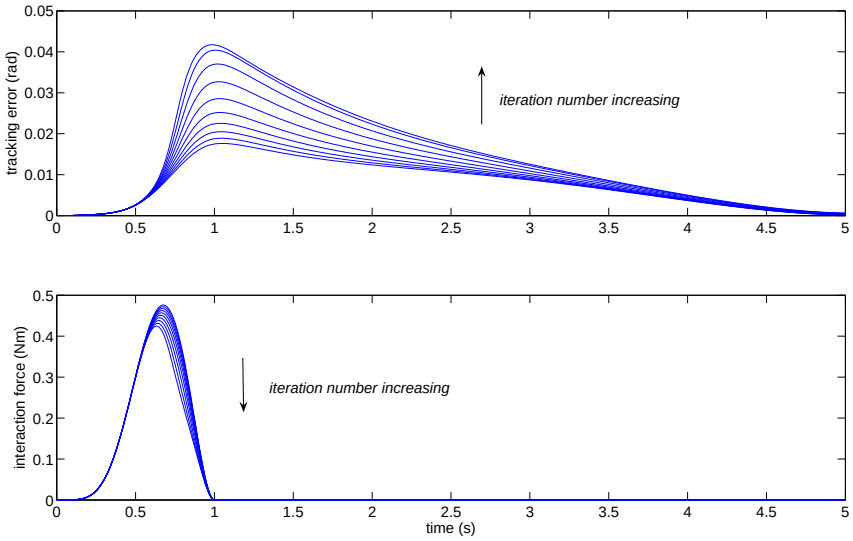

Fig. 4.6: Tracking errors and interaction forces in the second case

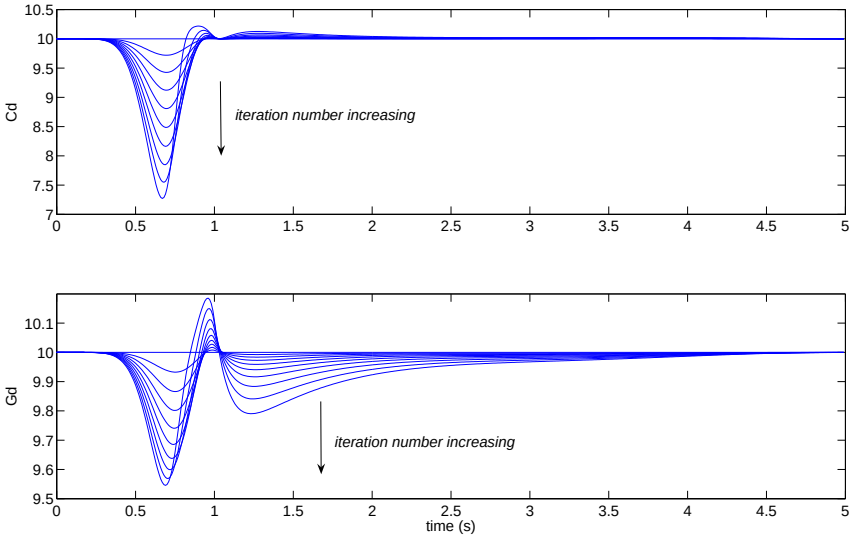

Fig. 4.7: Damping and stiffness parameters in the second case

4.4 Experiment

In this section, the proposed impedance learning is further examined on a real robot, Nancy, which is developed in Social Robotics Laboratory, National University of Singapore [102]. The motor which drives the joint is controlled by Maxon's EPOS2 70/10 dual loop controller. It works in the CANopen network and provides multiple operational modes including position, velocity, and current modes. An ATI mini-40 force/torque sensor is installed at the left wrist of Nancy to measure the force/torque exerted by environments.

In this experiment, the left wrist of Nancy follows a desired trajectory $q_d = 0.02t$ rad while it interacts with a human hand which plays the role of unknown environment, as shown in Fig. 4.8. In each iteration with a period of 18s, the interaction starts at $t = 5$s and ends at $t = 16$s. Similarly as in simulation studies, the interaction force drops to zero at $t = 16$s immediately, and thus there is discontinuity. Two cases with different control objectives are considered. In these two cases, M_d is fixed to equal to the apparent inertia and the initial values of C_d and G_d are $C_d^0(t) = 3.6$ and $G_d^0(t) = 3.6$. The parameters in (4.25) are $\alpha\beta_C = 40$ and $\alpha\beta_G = 40$. Other values of these parameters can be chosen to adjust the convergence rate of the learning process.

In the first case, we choose the cost function as $\Upsilon(t) = \|10e_x(t) - \int_0^t e_f(v)dv\|_2$ and then trajectory tracking is more important than zero force tracking. In Figs. 4.9 and 4.10, the results at $k = 0, 5, 10$ are shown. From Fig. 4.10, it is found that the tracking error becomes smaller when the iteration number increases. Correspondingly, the stiffness parameter G_d becomes larger and the defined cost function becomes smaller when the iteration number increases, as shown in Fig. 4.9. The result of the damping parameter C_d is similar to that of G_d, and is thus omitted. Similarly

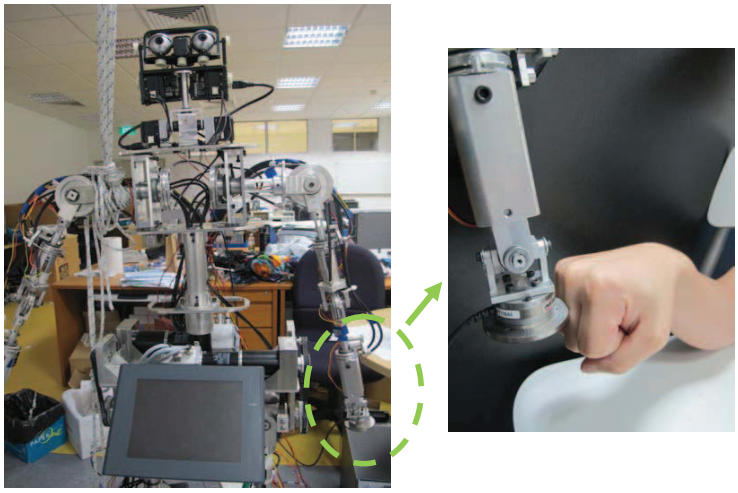

Fig. 4.8: Nancy and experiment scenario

as in simulation studies, the above results have revealed the expected interaction performance: impedance parameters become larger to make the robot arm stiffen up such that the interference from the environment is resisted, and they keep unchanged if there is no interference from the environment.

In the second case, we change the cost function to $\Upsilon(t) = \|e_x(t) - \int_0^t e_f(v)dv\|_2$, in which the weight of trajectory tracking is smaller and it is expected that the robot arm becomes more compliant. The results at $k = 0, 5, 10$ and in the second case are shown in Figs. 4.11 and 4.12. Different from that in Figs. 4.9 and 4.10, the tracking error becomes larger and correspondingly the stiffness parameter G_d becomes smaller when the iteration number increases. It is obvious that the robot arm becomes more compliant in this case. As the interaction force drops to zero immediately at $t = 6$s, there is an overshoot in the result of stiffness parameter in Fig. 4.11, but it does not have obvious effect on the motion of the robot arm. Besides, the force signal is typically noisy and the learning process is not as smooth as that in simulation studies. While the above results are acceptable, these practical issues need to be further considered for better interaction control.

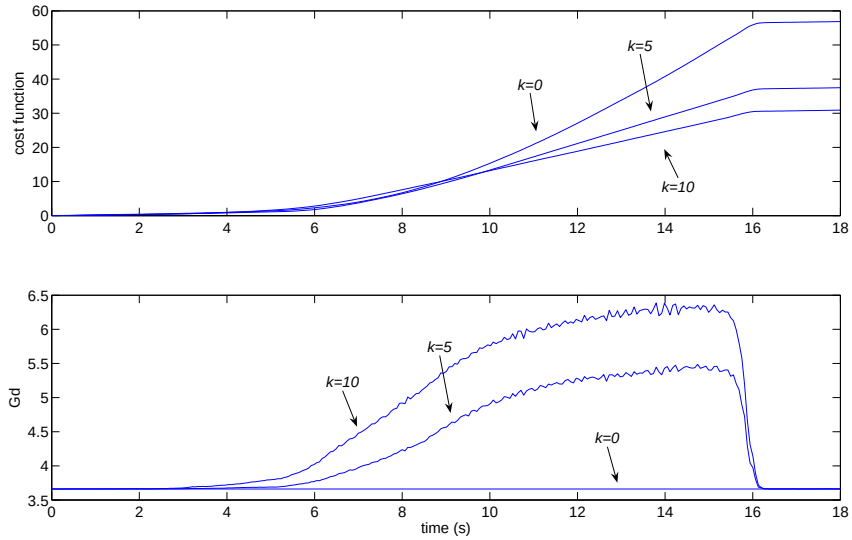

Fig. 4.9: Cost functions and stiffness parameters in the first case

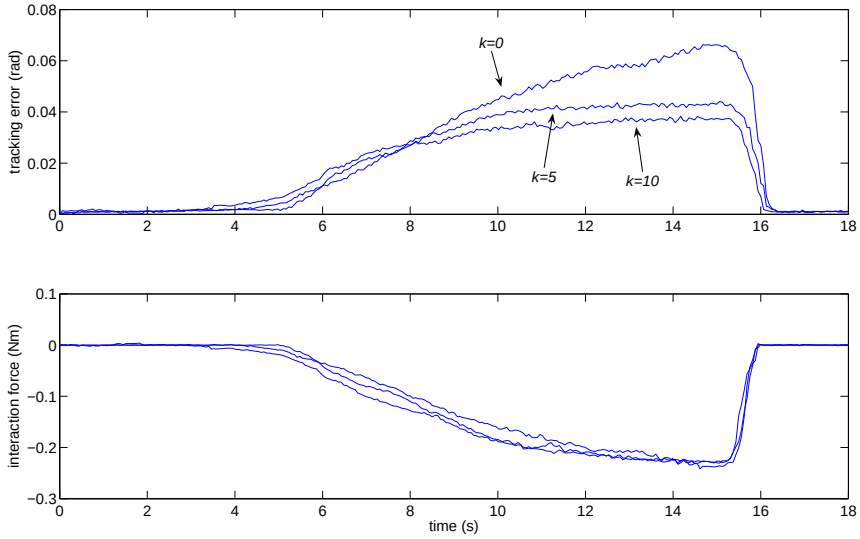

Fig. 4.10: Tracking errors and interaction forces in the first case

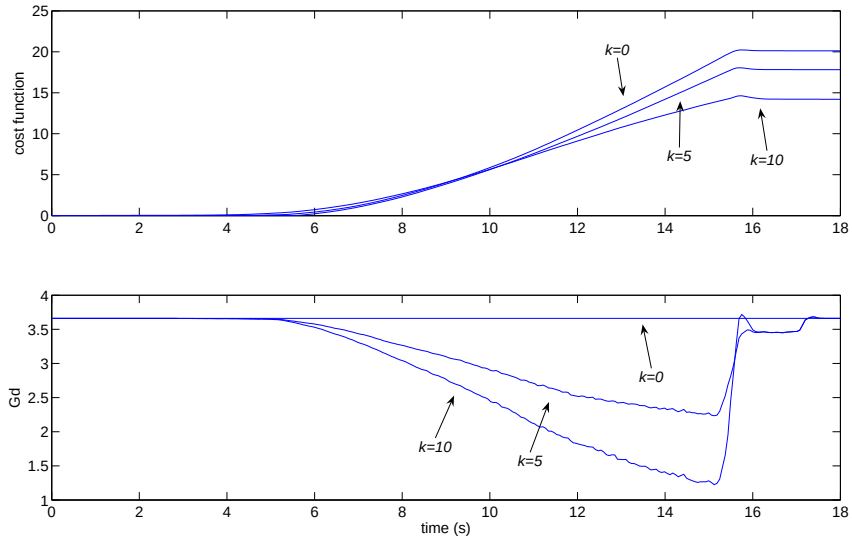

Fig. 4.11: Cost functions and stiffness parameters in the second case

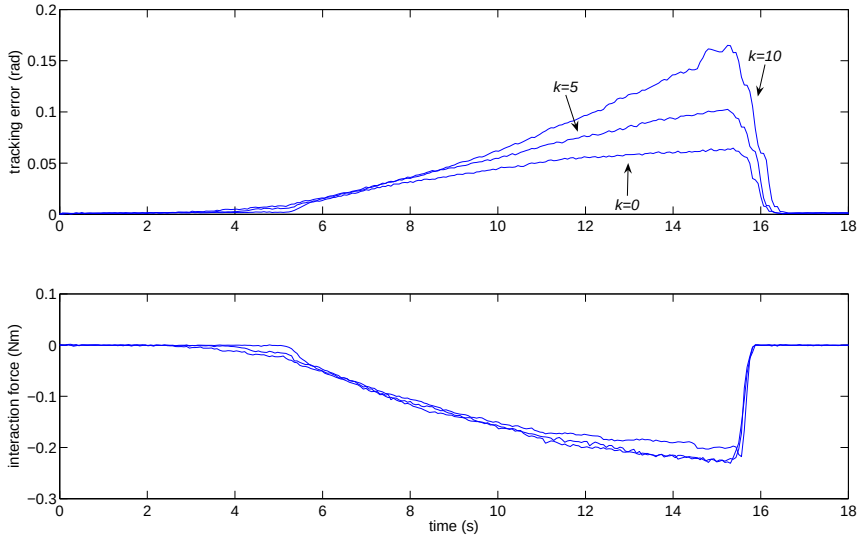

Fig. 4.12: Tracking errors and interaction forces in the second case

To summarize, by choosing different cost functions, it is determined that the control objective can be trajectory tracking, integral force tracking or the combination/compromise of these two. The proposed impedance learning guarantees that the defined cost function becomes smaller and subsequently the control objective is achieved, subject to unknown dynamic environments. The advantage of the proposed impedance learning over impedance control with fixed impedance parameters lies in: a modest performance can be obtained if a good set of fixed impedance parameters is predefined (when $k = 0$), and a better performance can be obtained only with variant impedance parameters because the environments are dynamically changing.

4.5 Conclusion

In this chapter, impedance learning for robots interacting with unknown environments has been investigated. Impedance learning has been developed to obtain desired impedance parameters subject to unknown dynamic environments. The proposed impedance learning has employed gradient-following and betterment schemes, which has a simple and straightforward formulation. Adaptive control without using the regressor has been developed for the trajectory tracking in the inner position control loop, and subsequently the control objective has been achieved. The feasibility and validity of the proposed method have been verified by simulation and experiment.

Chapter 5

Trajectory Adaptation: Intention Estimation

As the desired impedance parameters are obtained through impedance learning in the previous chapter, another question to be answered is how to determine the rest position in a desired impedance model. In the following two chapters, we consider a typical human-robot collaboration scenario and try to partially answer this question. In this scenario, the human partner stands for an unknown environment to the robot and he/she leads the robot along a trajectory that is unknown to the robot. The control objective is to make the robot "actively" follow the human partner and achieve the motion synchronization.

In this chapter, human motion intention is defined as the desired trajectory in the limb model of the human partner, which is extremely difficult to obtain considering the nonlinear and time-varying property of the limb model. NN are employed to cope with this problem, based on which an online estimation method is developed. The estimated motion intention is integrated into the developed adaptive impedance

control, which makes the robot follow a given target impedance model. Under the proposed method, the robot is able to actively collaborate with its human partner, which is verified through simulation and experiment studies.

The rest of this chapter is organized as follows. In Section 5.1, a specific human-robot collaboration system under study is described and the problem of unknown motion intention of the human partner is formulated. In Section 5.2, the proposed motion intention estimation method is introduced in details, and adaptive impedance control is developed. In Section 5.4, an intensive simulation study is used to verify the effectiveness of the proposed method. It is further examined through experiments in Section 5.5. Concluding remarks are given in Section 5.6.

5.1 Problem Statement

5.1.1 System Description

In this chapter, we investigate a typical human-robot collaboration system, which includes a human limb and a robot arm with a configurable end-effector and a force sensing handle, as shown in Fig. 5.1. The robot arm provides n DOF at the force sensing handle, which is mounted near the end-effector and measures the force exerted by the human partner to the robot arm. The end-effector is selected in order to flexibly pick and place objects with different sizes and shapes. According to the force exerted by the human partner and detected by the sensor mounted on the handle, the control system generates control input for each joint of the robot arm and drives the end-effector to the destination. In the whole system, human partner leads the task by simply applying force to the handle, and the robot arm carries the object load. The

critical problem to be discussed is how to estimate the motion intention of the human partner and make the robot achieve "active" following.

Assumption 3. *The object is tightly grasped by the robot arm and there is no relative motion between the object and the end-effector. Furthermore, the object is deemed as "a part" of the robot arm.*

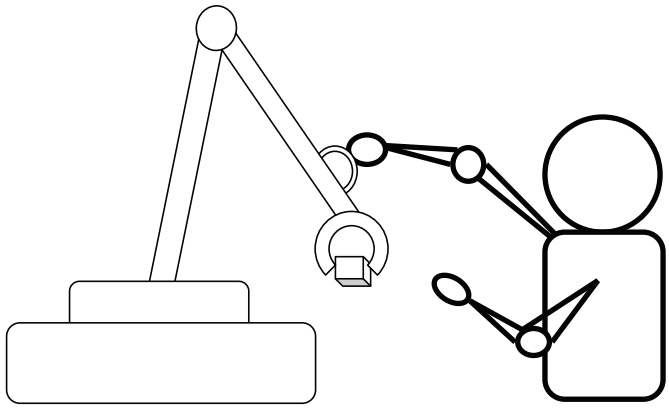

Fig. 5.1: Human-robot collaboration

Since the interaction is at the handle near the end-effector, we consider the robot dynamics in the Cartesian space, i.e., (2.6).

Property 5. *[83] Matrix $M_R(q)$ is symmetric and positive definite.*

Property 6. *[83] Matrix $2C_R(q,\dot{q}) - \dot{M}_R(q)$ is a skew-symmetric matrix if $C_R(q,\dot{q})$ is in the Christoffel form, i.e., $\xi^T(2C_R(q,\dot{q}) - \dot{M}_R(q))\xi = 0,\ \forall \xi \in \mathbb{R}^n$.*

Remark 23. *The above two properties are similar to Properties 1 and 2 as shown in Chapter 2. The only difference is that the former are in the Cartesian space and the latter are in the joint space.*

5.1.2 Problem Formulation

In a predefined task, the desired trajectory of the robot arm is prescribed and available for the control design. In the human-robot collaboration task under study in this chapter, the desired trajectory is determined by the human partner, which is unknown to the control design. In the literature, impedance control is employed such that the robot arm is controlled to be compliant to the force exerted by the human partner. Equivalently, the robot arm dynamics are governed by a target impedance model (4.1).

From the target impedance model in (4.1), we find that the actual position of the robot arm x will be refined according to the interaction force f. Seen from the perspective of the human partner, he will feel like moving an object with inertial/mass M_x, damping C_x, and stiffness G_x from the rest position x_0 to x, as shown in Fig. 5.2. In this regard, if x_0 is designed to be far away from x, the human partner need consume lots of energy to move the robot arm. Conversely, if the robot "knows" the motion intention of the human partner and changes x_0 accordingly, the human partner will consume much less energy to move the robot arm.

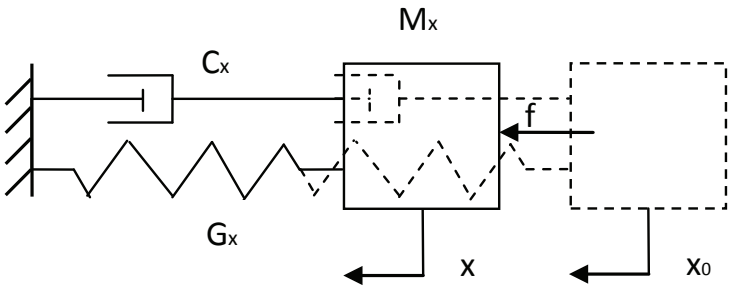

Fig. 5.2: Mass-damping-stiffness system

In many cases, x_0 can be designed based on the designer's prediction of the motion

intention of the human partner. For example, in the application of human-robot handshaking, although it is impossible to predict human's actual movement, it is still possible to design x_0 based on the basic understanding of the handshaking motion of the human partner. Nevertheless, this empirical method is obviously lack of flexibility and cannot guarantee a good performance. Therefore, in the first part of this chapter, we will propose a method to design x_0 based on the estimation of the motion intention of the human partner. Then, we will develop adaptive control to guarantee the robot dynamics (2.6) follow the target impedance model (4.1) subject to unknown robot dynamics.

5.2 Trajectory Adaptation

5.2.1 Human Limb Model

This section is dedicated to define the motion intention of the human partner by employing a human limb model. In [103], the equilibrium point control model is developed, which suggests that the CNS utilizes the spring-like property of the neuromuscular system in coordinating multi-DOF human limb movements and tends to drive the limb to equilibrium points. In the equilibrium point control model, only the spring-like property is taken into account. A more general model to describe human limb dynamics is supposed to consider its mass-damper-spring property, as in [45]

$$M_h\ddot{x} + C_h\dot{x} + K_h(x_h - x) = f, \tag{5.1}$$

where M_h, C_h, and K_h are the mass, damping, and stiffness matrices of the human limb model, respectively, and they are diagonal. x_h is the trajectory planned in the

human partner's CNS.

Note that when the human limb is motion-free, i.e., the interaction force $f = 0$, (5.1) leads to $x \to x_h$, considering that M_h, C_h, and K_h are positive definite. Thus, x_h is defined as the motion intention of the human partner in this thesis. As discussed and verified in [45], the damper and spring components usually dominate human limb model. Thus, we have the following model

$$C_h\dot{x} + K_h(x_h - x) + \delta(x, \dot{x}) = f, \tag{5.2}$$

where $\delta(x, \dot{x})$ is the uncertainty which may be resulted by the incomplete modeling, the time-varying property of C_h and K_h, and the external disturbances.

Based on the above human limb model (5.2), we assume that the motion intention x_h can be estimated by the interaction force f, actual position x, and velocity $\dot{x}$. Equivalently, we have the following assumption:

Assumption 4. *In a typical collaborative task, the motion intention of the human partner (in each direction), i.e., x_h in (5.2), is determined by the interaction force f, actual position x, and velocity $\dot{x}$ at the interaction point (in the corresponding direction) of the human limb and robot arm.*

Due to the existence of $\delta(x, \dot{x})$ in (5.2), it is improper to off-line estimate x_h from the collected data f, x, and $\dot{x}$. In the next section, we will utilize machine learning to develop an online estimation method.

5.2.2 Intention Estimation

For the analysis convenience, we consider the system dynamics in a single direction, i.e., M_x, C_x, G_x, x, x_0, f, C_h, K_h, and x_h are scalars.

Machine learning can discover intrinsic information, map unknown relationship, and approximate functions. As one of the popular machine learning methods, radial basis function neural networks (RBFNN) are employed in this chapter. In particular, the estimation of x_h is given by

$$\begin{aligned} \hat{x}_h(r) &= \sum_{i=1}^{p} \hat{w}_i s_i(r), \\ s_i(r) &= e^{\frac{-(r-\mu_i)^2}{\eta_i^2}}, \end{aligned} \tag{5.3}$$

where $r = [f^T, x^T, \dot{x}^T]^T$ is the input to RBFNN, p is the NN nodes number, μ_i is the center of the receptive field, η_i is the width of the Gaussian function, and $\hat{w}_i$ is an adjustable synaptic weight vector. Therefore, we have

$$x_h(t) = \hat{x}_h(t) + \varepsilon, \tag{5.4}$$

where ε is the estimation error, which is caused by both the NN approximation and the developed updating law. To determine the parameters in (5.3), the following rules of thumb can be considered [104]: a larger p normally results in the better approximation while it leads to a higher computational complexity, so usually p is chosen to be just large enough to meet the approximation requirement; the centers μ_i span evenly in the input space of r; and the widths η_i are chose as $\frac{d}{\sqrt{2}}$, where d is the distance between intermediate centers.

As $s_i(r)$ is available by collecting data r, we employ the back propagation algorithm [105] to obtain $\hat{w}_i$ in (5.3). According to the discussion in Section 5.1, the control objective is to make the robot "actively" move towards its human partner's intended position and thus the interaction force f as small as possible. Therefore, $\hat{w}_i$ is adjusted online in the direction of the steepest descent with respect to the cost function $E = \frac{1}{2}f^2$. Equivalently, we have

$$\begin{aligned} \dot{\hat{w}}_i(t) &= -\alpha_i' \frac{\partial E}{\partial \hat{w}_i} \\ &= -\alpha_i' \frac{\partial E}{\partial f} \frac{\partial f}{\partial x_h} \frac{\partial x_h}{\partial \hat{w}_i} \\ &= -\alpha_i' f \frac{\partial f}{\partial x_h} \frac{\partial x_h}{\partial \hat{w}_i}, \end{aligned} \tag{5.5}$$

where α_i' is a positive scalar. Theoretically, $\alpha_i' > 0$ will guarantee the convergence and a large α_i' will lead to a fast convergence. However, a large α_i' may also result in instability in practice. Therefore, a tradeoff between the convergence rate and stability has to be considered in implementations.

In the above equation, $\frac{\partial f_i}{\partial x_h}$ can be obtained according to (5.2) as follows

$$\frac{\partial f}{\partial x_h} = K_h, \tag{5.6}$$

and $\frac{\partial x_h}{\partial \hat{w}_i}$ can be obtained according to (5.4) as follows

$$\frac{\partial x_h}{\partial \hat{w}_i} = s_i(r). \tag{5.7}$$

Substituting (5.6) and (5.7) into (5.5) leads to

$$\dot{\hat{w}}_i(t) = -\alpha_i f s_i(r), \tag{5.8}$$

where $\alpha_i = \alpha_i' K_h$. As K_h is the parameter of human limb dynamics and unknown, it is absorbed by α_i which is set by the designer.

Then, we obtain the updating law of $\hat{w}_i$ as below

$$\hat{w}_i(t) = \hat{w}_i(0) - \alpha_i \int_0^t [f(v)s_i(r(v))]dv. \tag{5.9}$$

With the above equation, we obtain the estimated motion intention $\hat{x}_h$ according to (5.3).

Remark 24. *Note that $\hat{w}_i$ can be obtained online as in (5.9). This is a favorable property in the sense that the human partner may change his motion intention at any time.*

Remark 25. *In [72], the motion intention of the human partner is divided to two states: active and passive. It is assumed to be a stochastic process and thus can be estimated by the HMM. The robot is controlled in the following manner. If the motion intention of the human partner is passive, which indicates that the robot's current motion is coherent with the motion intention, then the robot is in an active state (stiff position control); if the motion intention is active, which indicates the human partner wants to lead the task or to change the motion, then the robot complies to the human limb motion (compliant control). Under this framework, the estimation of the motion intention is obtained based on the estimation of M_h, C_h, and K_h in (5.1). Different from that, the method proposed in this chapter is straightforward from the data collection to the intention estimation. And the estimated intention is a trajectory instead of two states.*

Remark 26. *In the practical implementation, the adaptation of $\hat{w}_i$ can be switched off to simplify the computation and improve the system robustness. The condition to*

switch the adaptation can be designed as: the adaptation is switched off if $f < \underline{f}$*, where* $\underline{f}$ *is a design parameter. This condition indicates that the adaptation is switched off when* x *is close to* x_h*.*

As the estimation error with NN is unavoidable and NN estimation usually falls into local minimum, $\hat{x}_h$ cannot be exactly the same as x_h. Therefore, it is improper to use position control to make the actual position x track the estimated motion intention $\hat{x}_h$. Instead of that, $\hat{x}_h$ can be used as the rest position in the target impedance model (4.1), such that the error between the actual position x and the estimated motion intention $\hat{x}_h$ can be accommodated partly by impedance control. This will be discussed in the following section. Nevertheless, it is important to note that this is different from the pure impedance control with a fixed rest position, where the error between the actual position and the motion intention is much larger and thus the human partner consumes much more energy to move the robot arm.

5.3 Adaptive Impedance Control

As $\hat{x}_h$ is obtained in the above section, we let $x_0 = \hat{x}_h$ and design adaptive impedance control to make the robot arm dynamics (2.6) track the given impedance model (4.1). The block diagram is shown in Fig. 5.3.

Remark 27. *Adaptive impedance control to be developed below follows the framework discussed in Chapters 2 and 3. The reason not to use learning impedance control developed in Chapters 2 and 3 lies in that the estimated motion intention can be integrated with adaptive impedance control but not learning impedance control which requires a learning process. Besides, it can be also shown that the framework discussed in Chapters 2 and 3 can be used for adaptive impedance control.*

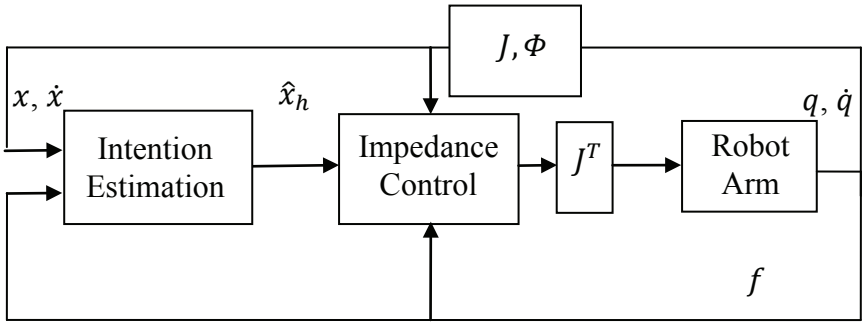

Fig. 5.3: Adaptive impedance control with estimated motion intention

Construct the error signal $w_x = M_x\ddot{e}_x + C_x\dot{e}_x + G_x e_x - f$ in the Cartesian space, where $e_x = x_0 - x$ as defined in Section 4.2. Then, similar augmented impedance error in the Cartesian space is

$$\bar{w}_x = K_{f,x} w_x = \ddot{e}_x + K_{d,x}\dot{e}_x + K_{p,x} e_x - K_{f,x} f, \tag{5.10}$$

where $K_{d,x} = M_x^{-1} C_x$, $K_{p,x} = M_x^{-1} G_x$, and $K_{f,x} = M_x^{-1}$. Choose two positive definite matrices Λ_x and Γ_x such that

$$\Lambda_x + \Gamma_x = K_{d,x},\ \dot{\Lambda}_x + \Gamma_x \Lambda_x = K_{p,x}. \tag{5.11}$$

Define the following variables in the Cartesian space similar to that in joint space

$$\dot{f}_l + \Gamma f_l = K_{f,x} f,\ z_x = \dot{e}_x + \Lambda e_x - f_l,\ \dot{x}_r = \dot{x}_0 - \Lambda e + f_l. \tag{5.12}$$

We propose the adaptive impedance control as below

$$u = -K_x z_x - \sum_{j=1}^{3} \frac{\hat{k}_j \varphi_j^2}{\varphi_j \|z_x\| + \sigma_j} z_x - f, \tag{5.13}$$

$$\dot{\hat{k}}_j = -a_j \hat{k}_j + \frac{b_j \varphi_j^2 \|z_x\|^2}{\varphi_j \|z_x\| + \sigma_j}, \tag{5.14}$$

where $j = 1, \ldots, 3$, $k_1 = k_M$, $k_2 = k_C$, $k_3 = k_G$, $\hat{k}_j$ is the estimate of k_j, and K_x is a positive definite matrix. $b_j > 0$, a_j and σ_j are time varying positive functions satisfying $\lim_{t\to\infty} a_j = 0$, $\int_0^t a_j(v)dv = c_j < \infty$, $\lim_{t\to\infty} \sigma_j = 0$, and $\int_0^t \sigma_j(v)dv = d_j < \infty$. $\varphi_1 = \|J^{-T}\|\|J^{-1}\|(\|\ddot{x}_r\| + \|J^{-1}\|\|\dot{J}\|\|\dot{x}_r\|)$, $\varphi_2 = \|J^{-T}\|\|J^{-1}\|\|\dot{q}\|\|\dot{x}_r\|$, and $\varphi_3 = \|J^{-T}\|$.

Considering (5.12), we rewrite (2.6) as

$$M_R \dot{z}_x + C_R z_x = u + f - (M_R \ddot{x}_r + C_R \dot{x}_r + G_R). \tag{5.15}$$

Substituting the control input (5.13) into the above equation, we have

$$\begin{aligned} & M_R \dot{z}_x + C_R z_x \\ & = -K_x z_x - \sum_{j=1}^{3} \frac{\hat{k}_j \varphi_j^2}{\varphi_j \|z_x\| + \sigma_j} z_x - (M_R \ddot{x}_r + C_R \dot{x}_r + G_R). \end{aligned} \tag{5.16}$$

Theorem 6. *Considering the robot dynamics described by (2.6), control (5.13) with the updating law (5.14) guarantees the following results:*

(i) the defined impedance error asymptotically converges to 0 *as* $t \to \infty$*, i.e.,* $\lim_{t\to\infty} z_x(t) = 0$*; and*

(ii) all the signals in the closed-loop are bounded.

Proof. Consider the following Lyapunov function candidate

$$V = \frac{1}{2} z_x^T M_R z_x + \sum_{j=1}^{4} \frac{1}{2b_i} \tilde{k}_j^2, \tag{5.17}$$

where $\tilde{k}_j = k_j - \hat{k}_j$.

The derivative of V with respect to time is

$$\dot{V} = \frac{1}{2} z_x^T \dot{M}_R z_x + z_x^T M_R \dot{z}_x + \sum_{j=1}^{4} \frac{1}{b_j} \tilde{k}_j \dot{\tilde{k}}_j. \tag{5.18}$$

Considering Property 2, we have

$$\dot{V} = z_x^T C_R z_x + z_x^T M_R \dot{z}_x + \sum_{j=1}^{4} \frac{1}{b_j} \tilde{k}_j \dot{\tilde{k}}_j. \tag{5.19}$$

According to the dynamics (5.16), we obtain

$$\begin{aligned} \dot{V} &= z_x^T (-K_x z_x - \sum_{j=1}^{4} \frac{\hat{k}_j \varphi_j^2}{\varphi_j \|z_x\| + \sigma_j} z_x \\ &\quad -(M_R \ddot{x}_r + C_R \dot{x}_r + G_R)) + \sum_{j=1}^{4} \frac{1}{b_j} \tilde{k}_j \dot{\tilde{k}}_j. \end{aligned} \tag{5.20}$$

According to (5.14), we have

$$\dot{\tilde{k}}_j = -\dot{\hat{k}}_j = a_j \hat{k}_j - \frac{b_j \varphi_j^2 \|z_x\|^2}{\varphi_j \|z_x\| + \sigma_j}. \tag{5.21}$$

Substituting the above equation to (5.20) leads to

$$\begin{aligned}\dot{V} &= z_x^T(-K_x z_x - \sum_{j=1}^{4} \frac{k_j \varphi_j^2}{\varphi_j \|z_x\| + \sigma_j} z_x \\ &\quad -(M_R \ddot{x}_r + C_R \dot{x}_r + G_R)) + \sum_{j=1}^{4} \frac{a_j}{b_j} \tilde{k}_j \hat{k}_j. \end{aligned} \tag{5.22}$$

Considering the definitions of φ_j, we have

$$\begin{aligned} & -z_x^T(M_R \ddot{x}_r + C_R \dot{x}_r + G_R) \\ \leq\ & \|z_x\|(\|M_R\|\|\ddot{x}_r\| + \|C_R\|\|\dot{x}_r\| + \|G_R\|) \\ =\ & \|z_x\|(\|J^{-T} M J^{-1}\|\|\ddot{x}_r\| \\ & +\|J^{-T}(C - MJ^{-1}\dot{J})J^{-1}\|\|\dot{x}_r\| + \|J^{-T} G\|) \\ \leq\ & \|z_x\|\|J^{-T}\|(\|M\|\|J^{-1}\|\|\ddot{x}_r\| \\ & +(\|C\| + \|M\|\|J^{-1}\|\|\dot{J}\|)\|J^{-1}\|\|\dot{x}_r\| + \|G\|) \\ \leq\ & \|z_x\|\|J^{-T}\|(k_M\|J^{-1}\|\|\ddot{x}_r\| \\ & +(k_C\|\dot{q}\| + k_M\|J^{-1}\|\|\dot{J}\|)\|J^{-1}\|\|\dot{x}_r\| + k_G) \\ =\ & \|z_x\|\{k_M\|J^{-T}\|\|J^{-1}\|(\|\ddot{x}_r\| + \|J^{-1}\|\|\dot{J}\|\|\dot{x}_r\|) \\ & +k_C\|J^{-T}\|\|J^{-1}\|\|\dot{q}\|\|\dot{x}_r\| + k_G\|J^{-T}\|\} = \|z_x\| \sum_{j=1}^{3} k_j \varphi_j. \end{aligned} \tag{5.23}$$

Substituting the above inequality to (5.22), we obtain

$$\begin{aligned}\dot{V} &\leq -z_x^T K_x z_x + \sum_{j=1}^{4} \sigma_j k_j + \sum_{j=1}^{4} \frac{a_j}{b_j} \tilde{k}_j \hat{k}_j \\ &\leq -z_x^T K_x z_x + \sum_{j=1}^{4} \sigma_j k_j + \frac{1}{4} \sum_{j=1}^{4} \frac{a_j}{b_j} k_j^2 \\ &= -z_x^T K_x z_x + \delta, \end{aligned} \tag{5.24}$$

where $\delta = \sum_{j=1}^{4} \sigma_j k_j + \frac{1}{4}\sum_{j=1}^{4} \frac{a_j}{b_j} k_j^2$, and the last inequality comes from

$$\tilde{k}_j \hat{k}_j = (k_j - \hat{k}_j)\hat{k}_j = \frac{1}{4}k_j^2 - (\frac{1}{2}k_j - \hat{k}_j)^2 \leq \frac{1}{4}k_j^2. \tag{5.25}$$

Because $\lim_{t\to\infty} a_j = 0$ and $\lim_{t\to\infty} \sigma_j = 0$, we have $\lim_{t\to\infty} \delta = 0$. It indicates that there exists t_1 such that when $t > t_1$, $\delta \leq \varepsilon$, where ε is a small finite constant. Then we obtain $z_x \in L_\infty^n$. According to the definition of z_x in (5.12), $x \in L_\infty^n$ and $\dot{x} \in L_\infty^n$, and thus $\ddot{x}_r \in L_\infty^n$ and $\dot{x}_r \in L_\infty^n$. Considering (5.16), we have $\dot{z}_x \in L_\infty^n$.

Integrating both sides of (5.24) leads to

$$V(t) - V(0) \leq -\int_0^t z_x^T(v) K_x z_x(v) dv + \int_0^t \delta(v) dv, \tag{5.26}$$

which leads to

$$\begin{aligned} \int_0^t z_x^T(v) K_x z_x(v) dv &\leq V(0) - V(t) + \int_0^t \delta(v) dv \\ &\leq V(0) + \int_0^t \delta(v) dv, \end{aligned} \tag{5.27}$$

because $V(t) \geq 0$.

According to the definition of δ, we have

$$\begin{aligned} \int_0^t \delta(v) dv &= \sum_{j=1}^{4} k_j \int_0^t \sigma_j(v) dv + \frac{1}{4}\sum_{j=1}^{4} \frac{k_j^2}{b_j} \int_0^t a_j(v) dv \\ &= \sum_{j=1}^{4} k_j d_j + \frac{1}{4}\sum_{j=1}^{4} \frac{k_j^2}{b_j} c_j. \end{aligned} \tag{5.28}$$

The above equation indicates that $\int_0^t \delta(v) dv$ is bounded.

According to (5.27), $\int_0^t z_x^T(v) K_x z_x(v) dv$ is bounded because $V(0)$ is bounded,

which results in $z_x \in L_2^n$. According to Barbalet's Lemma, $z_x \in L_2^n$ and $\dot{z}_x \in L_\infty^n$ lead to $z_x \to 0$ as $t \to \infty$, which completes the proof. □

Remark 28. *While the control input u is developed in the Cartesian space, we need transform it to the joint space for the control of each joint. In the non-redundancy case, the transformation is uniquely determined as $\tau = J^T u$, as discussed above and shown in Fig. 5.3. In the redundancy case, the transformation is not uniquely determined and there exists freedom to improve some measures of the system performance, such as singularity avoidance, obstacle avoidance, kinetic energy minimization, and posture control.*

In general, the control input in the joint space can be formulated as

$$\tau = J^T u + (I_n - J^T \bar{J}^T) u_o, \tag{5.29}$$

where u_o is the control input in the operational space to improve the measures mentioned above, and $\bar{J}$ is the dynamically consistent Jacobian inverse defined by

$$\bar{J} = \hat{M}^{-1} J^T (J \hat{M}^{-1} J^T)^{-1}. \tag{5.30}$$

For example, to produce a human-like motion, we may use the measure of "human muscle effort" proposed in [106], which is defined to compensate for the gravity and described by

$$\Pi = G_R^T (K_G K_G^T) G_R, \tag{5.31}$$

where K_G represents the joint "strength", and we obtain the following control input

by minimizing the above measure

$$u_o = -K_1 \nabla \Pi - K_2 \dot{q}, \tag{5.32}$$

where K_1 and K_2 are positive definite matrices. More details can be found in [107, 108, 109, 110, 106, 111].

5.4 Simulation Studies

In this section, we consider a scenario as described in Section 5.1 and shown in Fig. 5.1, where the human partner grasps the handle near the end-effector of a 2-DOF robot arm and moves it in a plane. The robot arm under study includes two revolute joints and it has a planar workspace. As the motion intention of the human partner is not available for the control design, it is estimated using the proposed method and integrated into the developed impedance control. The simulation is conducted with the Robotics Toolbox introduced in [90].

The robot arm parameters are: $m_1 = m_2 = 2.0$kg, $l_1 = l_2 = 0.2$m, $i_1 = i_2 = 0.02$kgm^2, and $l_{c1} = l_{c2} = 0.1$m. The initial positions of the robot arm are $q_1 = -\frac{\pi}{3}$ and $q_2 = \frac{2\pi}{3}$. The limb model of the human partner is assumed to be $f = 0.5\dot{x} + 11(x - x_h) - \frac{0.1x - 0.1\dot{x}}{1+x^2+\dot{x}^2+t^2}$, where $x_h = x_{h,X/Y}$ with $x_{h,X} = 0.2 + 0.1\sin(0.1t), x_{h,Y} = -0.1 + 0.1\cos(0.1t)$ and X, Y standing for X axis and Y axis, respectively. The desired trajectory of the human partner indicates that he intents to move the end-effector of the robot arm along a circle with the radius of 0.1m.

In the first step of this simulation study, we utilize impedance control with zero stiffness as the benchmark. It is acknowledged that zero stiffness is necessary for

impedance control in applications of physical human-robot interaction. In the second step, we employ the proposed method with the estimated motion intention. In both steps, the control parameters are the same, except the adaptation ratio in (5.9), $\alpha_{X/Y} = 0.06$, in the second step. In particular, the impedance parameters in (4.1) are $M_x = 0.1I_2,\ C_x = 10I_2$, and $G_x = 0$. With $k(0) = 0$, the parameters in control input (5.13) and updating law (5.14) are $K_x = I_2$, $a_j = \frac{1}{(t+10)^2}$, $\sigma_j = \frac{1}{(t+10)^2}$, and $b_j = 2$ for $j = 1, \ldots, 3$. The NN parameters to estimate $x_{h,X}$ and $x_{h,Y}$ are as follows: the input of the NN is $r_{X/Y} = [f_{X/Y}, x_{X/Y}, \dot{x}_{X/Y}]^T$, the number of NN nodes in (5.3) is $p_{X/Y} = 10$, the centers of the functions are $\mu_{i,X/Y} = [0, 0, 0]^T$, and the variances are $\eta_{i,X/Y} = 20$ for $i = 1, 2, \ldots, 10$.

The results with impedance control are shown in Figs. 5.4-5.9. It is clearly found from Fig. 5.4 that the robot arm fails to follow human partner's motion intention with impedance control. In the first 3s, there is an obvious oscillation, which happens at the beginning of the adaptive process. This is also illustrated in Fig. 5.8, where the defined impedance error z_x is shown to converge to 0 as $t \to \infty$. In Figs. 5.5 and 5.6, the tracking performance in a single axis is shown, which indicates that although the robot arm acts compliantly to the human limb, it cannot follow the motion intention of the human partner within an acceptable scale. Two ways can be considered to achieve the better performance. One is to choose smaller impedance parameters M_x and C_x, and make the robot arm "softer". Unfortunately, it has been proved that the desired inertia cannot be chosen to be arbitrarily small [47] and a large damping is required to stabilize the whole system in practical implementations [112]. The other one requires the human partner to stiffen his limb and make the limb impedance dominate the impedance of the coupled system, but more control effort from the human partner is the cost and it is not achievable when the robot arm has a

large weight (and thus a large inertia). In this regard, to make the robot arm actively follow human partner's motion cannot be achieved by impedance control with a fixed rest position. Fig. 5.7 shows the interaction force between the robot arm and human limb, which is very large and will be compared with that when the proposed method is employed. Besides, Fig. 5.9 indicates the convergence of the developed adaptive control.

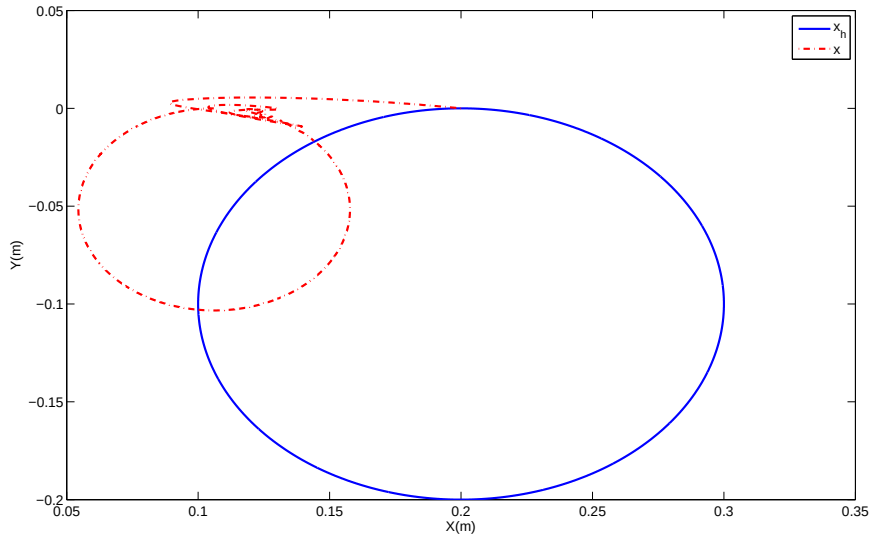

Fig. 5.4: Motion intention and actual trajectory with impedance control

The results with the proposed method are shown in Figs. 5.10-5.15. From Fig. 5.10, we can find that the actual trajectory of the robot arm almost tracks the motion intention of the human partner, which validates the effectiveness of the proposed method. This is further illustrated in the tracking results of single axis, as shown in Figs. 5.11 and 5.12. The interaction force with the proposed method is shown in Fig. 5.13, which is much smaller and about one tenth of that in Fig. 5.7. Therefore, it can be concluded that much less effort is required from the human partner with the proposed method, and the collaboration objective can be achieved more efficiently.

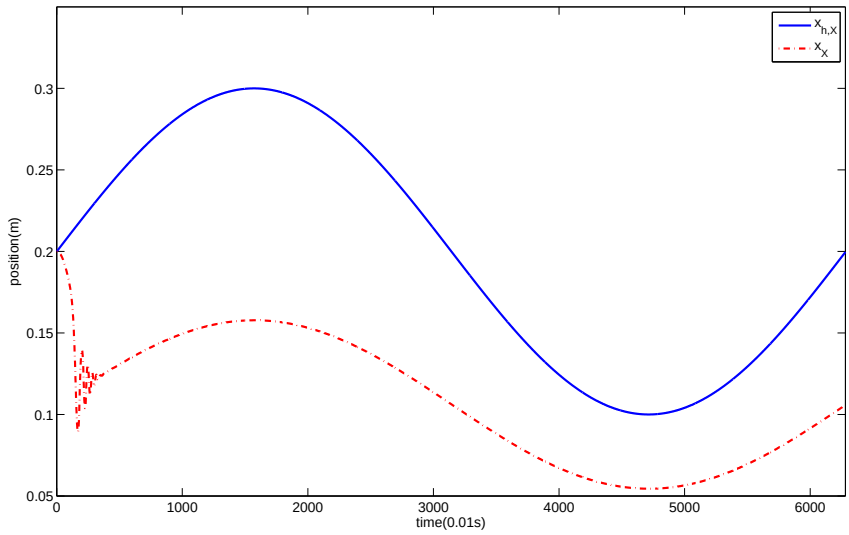

Fig. 5.5: Motion intention and actual trajectory with impedance control, X axis

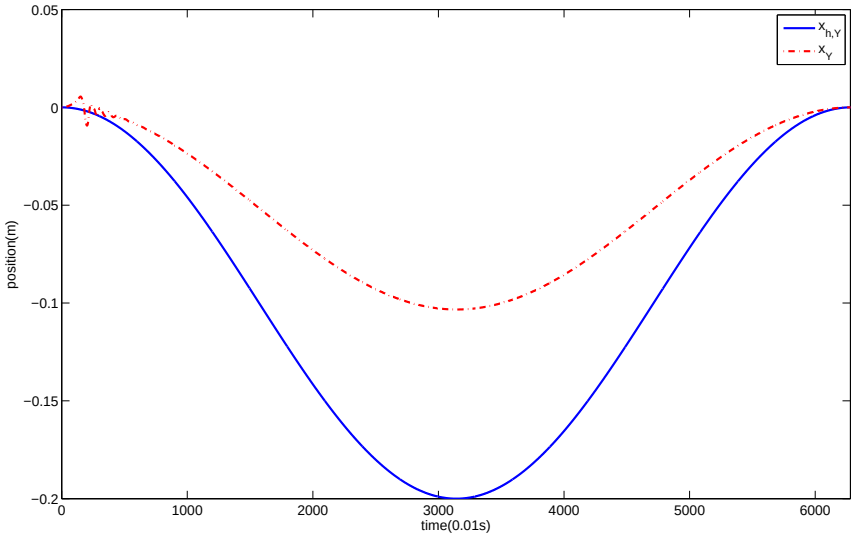

Fig. 5.6: Motion intention and actual trajectory with impedance control, Y axis

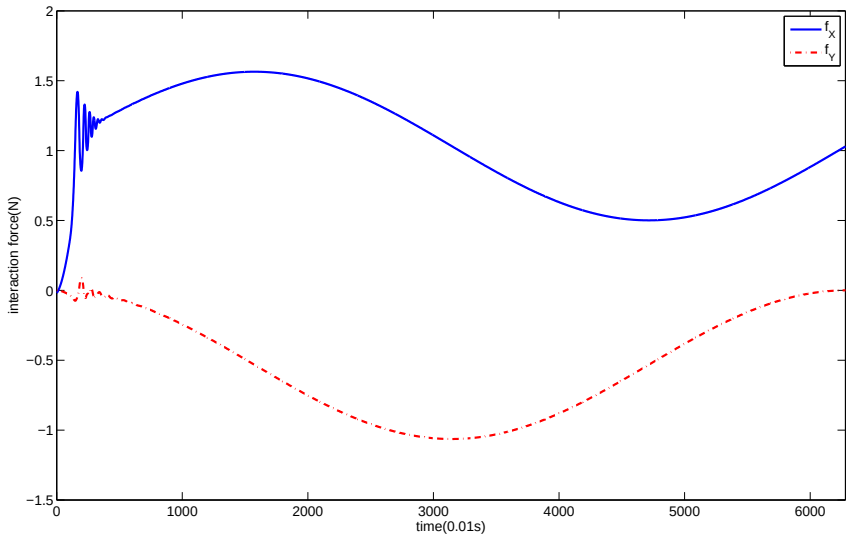

Fig. 5.7: Interaction force with impedance control

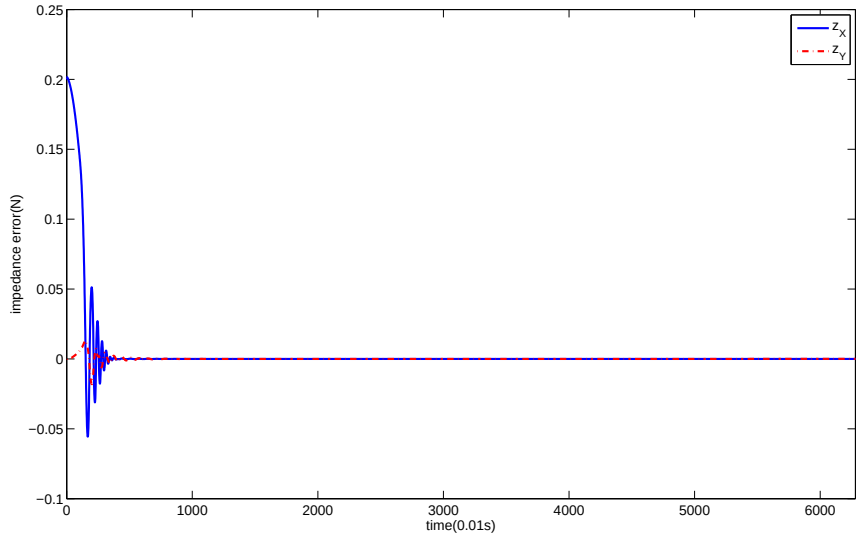

Fig. 5.8: Impedance error with impedance control

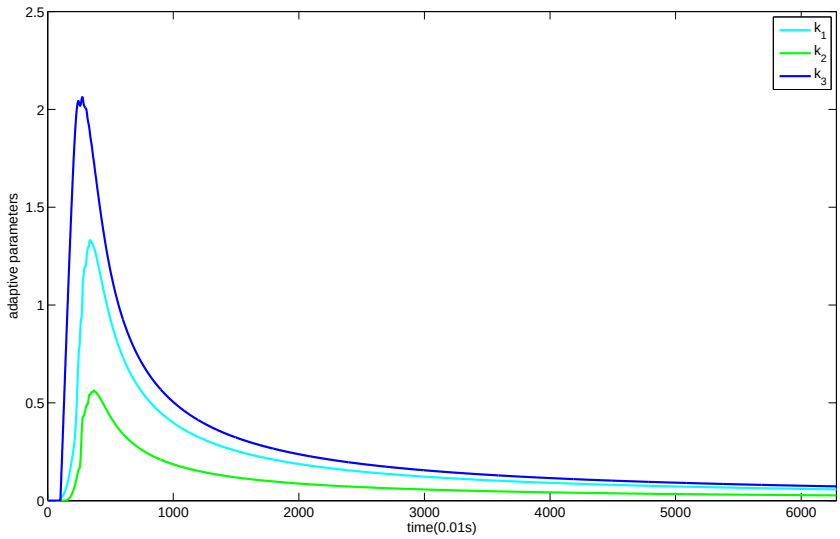

Fig. 5.9: Adaptive parameters with impedance control

Similarly to that in Figs. 5.8 and 5.9, good performance of the developed adaptive control can be seen in Figs. 5.14 and 5.15, which show the convergence of the defined impedance error z_x and the adaptive parameters.

5.5 Experiment

In this section, the proposed method is further examined through experiments. The experiments are carried out on Nancy which is a humanoid introduced in Chapter 4. In these experiments, the human partner holds a plate mounted on Nancy's left wrist, where there is an ATI mini-40 force/torque sensor, as shown in Fig. 5.16. Nancy's left wrist is moved by the human partner towards his intended position. Different from the simulation, the human partner's motion intention cannot be measured in the experiment. Therefore, the actual trajectory of the robot arm cannot be compared with the motion intention directly. In this situation, we can only understand the

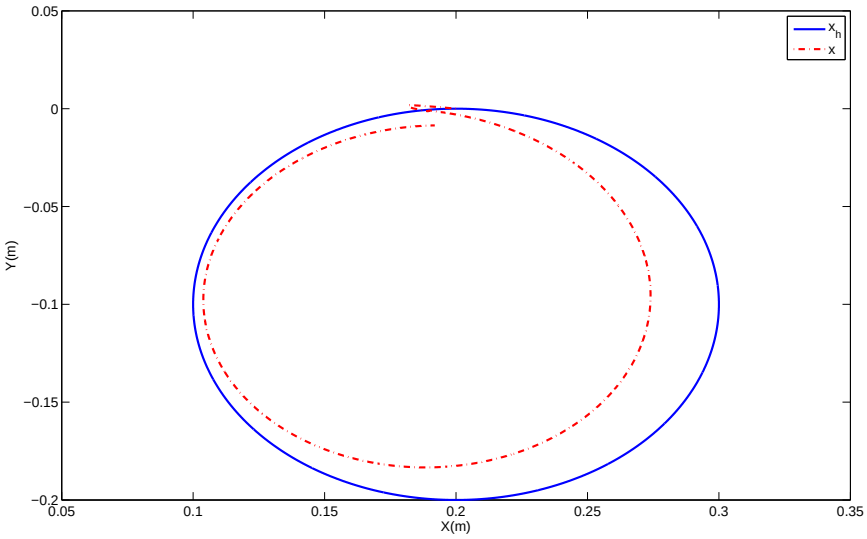

Fig. 5.10: Motion intention and actual trajectory with the proposed method

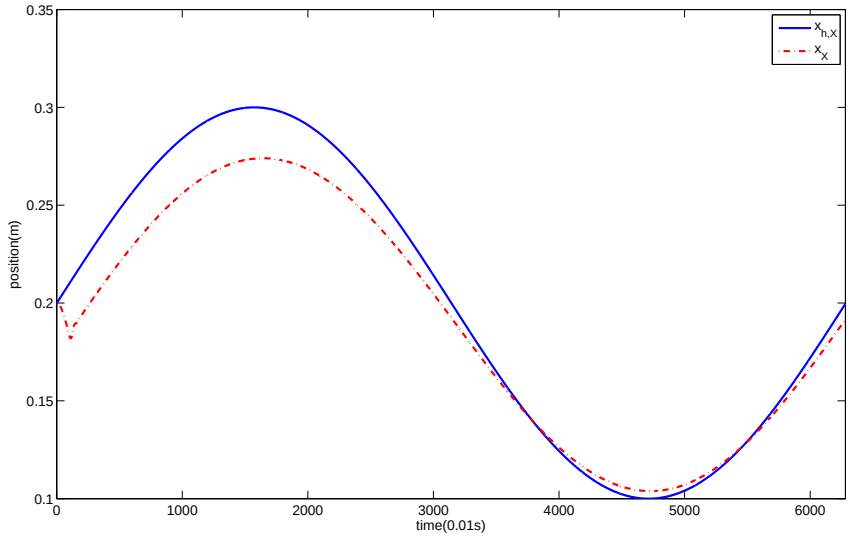

Fig. 5.11: Motion intention and actual trajectory with the proposed method, X axis

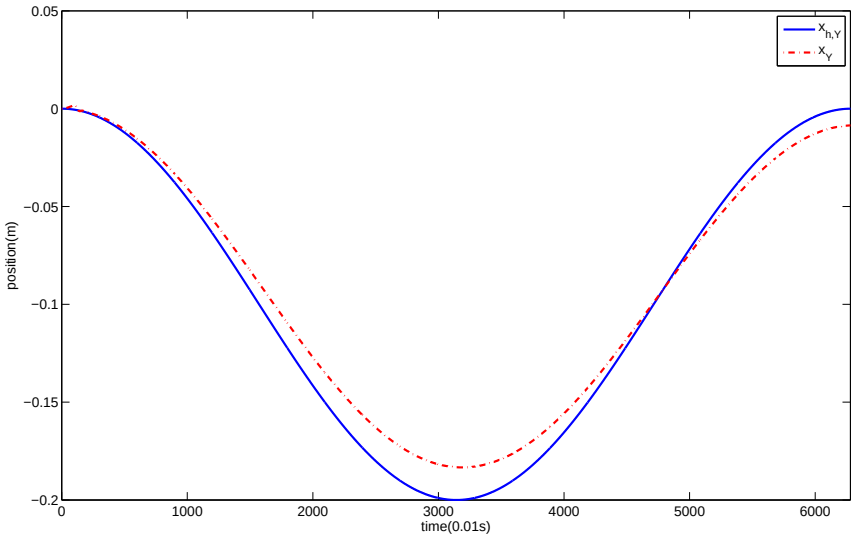

Fig. 5.12: Motion intention and actual trajectory with the proposed method, Y axis

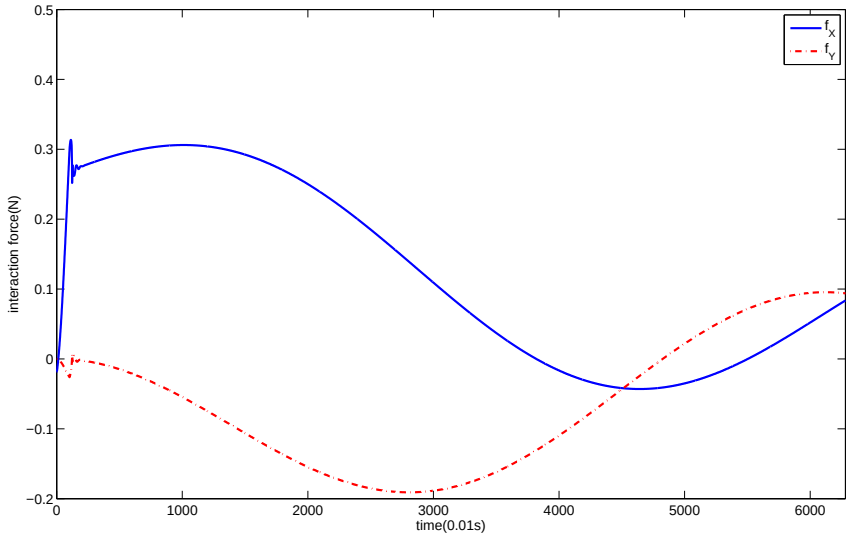

Fig. 5.13: Interaction force with the proposed method

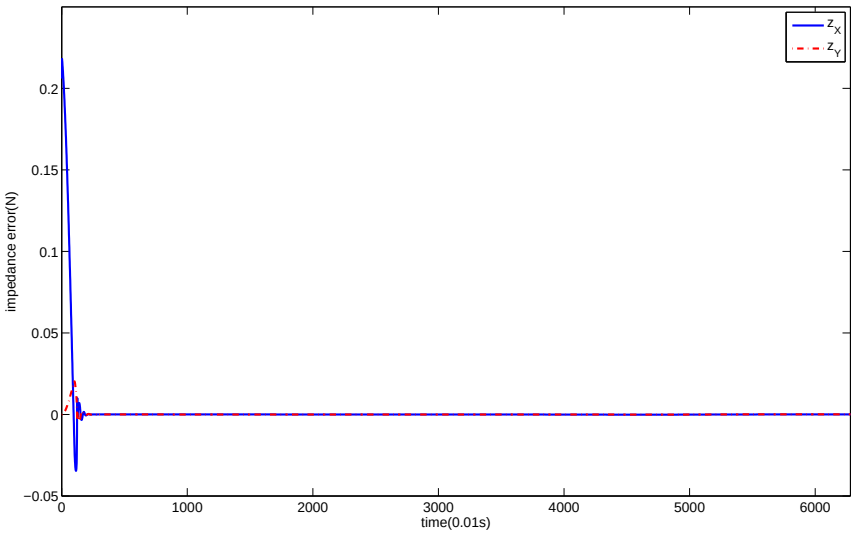

Fig. 5.14: Impedance error with the proposed method

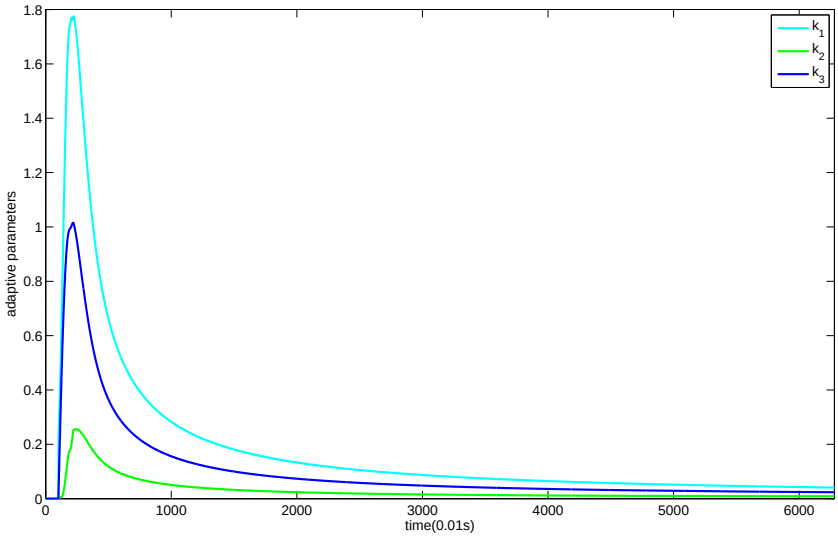

Fig. 5.15: Adaptive parameters with the proposed method

experiment results in an indirect way. In particular, a small external torque indicates a small error between the actual trajectory and the motion intention. This has been discussed when developing the intention estimation method in Section 5.2.

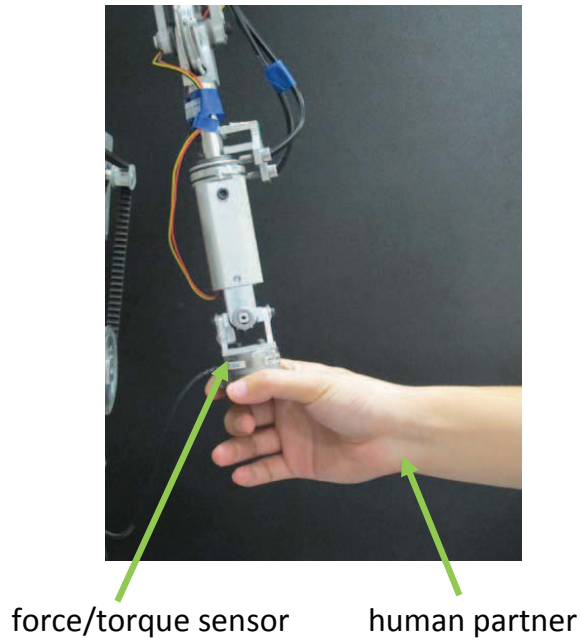

Fig. 5.16: Experiment scenario

Two cases of different motion intentions are considered. In the first case, the human partner aims to move the wrist to a fixed angle and thus the intended motion is a point-to-point movement. In the second case, the human partner aims to move the wrist forward and back, and the intended motion is a time-varying trajectory. In both cases, impedance control with zero stiffness is implemented for the comparison purpose. Impedance parameters in (4.1) are $M_x = 0.01$, $C_x = 0.8$, and $G_x = 0$. The number of NN nodes is $p = 10$, and the other parameters of NN in (5.3) are $\mu_i = 0$ and $\eta_i = 1$ for $i = 1, 2, \ldots, 10$. The adaptation ratio in (5.9) is $\alpha = 0.01$. Other values of the above parameters can be chosen to improve the control performance.

The results in the first case are shown in Figs. 5.17 and 5.18. In Fig. 5.17,

the wrist angles with impedance control and the proposed method are shown. The "target angle" in the figure stands for the position that the human partner intends to move the robot arm to. It is found that the response with the proposed method is faster than that with impedance control, which indicates that the wrist with the proposed method follows human partner's motion intention more "actively". While Fig. 5.17 illustrates that the wrist with two methods is moved to roughly the same angle (the target angle), it is clearly found in Fig. 5.18 that much less torque is needed with the proposed method. When the target angle is reached, the torque from the human partner becomes zero with both impedance control and the proposed method. Based on these results, it can be concluded that much less effort is required from the human partner with the proposed method, although both impedance control and the proposed method can be employed for human-robot collaboration in the case of point-to-point movement.

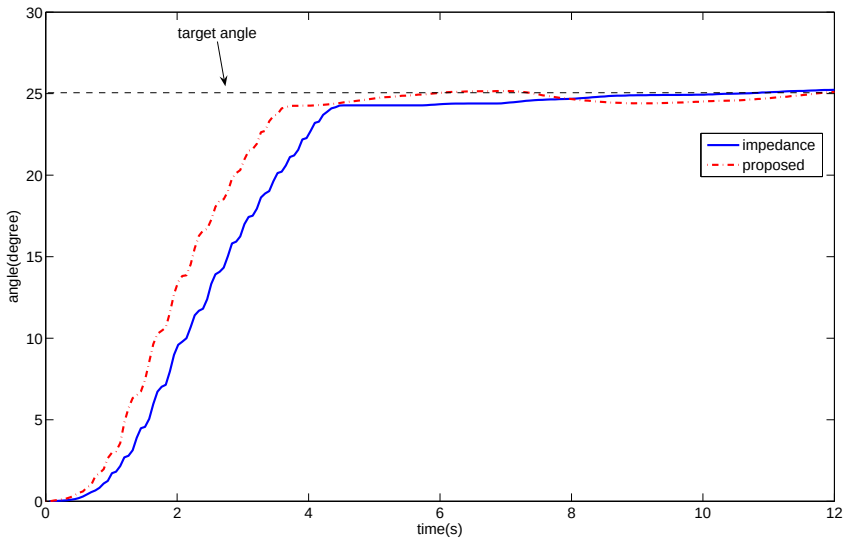

Fig. 5.17: Joint angle, in the case of point-to-point movement

Instead of point-to-point movement in the first case, a more common scenario in

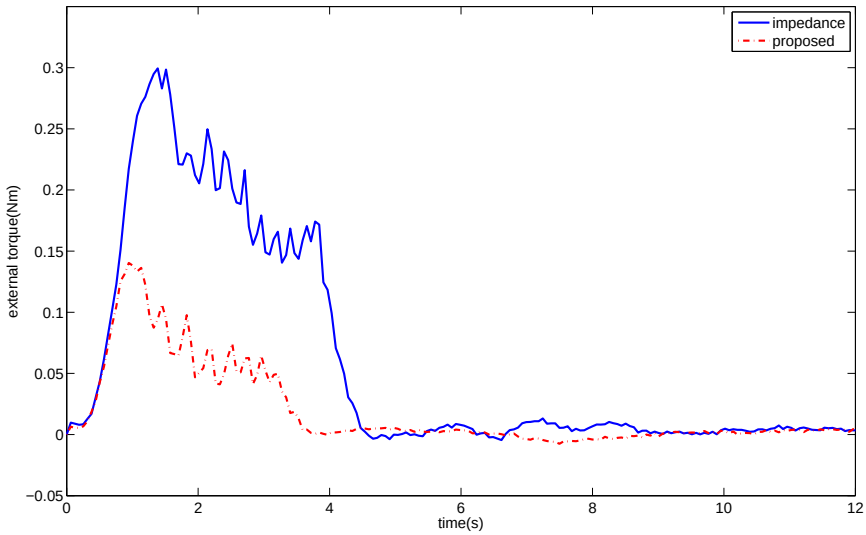

Fig. 5.18: External torque, in the case of point-to-point movement

practice is to move the robot arm along a time-varying trajectory. In the second case, Nancy's wrist is firstly moved toward a prescribed target position, and back to the other target position. The results in this case are shown in Figs. 5.19 and 5.20. The "target angle 1" and "target angle 2" in Fig. 5.19 stand for the target position in the forward motion and in the back motion, respectively. Similarly as in Fig. 5.17, a faster response is achieved with the proposed method as shown in Fig. 5.19. In Fig. 5.20, it is shown that the torque with the proposed method is about one fourth of that with impedance control. These results indicate that Nancy's wrist can be moved to the target position with much less effort under the proposed method, even if the human partner changes his motion intention. It has also well justified the validity of Assumption 4. Comparatively, although impedance control with zero stiffness can be employed in the case of time-varying trajectory, it makes the robot arm become a load to the human partner, as discussed before.

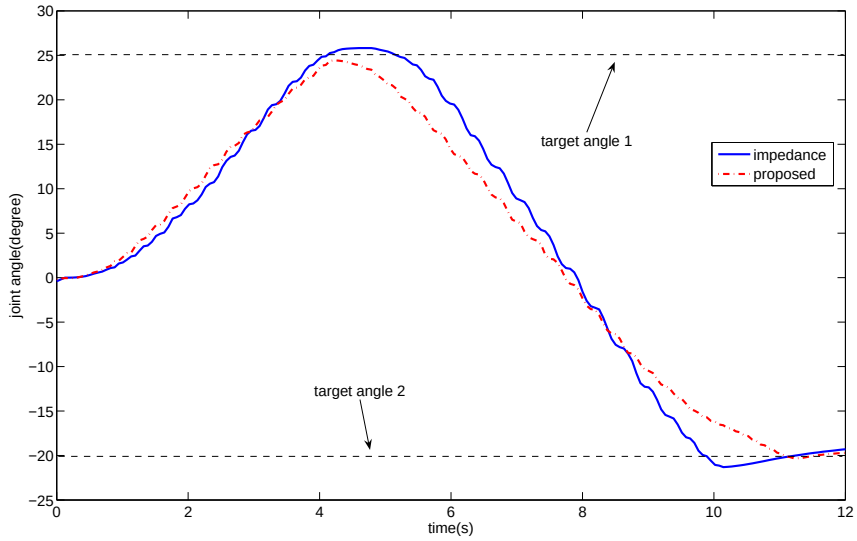

Fig. 5.19: Joint angle, in the case of time-varying trajectory

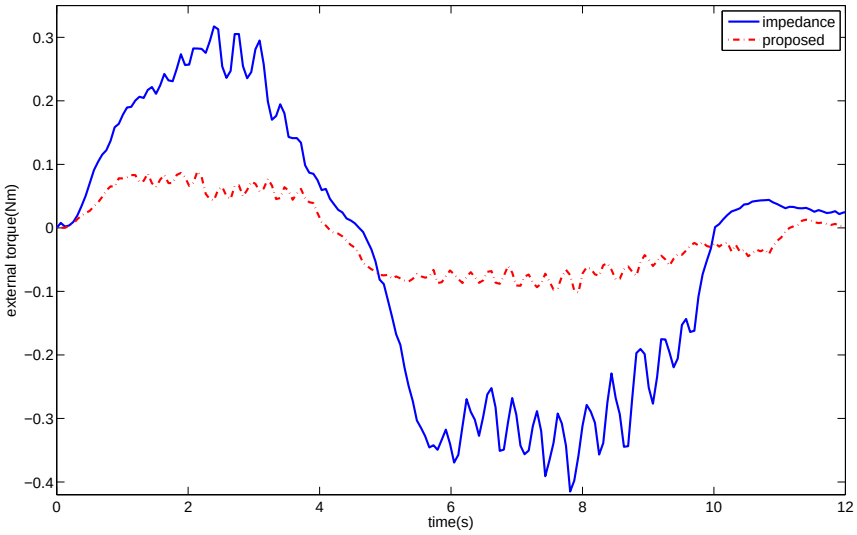

Fig. 5.20: External torque, in the case of time-varying trajectory

5.6 Conclusion

In this chapter, trajectory adaptation for human-robot collaboration has been investigated, in which the motion intention of the human partner has been observed by employing the human limb model and estimating the desired trajectory. A NN method has been proposed to cope with the problem of unknown human limb model. The estimated motion intention has been integrated into impedance control of the robot arm, such that it actively follows its human partner. Simulation and experiment results have been provided to verify the validity of the proposed method.

In the discussion throughout this chapter, human partner and robot are considered to be two separated subsystems. In particular, the motion intention of the human partner is estimated by considering the human limb dynamics. The estimated motion intention is integrated to impedance control of the robot arm. The performance of the whole coupled collaboration system is yet to be rigorously analyzed, which is the motivation of the following chapter.

Chapter 6

Trajectory Adaptation: Zero Force Regulation

In this chapter, human limb dynamics are described by the model introduced in the previous chapter. Zero force regulation under the impedance control framework is proposed to achieve natural human-robot collaboration, subject to uncertain human limb dynamics. Adaptive control is proposed to deal with the point-to-point movement, and learning control and NN control are developed to generate periodic and non-periodic trajectories, respectively. The stability and tracking performance of the whole coupled system are discussed through the rigorous analysis.

The rest of this chapter is organized as follows. In Section 6.1, the human-robot collaboration system under study is introduced and the control objective of force regulation is discussed. In Section 6.2, three cases of trajectory adaptation are discussed and the system performance for each case is rigorously analyzed. Section 6.3 is dedicated to discuss the system performance when the inner-loop dynamics are taken into account. In Section 6.4, the simulation study is used to verify the effectiveness

of the proposed method. In Section 6.5, further examination of the proposed method is carried out with the practical implementation. Concluding remarks are given in Section 6.6.

6.1 Problem Formulation

In this chapter, we further investigate the human-robot collaboration system introduced in the previous chapter, which includes a robot arm and a human limb. The human limb holds the end-effector of the robot arm and aims to move it along a certain trajectory which is unknown to the robot arm.

For the analysis convenience, we consider the system dynamics in a single direction as in the previous chapter. Considering the target impedance model (4.1), we have

$$x = x_0 - f'. \tag{6.1}$$

The Laplace transformation of the signal f', i.e., $f'(s)$, satisfies

$$f'(s) = \frac{f(s)}{M_x s^2 + C_x s + G_x}, \tag{6.2}$$

where $f(s)$ is the Laplace transformation of the signal f.

The human limb model (5.2) has the following property:

Property 7. *$\frac{\partial \delta}{\partial x}$ and $\frac{\partial \delta}{\partial \dot{x}}$ are bounded, and $|\delta(x, \dot{x})| < b_1|x| + b_2|\dot{x}|$, where b_1 and b_2 are unknown positive constants.*

If no uncertainty is in (5.2), it is found that $f \to 0$ leads to $x \to x_h$ which means that the robot arm moves to the trajectory planned by the human partner and the

collaboration objective is achieved. Therefore, the control objective in the following is to make $f \to 0$.

By substituting (6.1) into (5.2), we obtain

$$\begin{aligned} \frac{f}{K_h} &= x - x_h + \frac{C_h\dot{x}}{K_h} + \frac{\delta(x,\dot{x})}{K_h} \\ &= x_0 - f' - x_h + \frac{C_h\dot{x}}{K_h} + \frac{\delta(x,\dot{x})}{K_h}. \end{aligned} \tag{6.3}$$

Let

$$x_0 = f' + \hat{x}_h - \hat{C}_h\dot{x} + x_\delta, \tag{6.4}$$

where $\hat{x}_h$ and $\hat{C}_h$ are the estimates of x_h and $\frac{C_h}{K_h}$, respectively, and

$$x_\delta = \hat{b}_1 \mathrm{sgn}(xf)x + \hat{b}_2 \mathrm{sgn}(\dot{x}f)\dot{x} \tag{6.5}$$

with $\hat{b}_1$ and $\hat{b}_2$ as the estimates of $\frac{b_1}{K_h}$ and $\frac{b_2}{K_h}$, respectively.

Remark 29. *It will be shown in the analysis below that x_δ is used to compensate for $\frac{\delta(x,\dot{x})}{K_h}$. Besides, for the rigorous analysis in the proof of Theorem 7, it is required that the sign function in x_δ is replaced by a smooth threshold function such that its derivative is bounded and it is the function of only x and $\dot{x}$. This function can be easily constructed in practice.*

According to (6.3) and (6.4), we have

$$\frac{f}{K_h} = \tilde{x}_h - \tilde{C}_h\dot{x} + (x_\delta + \frac{\delta(x,\dot{x})}{K_h}), \tag{6.6}$$

where $\tilde{x}_h = \hat{x}_h - x_h$ and $\tilde{C}_h = \hat{C}_h - \frac{C_h}{K_h}$.

Lemma 5. $(x_\delta + \frac{\delta(x,\dot{x})}{K_h})f \leq -\tilde{b}_1 sgn(xf)xf - \tilde{b}_2 sgn(\dot{x}f)\dot{x}f$, *where* $\tilde{b}_1 = \hat{b}_1 - \frac{b_1}{K_h}$ *and* $\tilde{b}_2 = \hat{b}_2 - \frac{b_2}{K_h}$.

Proof. Considering Property 7 and (6.5), we obtain

$$\begin{aligned} & (x_\delta + \frac{\delta(x,\dot{x})}{K_h})f \\ \leq\ & x_\delta f + |\frac{\delta(x,\dot{x})}{K_h}||f| \\ \leq\ & x_\delta f + (\frac{b_1}{K_h}|x| + \frac{b_2}{K_h}|\dot{x}|)|f| \\ =\ & x_\delta f + [\frac{b_1}{K_h}\mathrm{sgn}(xf)xf + \frac{b_2}{K_h}\mathrm{sgn}(\dot{x}f)\dot{x}f] \\ =\ & -\tilde{b}_1\mathrm{sgn}(xf)xf - \tilde{b}_2\mathrm{sgn}(\dot{x}f)\dot{x}f. \end{aligned} \tag{6.7}$$

□

6.2 Zero Force Regulation

In the following, we discuss three cases where x_h is assumed to be constant, periodic and non-periodic, respectively. Zero force regulation for each case is accordingly developed, i.e., to design x_0 in (6.4) to make $\lim_{t\to\infty} f = 0$.

6.2.1 Point-to-Point Movement

In the case of point-to-point movement, we have the following assumption:

Assumption 5. *The desired trajectory of the human limb* x_h *is a constant, i.e.,* $\dot{x}_h = 0$.

We develop the following updating law to obtain $\hat{x}_h$, $\hat{C}_h$ and x_δ in (6.4):

$$\dot{\hat{x}}_h = -\gamma f,\ \dot{\hat{C}}_h = -\gamma \dot{x} f,\ \dot{\hat{b}}_1 = -\gamma \mathrm{sgn}(xf) xf,\ \dot{\hat{b}}_2 = -\gamma \mathrm{sgn}(\dot{x}f)\dot{x}f, \tag{6.8}$$

where γ is a positive scalar.

Theorem 7. *Considering the closed-loop dynamics described by (6.6), the rest position (6.4) with the updating law (6.8) guarantees the following results:*

(i) the interaction force asymptotically converges to 0 *as* $t \to \infty$*, i.e.,* $\lim_{t\to\infty} f(t) = 0$*, and*

(ii) all the signals in the closed-loop system are bounded.

Proof. Denote $\theta = [x_h, \frac{C_h}{K_h}, \frac{b_1}{K_h}, \frac{b_2}{K_h}]^T$, $\hat{\theta} = [\hat{x}_h, \hat{C}_h, \hat{b}_1, \hat{b}_2]^T$, $\tilde{\theta} = [\tilde{x}_h, \tilde{C}_h, \tilde{b}_1, \tilde{b}_2]^T$, and

$$\phi = [1, \dot{x}, \mathrm{sgn}(xf)x, \mathrm{sgn}(\dot{x}f)\dot{x}]^T. \tag{6.9}$$

Then, according to (6.8), we have

$$\dot{\hat{\theta}} = -\gamma \phi f. \tag{6.10}$$

Consider a Lyapunov function candidate

$$V_1 = \frac{1}{2\gamma}\tilde{\theta}^T\tilde{\theta}. \tag{6.11}$$

Considering $\dot{\tilde{\theta}} = \dot{\hat{\theta}}$, (6.10), (6.6), and Lemma 5, the derivative of V_1 with respect to

time is

$$\begin{aligned}\dot{V}_1 &= \frac{1}{\gamma}\tilde{\theta}^T\dot{\tilde{\theta}} = \frac{1}{\gamma}\tilde{\theta}^T\dot{\hat{\theta}} = -\tilde{\theta}^T\phi f \\ &\leq -[\tilde{x}_h - \tilde{C}_h\dot{x} + (x_\delta + \frac{\delta(x,\dot{x})}{K_h})]f \\ &= -\frac{f^2}{K_h} \leq 0. \end{aligned} \tag{6.12}$$

As V_1 is positive definite, the above equation shows that $V_1 \in L_\infty$. According to the inequality $\dot{V}_1 \leq -\frac{f^2}{K_h}$, we have $\int_0^t \frac{f(v)^2}{K_h}dv \leq V_1(0) - V_1(t) \leq V_1(0)$, which indicates that $f \in L_2$ and $f \in L_\infty$.

According to (6.4), we have $x = \hat{x}_h - \hat{C}_h\dot{x} + x_\delta$ and taking its derivative with reference to time leads to $\dot{x} = \dot{\hat{x}}_h - \dot{\hat{C}}_h\dot{x} - \hat{C}_h\ddot{x} + \dot{x}_\delta$. Note that $\dot{x}$, $\dot{\hat{x}}_h$, $\dot{\hat{C}}_h\dot{x}$, and $\hat{C}_h$ are bounded. To obtain $\ddot{x} \in L_\infty$, it is required to replace the sign function in (6.5) by a smooth threshold function as mentioned in Remark 29. Considering Property 7 and $\dot{\delta}(x,\dot{x}) = \frac{\partial\delta}{\partial x}\dot{x} + \frac{\partial\delta}{\partial\dot{x}}\ddot{x}$, we have $\dot{\delta}(x,\dot{x}) \in L_\infty$. Taking derivative of (5.2) with reference to time, we have $\dot{f} = C_h\ddot{x} + K_h(\dot{x} - \dot{x}_h) + \dot{\delta}(x,\dot{x})$. Thus, $\dot{f} \in L_\infty$ and f is uniformly continuous. According to Barbalet's lemma, $f \in L_2$ and the uniform continuity of f lead to $f \to 0$ when $t \to \infty$. This completes the proof. □

6.2.2 Periodic Trajectory

It is noted that x_h in the the previous section is assumed to be a constant, which is valid in the case of point-to-point movement. However, in many practical applications, x_h is usually a time-varying trajectory, which will be handled in this subsection and the following subsection.

From the performance analysis in the previous section, it is found that the adaptive

method is not applicable to the case of time-varying trajectory. In particular, the existence of $\dot{x}_h$ will result in the interaction force. In the following, we develop an iterative learning method to deal with the periodic time-varying trajectory.

Assumption 6. *The desired trajectory of the human limb x_h is periodic with a known period T, i.e.,*

$$\begin{aligned} x_h(t) &= x_h(t-T), \\ x_h(t) &= 0,\ t<0. \end{aligned} \tag{6.13}$$

Considering the rest position (6.4), we replace the updating law for $\dot{\hat{x}}_h$ in (6.8) by the following learning law

$$\begin{aligned} \hat{x}_h(t) &= \hat{x}_h(t-T) - \gamma f, \\ \hat{x}_h(t) &= 0,\ t<0. \end{aligned} \tag{6.14}$$

Theorem 8. *Considering the closed-loop dynamics described by (6.6), the rest position (6.4) with the updating laws (6.8) and (6.14) guarantees the following results:*

(i) the interaction force asymptotically converges to 0 *as* $t \to \infty$, *i.e.,* $\lim_{t\to\infty} f(t) = 0$, *and*

(ii) all the signals in the closed-loop system are bounded.

Proof. Denote $\xi = [\frac{C_h}{K_h}, \frac{b_1}{K_h}, \frac{b_2}{K_h}]^T$, $\hat{\xi} = [\hat{C}_h, \hat{b}_1, \hat{b}_2]^T$, $\tilde{\xi} = [\tilde{C}_h, \tilde{b}_1, \tilde{b}_2]^T$, and

$$\varphi = [\dot{x}, \mathrm{sgn}(xf)x, \mathrm{sgn}(\dot{x}f)\dot{x}]^T. \tag{6.15}$$

Then, we have $\dot{\tilde{\xi}} = -\gamma\varphi f$. Consider a Lyapunov function candidate

$$\begin{aligned} V_2 &= U + W,\ U = \frac{1}{2\gamma}\tilde{\xi}^T\tilde{\xi}, \\ W &= \begin{cases} \frac{1}{2\lambda}\int_0^t \tilde{x}_h^2(\tau)\tau, & 0 \le t < T; \\ \frac{1}{2\lambda}\int_{t-T}^t \tilde{x}_h^2(\tau)\tau, & T \le t < \infty. \end{cases} \end{aligned} \tag{6.16}$$

where λ is a positive scalar.

The derivative of U with respect to time is

$$\begin{aligned} \dot{U} &= \frac{1}{\gamma}\tilde{\xi}^T\dot{\tilde{\xi}} \\ &= -\tilde{\xi}^T\varphi f \\ &\le -[-\tilde{C}_h\dot{x} + (x_\delta + \frac{\delta(x,\dot{x})}{K_h})]f \\ &= -(\frac{f}{K_h} - \tilde{x}_h)f. \end{aligned} \tag{6.17}$$

For $0 \le t < T$, the derivative of W with respect to time is

$$\begin{aligned} \dot{W} &= \frac{1}{2\lambda}\tilde{x}_h^2 \\ &= \frac{1}{2\lambda}(\hat{x}_h^2 - 2\hat{x}_h x_h + x_h^2) \\ &\le \frac{1}{2\lambda}(2\hat{x}_h^2 - 2\hat{x}_h x_h + x_h^2) \\ &= \frac{1}{2\lambda}(2\hat{x}_h\tilde{x}_h + x_h^2) \\ &= \frac{1}{2\lambda}(-2\lambda\tilde{x}_h f + x_h^2) \\ &= -\tilde{x}_h f + \frac{1}{2\lambda}x_h^2. \end{aligned} \tag{6.18}$$

Therefore, for $0 \leq t < T$, we have

$$\dot{V}_2 = \dot{U} + \dot{W} \leq -\frac{f^2}{K_h} + \frac{1}{2\lambda} x_h^2. \tag{6.19}$$

Since x_h is bounded, $\dot{V}_2$ is bounded for $0 \leq t < T$, and thus V_2 is bounded for $0 \leq t < T$.

For $T \leq t < \infty$, the derivative of W with respect to time is

$$\begin{aligned} \dot{W} &= \frac{1}{2\lambda}[\tilde{x}_h(t)^2 - \tilde{x}_h(t-T)^2] \\ &= \frac{1}{2\lambda}[\tilde{x}_h(t)^2 - (\tilde{x}_h(t) + \lambda f)^2] \\ &= \frac{1}{2\lambda}(-2\lambda \tilde{x}_h f - \lambda^2 f^2) \\ &= -\tilde{x}_h f - \frac{\lambda}{2} f^2. \end{aligned} \tag{6.20}$$

Therefore, for $T \leq t < \infty$, we have

$$\begin{aligned} \dot{V}_2 &= \dot{U} + \dot{W} \\ &\leq -(\frac{1}{K_h} + \frac{\lambda}{2}) f^2. \end{aligned} \tag{6.21}$$

The following is similar to that in the proof of Theorem 7, and thus omitted. □

Remark 30. *In the case discussed in this section, x_h is assumed to be periodic and learning control is thus developed. For learning control, usually the repositioning condition is required [113], i.e., the robot arm is required to move to the initial position at the beginning of each period. To relax this assumption, much effort has been made by adopting alignment condition instead, i.e., the robot arm is only required to start from where it stops [114]. Motivated by adaptive learning control in [115], the method proposed in this chapter requires neither the repositioning condition nor the alignment*

condition, which has been shown in the above proof.

6.2.3 Non-Periodic Trajectory

In the previous section, it is assumed in Assumption 6 that x_h is periodic. Although this is acceptable in many scenarios, it obviously limits the applications of the proposed method. In this section, we make use of the linearly parameterized function approximators, such as higher-order NN, fuzzy systems and splines, to relax this assumption. The basic idea is to approximate a non-periodic trajectory by a linearly parameterized function, and the adaptive method is developed to estimate the ideal weights. As in the previous chapter, RBFNN is employed in this chapter as the linearly parameterized function approximator.

The structure of RBFNN is expressed as

$$\begin{aligned} x_{NN}(r) &= \sum_{i=1}^{p} w_i s_i(r), \\ s_i(r) &= e^{\frac{-(r-\mu_i)^2}{\eta_i^2}}, \end{aligned} \tag{6.22}$$

where $r,\ p,\ \mu_i$, and η_i have the same meanings as in (5.3), and w_i is the ideal weight vector.

According to Assumption 4, $x_h(r)$ is a smooth function over a compact set Ω_r. Then, given a small constant real number $\varepsilon > 0$, if p is sufficiently large, there exist a set of ideal bounded weights w_i such that

$$|x_h(r) - x_{NN}(r)| < \varepsilon. \tag{6.23}$$

Considering the rest position (6.4), we replace the updating law for $\dot{\hat{x}}_h$ in (6.8) by the following updating law

$$\begin{aligned} \hat{x}_h &= \sum_{i=1}^{p} \hat{w}_i s_i(r) - \text{sgn}(f)\varepsilon, \\ \dot{\hat{w}}_i &= -\gamma s_i f, \text{ for } i = 1, \ldots, p. \end{aligned} \tag{6.24}$$

The following analysis will show that $\text{sgn}(f)\varepsilon$ is to compensate for the NN modeling error.

Theorem 9. *Considering the closed-loop dynamics described by (6.6), the rest position (6.4) with the updating laws (6.8) and (6.24) guarantees the following results:*

(i) the interaction force asymptotically converges to 0 *as* $t \to \infty$*, i.e.,* $\lim_{t\to\infty} f(t) = 0$*, and*

(ii) all the signals in the closed-loop system are bounded.

Proof. The proof is similar to that of Theorem 7, so we only highlight the differences.

First, we denote

$$\begin{aligned} \vartheta &= [w_1, \ldots, w_p, \frac{C_h}{K_h}, \frac{b_1}{K_h}, \frac{b_2}{K_h}]^T, \\ \hat{\vartheta} &= [\hat{w}_1, \ldots, \hat{w}_p, \hat{C}_h, \hat{b}_1, \hat{b}_2]^T, \\ \tilde{\vartheta} &= [\tilde{w}_1, \ldots, \tilde{w}_p, \tilde{C}_h, \tilde{b}_1, \tilde{b}_2]^T, \\ \psi &= [s_1, \ldots, s_p, \dot{x}, \text{sgn}(xf)x, \text{sgn}(\dot{x}f)\dot{x}]^T. \end{aligned} \tag{6.25}$$

Then, we obtain $\dot{\hat{\vartheta}} = -\gamma\psi f$. Consider a Lyapunov function candidate

$$V_3 = \frac{1}{2\gamma}\tilde{\vartheta}^T\tilde{\vartheta}. \tag{6.26}$$

The derivative of V_3 along the time is

$$\begin{aligned}
\dot{V}_3 &= \frac{1}{\gamma}\tilde{\vartheta}^T\dot{\tilde{\vartheta}} \\
&= -\tilde{\vartheta}^T\psi f \\
&\leq -[\tilde{x}_h - \tilde{C}_h\dot{x} + (x_\delta + \frac{\delta(x,\dot{x})}{K_h}) + (x_h - x_{NN} + \mathrm{sgn}(f)\varepsilon)]f \\
&\leq -[\tilde{x}_h - \tilde{C}_h\dot{x} + (x_\delta + \frac{\delta(x,\dot{x})}{K_h})]f \\
&= -\frac{f^2}{K_h} \leq 0. \qquad (6.27)
\end{aligned}$$

The following is similar to that in the proof of Theorem 7, and thus omitted. □

Remark 31. *Comparing (5.8) and (6.24), we find that they have a similar formulation. This is reasonable because two methods proposed in the previous chapter and this chapter are based on the same control objective: to make the interaction force as small as possible. By further observing (5.8) and (6.24), we find that in the rigorous proof in the above,* $\mathrm{sgn}(f)\varepsilon$ *is needed to compensate for the NN modeling error. Therefore, the proposed method in the previous chapter is an incomplete version of the NN method developed in this chapter.*

6.3 Inner-Loop Dynamics

In the above discussion, it is assumed that the robot dynamics perfectly follow the target impedance model (4.1). In other words, the transient performance of the robot dynamics during learning/adaptive impedance control have not been considered. In this section, we aim to illustrate that zero force regulation will not be affected by the transient performance of the robot dynamics, subject to a certain condition.

For the analysis convenience, position-based impedance control as shown in Fig. 6.1 is considered. In this framework, the outer-loop is dedicated to generate $q_d = \int_0^t J^{-1}(q(v))\dot{x}_d(v)dv$ according to the target impedance model (4.1), where x is replaced by x_d. The inner-loop is to guarantee the trajectory tracking, i.e., $\lim_{t\to\infty} q(t) = q_d(t)$ and thus $\lim_{t\to\infty} x(t) = x_d$.

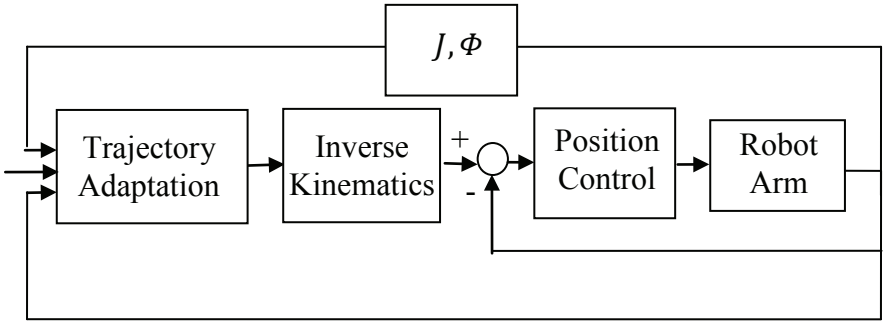

Fig. 6.1: Trajectory adaptation and its implementation

Denoting $e_1 = x_d - x$, we evaluate the force regulation performance under the following condition: $\lim_{t\to\infty} e_1(t) = 0$ and $e_1 \in L_2$. Similar arguments discussed in this section can be found in [116].

Instead of (4.1), the target impedance model is given by

$$M_x(\ddot{x}_d - \ddot{x}_0) + C_x(\dot{x}_d - \dot{x}_0) + G_x(x_d - x_0) = -f. \tag{6.28}$$

Accordingly, we have the below equation instead of (6.1)

$$x_d = x_0 - f'. \tag{6.29}$$

Then, instead of (6.6), the closed-loop dynamics including the human limb dynamics

(5.2) become

$$\frac{f}{K_h} = \tilde{x}_h - \tilde{C}_h\dot{x} + (x_\delta + \frac{\delta(x,\dot{x})}{K_h}) - e_1. \tag{6.30}$$

Lemma 6. *The results in Theorem 7, 8 and 9 are guaranteed if* $\lim_{t\to\infty} e_1(t) = 0$ *and* $e_1 \in L_2$.

Proof. Since $e_1 \in L_2$, we have the following inequality

$$\int_0^t e_1^2(v)dv \leq c, \tag{6.31}$$

where c is a positive constant.

Consider a Lyapunov-like function

$$V = V_j + \frac{c}{4c_j} - \frac{1}{4c_j}\int_0^t e_1^2(v)dv, \text{ for } j = 1,2,3, \tag{6.32}$$

where $c_1 = c_3 = \frac{1}{K_h}$ and $c_2 = \frac{1}{K_h} + \frac{\lambda}{2}$. Then, the derivative of V with respect to time is

$$\begin{aligned} \dot{V} &= \dot{V}_j - \frac{1}{4c_j}e_1^2 \\ &\leq -c_j f^2 + e_1 f - \frac{1}{4c_j}e_1^2 \\ &= -(\sqrt{c_j}f - \frac{1}{2\sqrt{c_j}}e_1)^2 \leq 0. \end{aligned} \tag{6.33}$$

Similarly as in the proofs of Theorem 7, 8 and 9, we have $\lim_{t\to\infty}(\sqrt{c_j}f(t) - \frac{1}{2\sqrt{c_j}}e_1(t)) = 0$. Because $\lim_{t\to\infty} e_1(t) = 0$, we finally obtain $\lim_{t\to\infty} f(t) = 0$, and all the other signals are bounded. □

6.4 Simulation Studies

In this section, we consider the human-robot collaboration system as discussed in the simulation study in Chapter 5. Three cases will be discussed and the desired trajectory of the human limb will be a point-to-point movement, a periodic trajectory and a non-periodic trajectory, respectively. The simulation is conducted with the Robotics Toolbox [90]. Recalling the simulation results in Chapter 5, impedance control with zero stiffness has been used as the benchmark and it has been shown that the better performance can be guaranteed by the method developed in Chapter 5. As the following simulation conditions are similar to that in Chapter 5, impedance control with zero stiffness will not be considered in this chapter, and only the results with the proposed method in this chapter will be shown.

The robot arm includes two revolute joints and its parameters are: $m_1 = m_2 = 2.0\text{kg}$, $l_1 = l_2 = 0.2\text{m}$, $i_1 = i_2 = 0.027\text{kgm}^2$, and $l_{c1} = l_{c2} = 0.1\text{m}$. The initial positions of the robot arm are $q_1 = -\frac{\pi}{3}$ and $q_2 = \frac{2\pi}{3}$. It is assumed that the human limb exerts the force only in X direction and thus the robot arm in Y direction is interaction-free. Nevertheless, note that in the inner position control loop, the dynamics in two directions are still coupled, i.e., the control performance in one direction still affects that in the other direction. The human limb model is described by $f = \dot{x} + 50(x - x_h) - \frac{0.4x - 0.1\dot{x}}{1+x^2+\dot{x}^2+t^2}$, where the last component $\frac{0.4x-0.1\dot{x}}{1+x^2+\dot{x}^2+t^2}$ stands for the uncertainty.

By adopting the computed-torque control in [28], we set $Y = [\ddot{q}_{r1}, 2\cos(q_2)\ddot{q}_{r1} + \cos(q_2)\ddot{q}_{r2} - \sin(q_2)\dot{q}_{r1} - \sin(q_2)(2\dot{q}_1 + \dot{q}_2)\dot{q}_{r2}, \ddot{q}_{r2}; 0, \cos(q_2)\ddot{q}_{r1} + \sin(q_2)\dot{q}_1\dot{q}_{r1}, \ddot{q}_{r1} + \ddot{q}_{r2}]$. The updating ratio in (6.8), (6.14) and (6.24) is $\gamma = 0.01$.

In the first case, the desired trajectory of the human limb is $x_h = 0.25$ and the

updating law (6.8) is applied. The results in this case are shown in Figs. 6.2-6.6. In Fig. 6.2, it is shown that the obtained desired trajectory of the robot arm, as well as the actual trajectory, tracks the desired trajectory of the human limb. Accordingly, it is found in Fig. 6.3 that the interaction force goes to zero. The above results indicate that the robot arm follows the human limb in such a way that it is able to predict the motion of the human limb. The result of the adaptation parameters is shown in Fig. 6.4, which illustrates that the parameters converge to some constants. The control performance of the inner position control loop is also investigated and the results are shown in Figs. 6.5 and 6.6. Fig. 6.5 shows that the tracking error goes to zero and Fig. 6.6 indicates the convergence of the adaptation parameters.

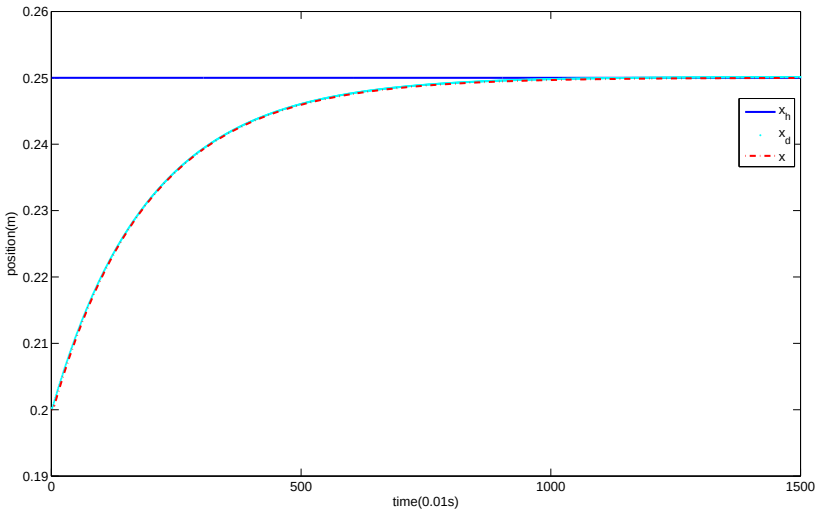

Fig. 6.2: Desired trajectory of human limb, desired trajectory of robot arm, and actual trajectory, in the case of point-to-point movement

In the second case, we consider that the desired trajectory of the human limb is time-varying and periodic, which is given by $x_h = 0.2 + 0.1\sin(\frac{\pi}{2}t)$. Before evaluating the developed updating law (6.14), we still employ the updating law (6.8) used in the first case. The tracking performance and interaction force are shown in Figs. 6.7 and

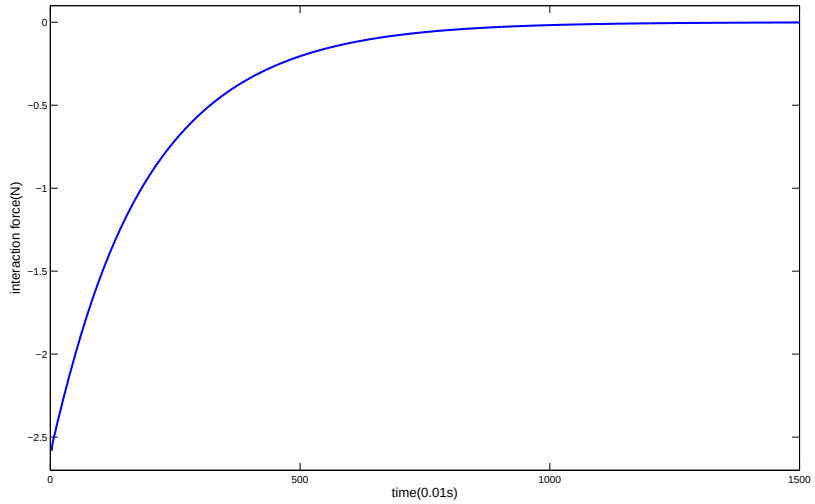

Fig. 6.3: Interaction force, in the case of point-to-point movement

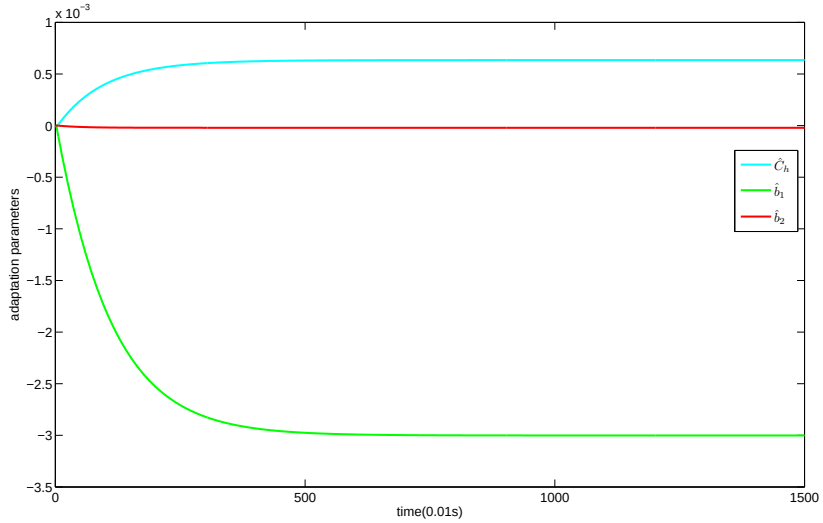

Fig. 6.4: Adaptation parameters, in the case of point-to-point movement

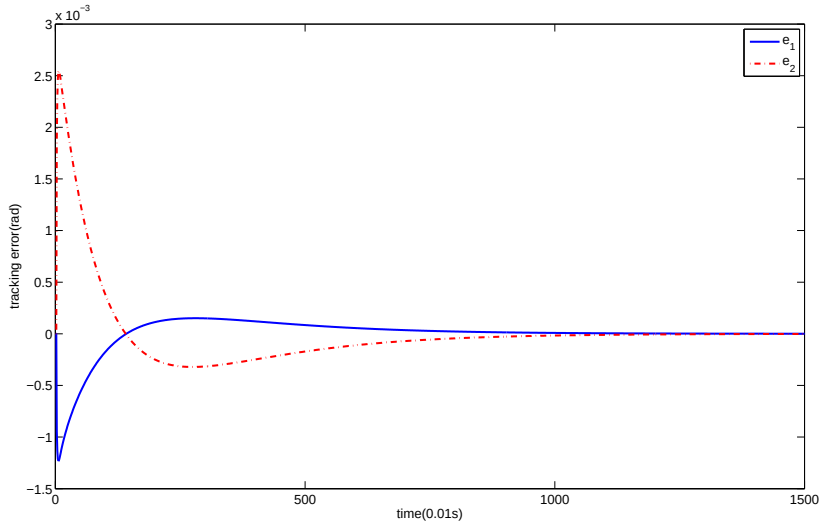

Fig. 6.5: Tracking error of the inner position control loop, in the case of point-to-point movement

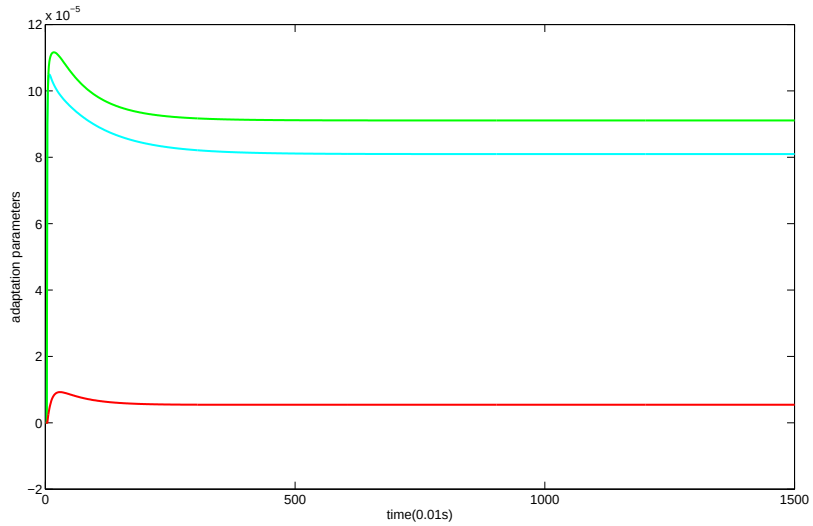

Fig. 6.6: Adaptation parameters of the inner position control loop, in the case of point-to-point movement

6.8, respectively. Obviously, due to the existence of the derivative of x_h, the updating law (6.8) used in the first case fails to guarantee the actual trajectory of the robot arm to track the desired trajectory of the human limb, and thus the interaction force is resulted. Therefore, we employ the updating law (6.14) instead and show the results in Figs. 6.9 and 6.10. In Fig. 6.9, it is shown that after several iterations, the actual trajectory tracks the desired trajectory of the human limb. In Fig. 6.10, it is shown that the interaction force becomes smaller as the iteration number increases. The control performance of the inner position control loop is similar to that in Figs. 6.5 and 6.6, and thus it is omitted. Note that the point-to-point movement in the first case can be considered as a special case of the periodic time-varying trajectory, so the updating law (6.14) is also applicable in the first case. In this regard, the updating law (6.14) can be used in a more general class of applications.

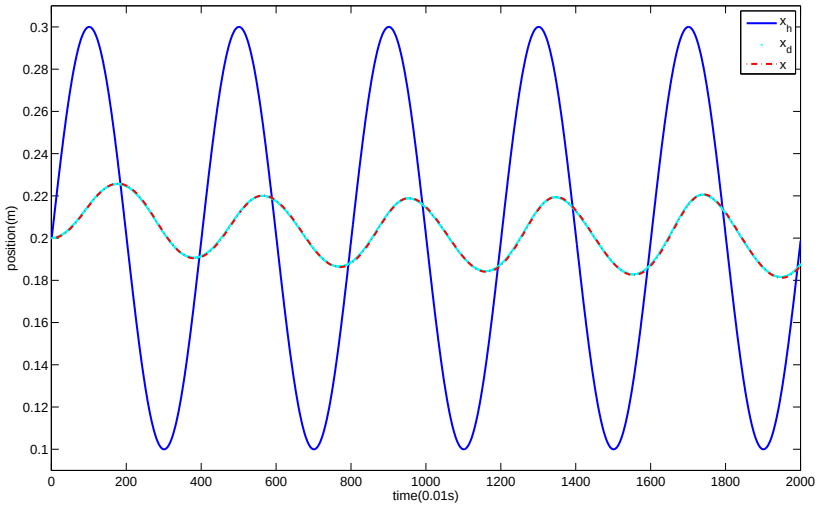

Fig. 6.7: Desired trajectory of human limb, desired trajectory of robot arm, and actual trajectory, in the case of periodic trajectory, with updating law (6.8)

In the last case, we consider a non-periodic trajectory and illustrate that the updating law (6.24) is applicable in this more general case by adopting NN. The

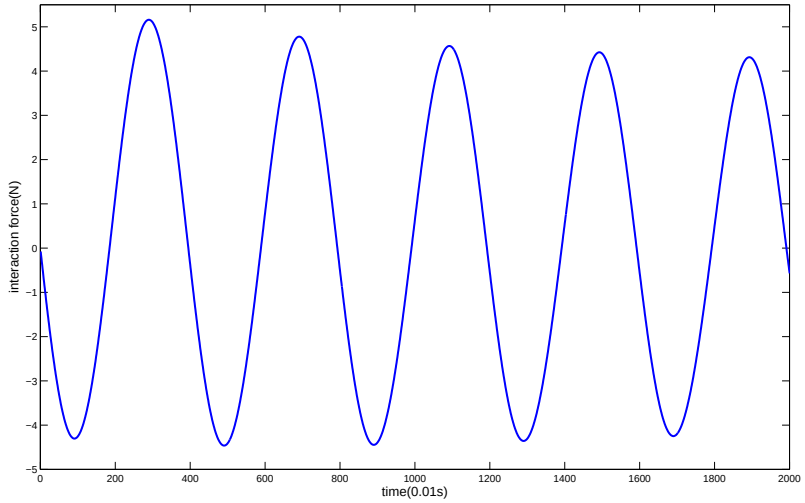

Fig. 6.8: Interaction force, in the case of periodic trajectory, with updating law (6.8)

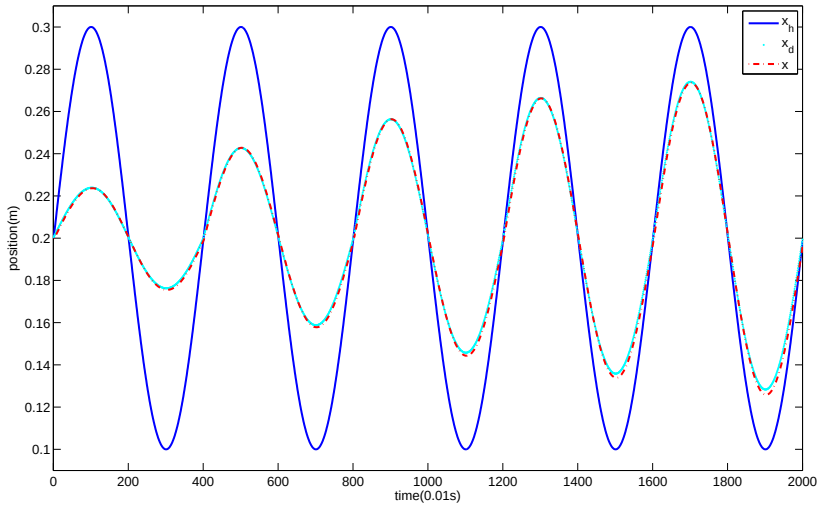

Fig. 6.9: Desired trajectory of human limb, desired trajectory of robot arm, and actual trajectory, in the case of periodic trajectory

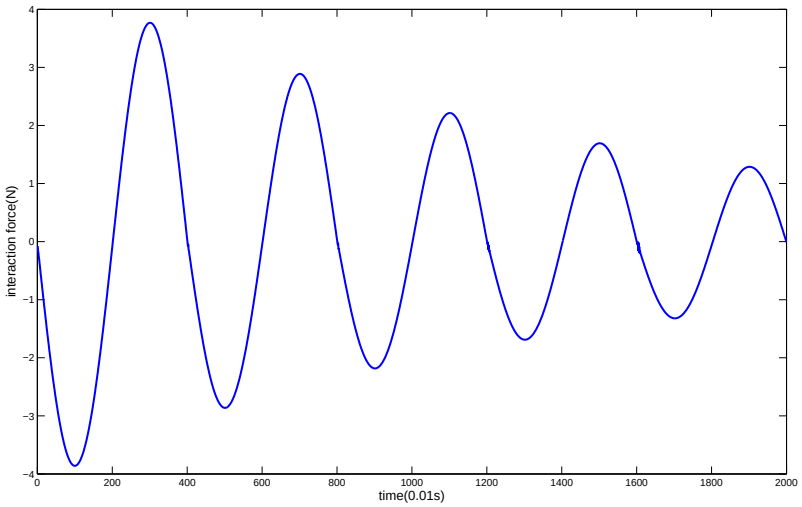

Fig. 6.10: Interaction force, in the case of periodic trajectory

desired trajectory of the human limb is the same as in the second case, which is given by $x_h = 0.2 + 0.1\sin(\frac{\pi}{2}t)$. Only one period is considered so it is non-periodic. The results of trajectory tracking and interaction force are shown in Figs. 6.11 and 6.12, respectively, which validate that the proposed method guarantees the robot arm to follow the human limb actively. Note that the point-to-point movement and periodic trajectory are two special cases of the non-periodic trajectory, so the NN method in the third case is also applicable to the first two cases.

6.5 Experiment

In this section, the proposed method is examined on the robot Nancy which is introduced in Chapters 4 and 5. In this experiment, the human partner uses his hand to move the left wrist of Nancy as shown in Fig. 5.16. Nancy is under position control while its rest position is 0 and its desired trajectory is generated by the proposed

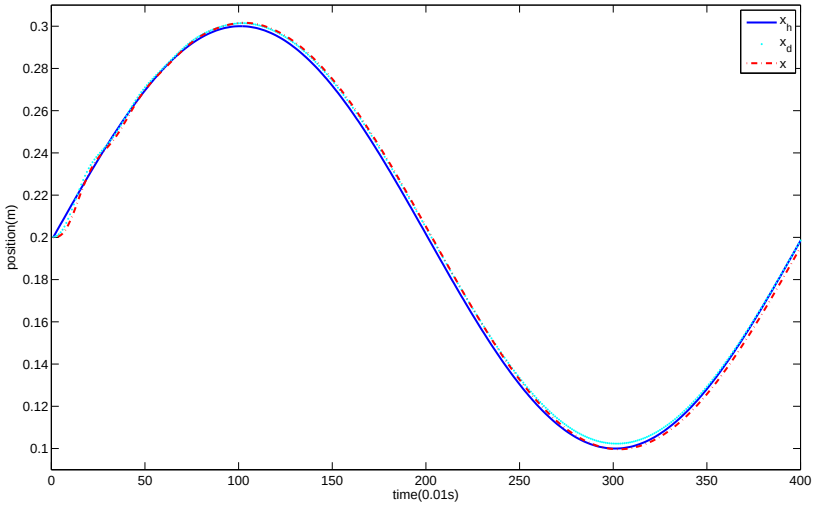

Fig. 6.11: Desired trajectory of human limb, desired trajectory of robot arm, and actual trajectory, in the case of non-periodic trajectory

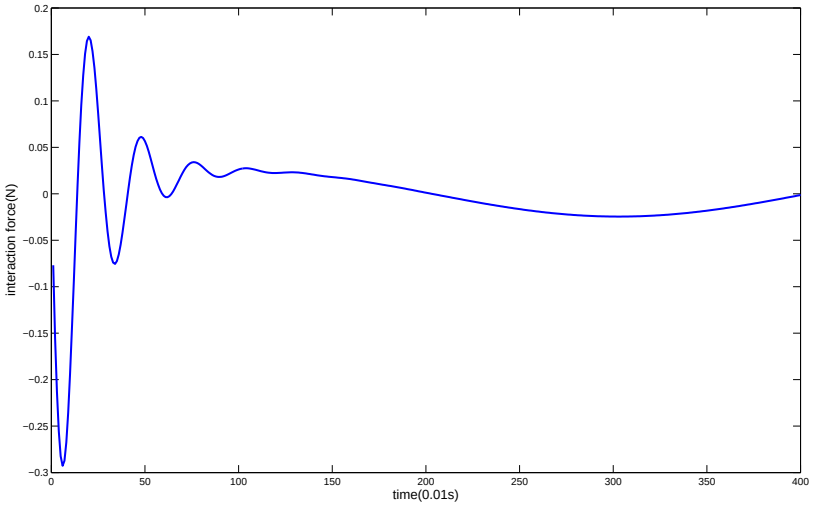

Fig. 6.12: Interaction force, in the case of non-periodic trajectory

method. The objective is to make the left wrist of Nancy follow the movement of human limb and the interaction force measured by the force sensor go to zero. Similarly as in Chapter 5, the human partner's motion intention cannot be measured in the experiment, and the actual trajectory of the robot arm cannot be compared with the motion intention directly. In this situation, we can only understand the experiment results through the actual trajectory and external torque. For the comparison purpose, impedance control with zero stiffness in the previous chapter is employed. Three cases are to be considered in the following, and impedance parameters in (4.1) are $M_x = 0.01$, $C_x = 0.8$, and $G_x = 0$.

In the first case, Nancy's wrist is moved to a target angle and the updating law (6.8) is adopted. The updating ratio is $\gamma = 0.06$. The joint angle and external torque are shown in Figs. 6.13 and 6.14, respectively. It is found that Nancy's wrist can be moved to the target angle and the external torque goes to zero. Compared to the result obtained with impedance control, the external torque with the proposed adaptive control is smaller while the performance of the joint angle is similar. This indicates that the updating law (6.8) is applicable in the case of point-to-point movement. Besides, less effort is needed from the human partner with the proposed method, so the collaboration efficiency can be increased. To show that the updating law (6.8) is only applicable for the point-to-pint movement, Nancy's wrist is moved forward and back between two target angles. The joint angle and external torque with the updating law (6.8) in this case are shown in Figs. 6.15 and 6.16, respectively. These results illustrate that an external torque of around 0.3Nm is needed when the motion direction is changed, and Nancy's wrist cannot follow the motion of human limb "actively".

In the second case, a periodic trajectory is considered. Particularly, Nancy's wrist

is moved forward and back between two target angles in every 12.6s. The updating law (6.14) with the updating ratio $\gamma = 0.36$ is employed in this case. The results are shown in Figs. 6.17 and 6.18. Note that in the first iteration, Nancy's wrist is very "stiff" so an external torque of around 0.4 Nm is needed to move it to the two target angles. As the iteration number increases, the external torque becomes smaller. At the 6th iteration, an external torque of smaller than 0.1Nm is needed to move Nancy's wrist to the target angles. These results indicate that Nancy's wrist starts "actively" following human partner's motion intention, after several iterations. And the validity of the learning method is verified.

In the third case, we consider the time-varying trajectory which has been discussed at the end of the first case. Particularly, Nancy's wrist is moved forward and back between two target angles. The desired trajectory of the human limb in this case is deemed to be an non-periodic trajectory, although it cannot be measured. As discussed before, it stands for a more general situation. The NN method is employed and the updating law (6.24) is adopted with the following parameters: $p = 10$, $\eta_i = 1$, $\mu_i = 0$, and $\gamma = 0.01$. The results in this case are shown in Figs. 6.19 and 6.20. It is noted that a small external torque of about 0.1Nm still exists, which is different from that claimed in Theorem 9 and the simulation results. This may be explained by the following fact. During the experiments, we note that the human partner may change his motion intention according to robot trajectory. This is an interesting issue but was not considered when developing the proposed method. In particular, we assume implicitly that the human motion intention is stationary with respect to the actual robot trajectory, i.e., the adaptation of the robot trajectory has no effect on the human motion intention. However, human motion is also an output of the neuromuscular control system, so the dynamic interaction with the

robot could well result in concurrent adaptations in the human motion intention. This makes the problem more tricky and it will be further investigated in the future work. Nevertheless, it is found that the proposed NN method leads to a faster response and smaller external torque, compared to impedance control with zero stiffness. Recalling the experiment results in Chapter 5, there is not an obvious difference between the method in this chapter and that in Chapter 5. Both of them can be used to guarantee the robot arm to follow human partner "actively", even in the case of non-periodic trajectory.

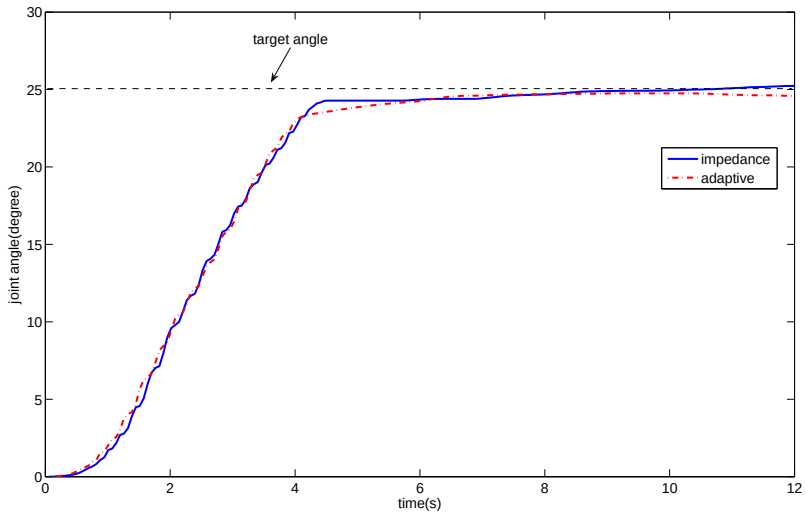

Fig. 6.13: Joint angle, in the case of point-to-point movement, with updating law (6.8)

6.6 Conclusion

In this chapter, zero force regulation has been investigated for human-robot collaboration, such that the robot is able to "actively" follow its human partner. Force

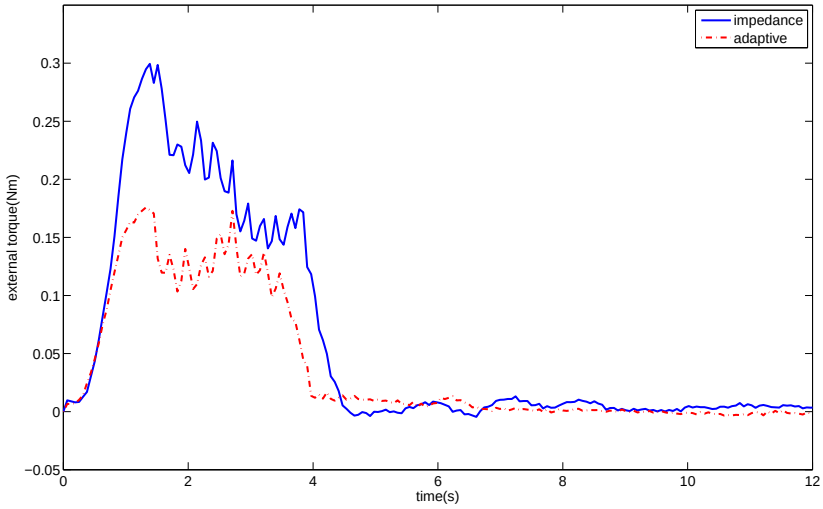

Fig. 6.14: External torque, in the case of point-to-point movement, with updating law (6.8)

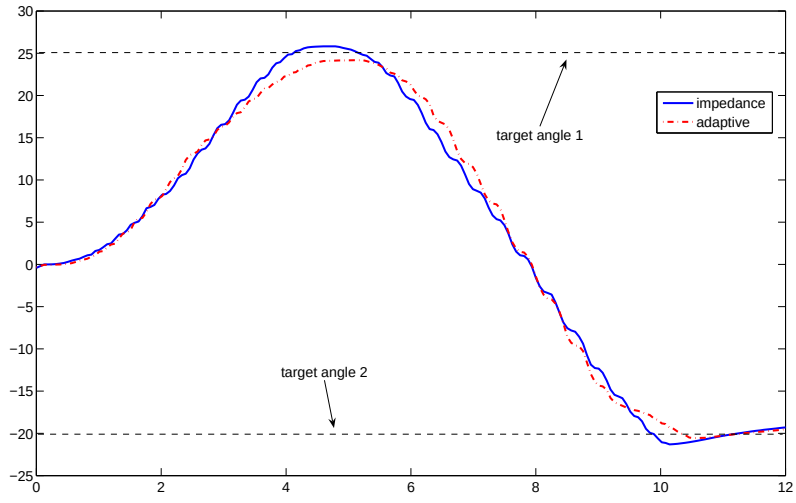

Fig. 6.15: Joint angle, in the case of time-varying trajectory, with updating law (6.8)

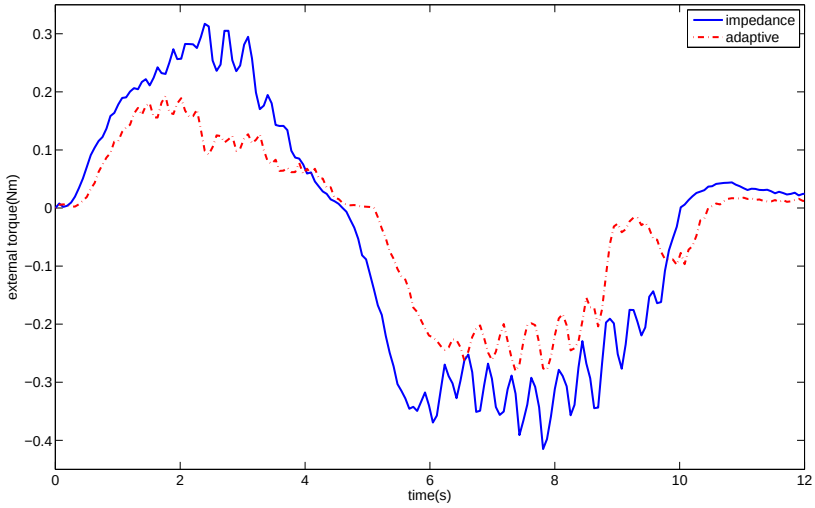

Fig. 6.16: External torque, in the case of time-varying trajectory, with updating law (6.8)

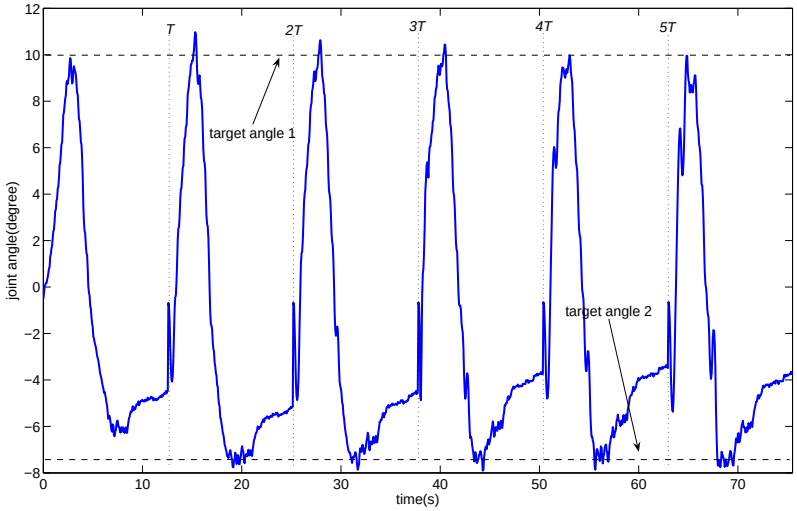

Fig. 6.17: Joint angle, in the case of periodic trajectory

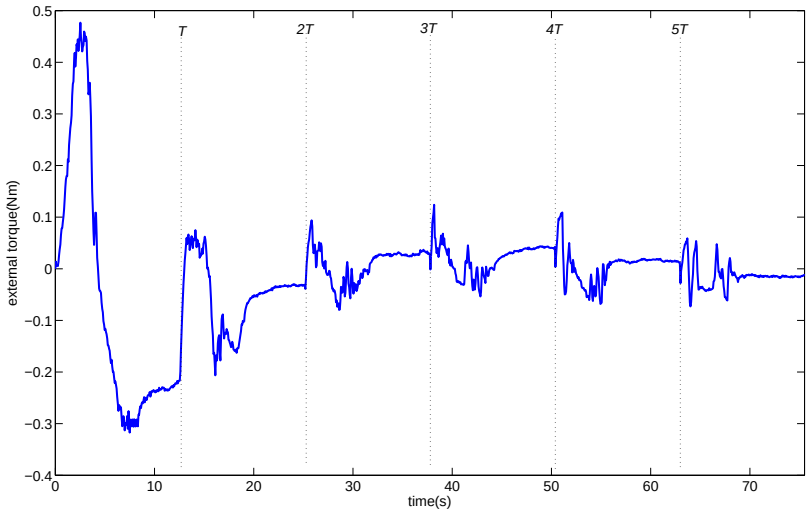

Fig. 6.18: External torque, in the case of periodic trajectory

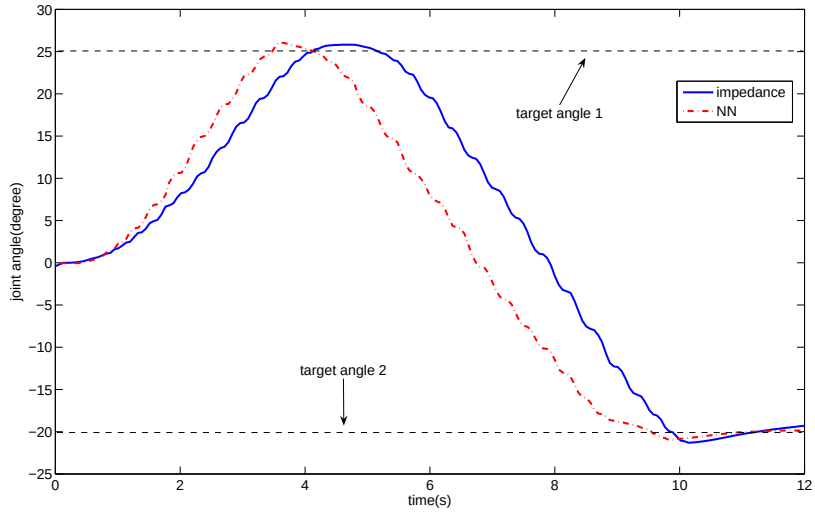

Fig. 6.19: Joint angle, in the case of non-periodic trajectory

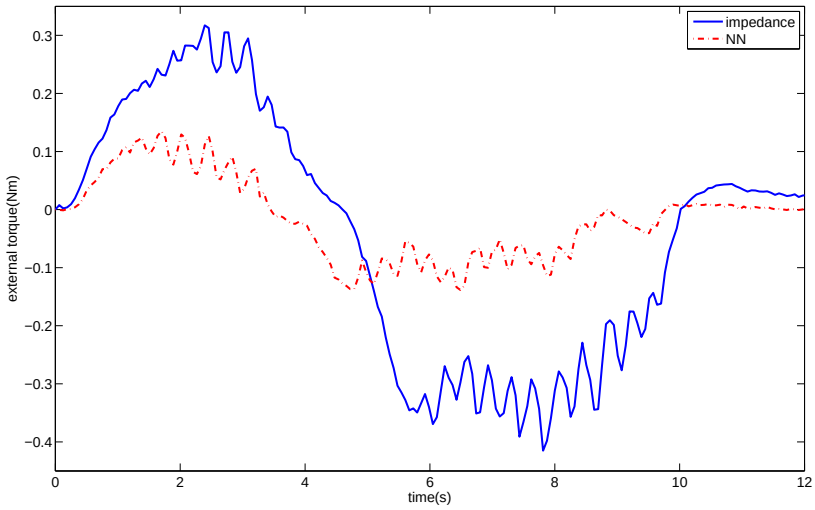

Fig. 6.20: External torque, in the case of non-periodic trajectory

regulation has been achieved under the impedance control framework, subject to uncertain human limb dynamics. Adaptive control has been proposed to deal with the point-to-point movement, and learning control and NN control have been developed to generate periodic and non-periodic trajectories, respectively. The stability and tracking performance of the whole coupled system have been discussed through the rigorous analysis. The validity of the proposed method has been verified through simulation and experiment studies.

Together with Chapter 5, trajectory adaptation has been investigated for a typical human-robot collaboration system. Therefore, the answer of how to obtain the desired rest position in a target impedance model has been partially given. Nevertheless, the discussion only focuses on such a specific case where the control objective is zero force regulation. In many other applications where the control objectives are different, how to obtain the desired rest position is still an open problem and needs to be resolved in the future work.

Chapter 7

Conclusion and Future Work

Robots are expected to participate in and learn from intuitive, long term interaction with humans, and be safely deployed in myriad social applications ranging from elderly care, entertainment to education. They are also envisioned to collaborate and co-work with human beings in the foreseeable future for productivity, service, and operations with guaranteed quality. In all these applications, robots which are stiff and tightly controlled in position will face problems such as saturation, instability, and physical failure, when they interact with unknown environments. In this thesis, we have investigated the control problems of robots interacting with unknown environments. The achievements, possible limitations, and possible future works are summarized in the following sections.

7.1 Conclusion

7.1.1 Impedance Control Design

Impedance control has been employed as the fundamental of this thesis. Impedance control design subject to unknown and uncertain robot dynamics has been discussed in the first part of this thesis. First, an auxiliary error variable has been introduced such that it is possible to extend existing methods in position control to impedance control. Based on the LIP property, learning impedance control has been developed but it requires the knowledge of the robot structure. Based on the boundedness property, learning impedance control which requires neither the knowledge of the robot structure nor that of physical parameters has been developed. As further discussed, if the bounds of the robot dynamics are known, the learning process is avoided while the high-gain scheme can be adopted. Although the method based on the boundedness property provides the design simplicity, it is found that there is chattering when the defined impedance error becomes very small. This problem has been resolved by utilizing function approximators. Finally, neither the LIP property nor the boundedness property was needed in the proposed NN method. The control performance of all the proposed methods has been discussed through rigorous proof and remarking arguments. The simulation results have shown the validity of the proposed methods and superiority over the existing methods.

7.1.2 Impedance Learning

Impedance learning for robots interacting with unknown environments has been investigated in Chapter 4. A learning framework has been developed to obtain desired

impedance parameters subject to unknown dynamic environments. The proposed impedance learning has employed gradient-following and betterment schemes, which has a simple and straightforward formulation. It is applicable for different control objectives such as trajectory tracking, force regulation and the combination/comprimise of these two. The resulted variant impedance control is preferred than impedance control with fixed impedance parameters because the environments are dynamically changing. Besides, the learning capability of the proposed method makes the control design easier which is simply to choose a cost function determining the interaction performance. The feasibility and validity of the proposed method have been verified by simulation and experiment studies.

7.1.3 Trajectory Adaptation

Besides impedance learning, trajectory adaptation is another human skill which can be realized by robot control. In Chapters 5 and 6, trajectory adaptation has been investigated for a typical human-robot collaboration system. In Chapter 5, the motion intention of the human partner has been observed by employing the human limb model and estimating the desired trajectory. A NN method has been proposed to cope with the problem of unknown human limb model. The estimated motion intention has been integrated into impedance control of the robot arm, such that it actively follows its human partner. As human partner and robot are considered to be two subsystems in Chapter 5, the performance of the whole coupled collaboration system has been analyzed in Chapter 6. In particular, zero force regulation has been investigated for human-robot collaboration and it has been achieved under the impedance control framework, subject to uncertain human limb dynamics. Adaptive control has been proposed to deal with the point-to-point movement, and learning

control and NN control have been developed to generate periodic and non-periodic trajectories, respectively. The stability and tracking performance of the whole coupled system have been discussed through the rigorous analysis. The validity of the proposed methods has been verified through simulation and experiment studies.

7.2 Future Work

By employing the methods discussed above, robots can be deployed in a large class of applications where they interact with unknown environments, such as robotic rehabilitation [117], teleoperation [118], dexterous manipulation [119], and human-robot collaboration [68]. However, it is obvious that robots are still not "intelligent" enough to understand circumstances, make decisions and solve problems, like human beings. One possible reason is sensory information limit. For example, the noncontact measurement of the environment is allowed with the help of cameras in image-based control, which will make robots to make decisions more easily [120]. Therefore, it is important to take other sensory information (e.g, image), rather than only position and force, into account for robots interacting with unknown environments. This will be investigated in our future work.

Compared to impedance learning discussed in this thesis, impedance adaptation seems more interesting but it is also more challenging. It is interesting because it does not require the robot to repeat operations to learn the desired impedance parameters. This is important because to make the robot repeat operations may cause inconvenience in many situations. It is challenging because to develop an adaptive scheme usually requires that a certain variable is invariant but this is difficult to satisfy in the case of dynamically changing environment. There has been research effort made

on impedance adaptation in the literature [121], but it is limited in the case of known environments. Therefore, how to adjust impedance parameters adaptively subject to unknown dynamically changing environments needs to be further investigated. For trajectory adaptation, the discussion in this thesis only focuses on human-robot collaboration which is a specific case of robots interacting with unknown environments, and the control objective is zero force regulation. In many other applications where the control objectives are different, how to obtain the desired rest position is still an open problem [122]. Besides, impedance learning and trajectory adaptation have been individually discussed in this thesis. From the experience of human beings physically interacting with environments, it seems that impedance parameters and rest position are supposed to be simultaneously adjusted during the interaction. This hypothesis will be thoroughly justified and considered in the future work and applied to robot control.

Furthermore, practical issues such as time-delay and human factor in the real-world implementations will also be taken into account. For example, in the part of trajectory adaptation in this thesis, we assume implicitly that the human motion intention is stationary with respect to the actual robot trajectory. In other words, the adaptation of the robot trajectory is assumed to have no effect on the human motion intention. However, human motion is also an output of the neuromuscular control system, so the dynamic interaction with the robot could well result in concurrent adaptations in the human motion intention. This makes the problem more tricky but also more interesting, which will be investigated in the future work.

Bibliography

[1] S. Katsura and K. Ohnishi, "Human cooperative wheelchair for haptic interaction based on dual compliance control," *IEEE Transactions on Industrial Electronics*, vol. 51, no. 1, pp. 221–228, 2004.

[2] K. Morioka, J.-H. Lee, and H. Hashimoto, "Human-following mobile robot in a distributed intelligent sensor network," *IEEE Transactions on Industrial Electronics*, vol. 51, no. 1, pp. 229–237, 2004.

[3] S. S. Ge, "People in control," *IEEE Control Systems Magazine*, vol. 31, pp. 29–34, 2011.

[4] C. L. Breazeal, *Designing Sociable Robots*. Cambridge: The MIT Press, 2002.

[5] H. Kazerooni, T. B. Sheridan, and P. K. Houpt, "Robust compliant motion for manipulators, part I: the fundamental concepts of compliant motion," *IEEE Journal of Robotics and Automation*, vol. RA-2, no. 2, pp. 83–92, 1986.

[6] M. D. Queiroz, J. Hu, D. Dawson, T. Burg, and S. Donepudi, "Adaptive position/force control of robot manipulators without velocity measurements: Theory and experimentation," *IEEE Transactions on Systems, Man and Cybernetics-Part B: Cybernetics*, vol. 27, no. 5, pp. 796–809, 1997.

[7] K. Dupree, C. H. Liang, G. Hu, and W. E. Dixon, "Adaptive Lyapunov-based control of a robot and mass-spring system undergoing an impact collision," *IEEE Transactions on Systems, Man and Cybernetics-Part B: Cybernetics*, vol. 38, no. 4, pp. 1050–1061, 2008.

[8] J. T. Wen and S. Murphy, "Stability analysis of position and force control for robot arms," *IEEE Transactions on Automatic Control*, vol. 36, no. 3, pp. 365–369, 1991.

[9] W. S. Newman, "Stability and performance limits of interaction controllers," *ASME Journal of Dynamic Systems, Measurement, and Control*, vol. 114, pp. 563–570, 1992.

[10] R. Volpe and P. Khosla, "A theoretical and experimental investigation of explicit force control strategies for manipulators," *IEEE Transactions on Automatic Control*, vol. 38, no. 11, pp. 1634–1650, 1993.

[11] L. Huang, S. S. Ge, and T. H. Lee, "Fuzzy unidirectional force control of constrained robotic manipulators," *Fuzzy Sets and Systems*, vol. 134, no. 1, pp. 135–146, 2003.

[12] ——, "Position/force control of uncertain constrained flexible joint robots," *Mechatronics*, vol. 16, no. 2, pp. 111–120, 2006.

[13] N. Hogan, "Impedance control: an approach to manipulation-Part I: Theory; Part II: Implementation; Part III: Applications," *Journal of Dynamic Systems, Measurement, and Control*, vol. 107, no. 1, pp. 1–24, 1985.

[14] J. E. Colgate and N. Hogan, "Robust control of dynamically interacting systems," *International Journal of Control*, vol. 48, no. 1, pp. 65–88, 1988.

[15] J. J. Gonzalez and G. R. Widmann, "A force commanded impedance control scheme for robots with hard nonlinearities," *IEEE Transactions on Control Systems Technology*, vol. 3, no. 4, pp. 398–408, 1995.

[16] C. H. Wu, , K. S. Hwang, and S. L. Chang, "Analysis and implementation of a neuromuscular-like control for robotic compliance," *IEEE Transactions on Control Systems Technology*, vol. 5, no. 6, pp. 586–597, 1997.

[17] R. B. Gillespie, J. E. Colgate, and M. A. Peshkin, "A general framework for cobot control," *IEEE Transactions on Robotics and Automation*, vol. 17, no. 4, pp. 391–401, August 2001.

[18] Y. Hirata, T. Takagi, K. Kosuge, H. Asama, H. Kaetsu, and K. Kawabata, "Manipulation of a large object by multiple dr helpers in cooperation with a human," *Proceedings of the IEEE/RSJ International Conference on Intelligent Robots and Systems*, pp. 126–131, 2001.

[19] K. M. Lynch, C. Liu, A. Sorensen, S. Kim, M. Peshkin, J. E. Colgate, T. Tickel, D. Hannon, and K. Shiels, "Motion guides for assisted manipulation," *The International Journal of Robotics Research*, vol. 21, no. 1, pp. 27–43, January 2002.

[20] E. Lee, J. Park, K. A. Loparo, C. B. Schrader, and P. H. Chang, "Bang-bang impact control using hybrid impedance/time-delay control," *IEEE/ASME Transactions on Mechatronics*, vol. 8, no. 2, pp. 272–277, 2003.

[21] Y. Hirata, H. Song, Z. Wang, and K. Kosuge, "Control of passive object handling robot with free joint for reducing human assistive force," *Proceedings of the IEEE/RSJ International Conference on Intelligent Robots and Systems*, pp. 1154–1159, October 2007.

[22] Y. Hirata, Y. Ojima, and K. Kosuge, "Variable motion characteristics control of an object by multiple passive mobile robots in cooperation with a human," *Proceedings of the International Conference on Robotics and Automation*, pp. 1346–1351, May 2008.

[23] Y. Hirata, Z. Wang, K. Fukaya, and K. Kosuge, "Transporting an object by a passive mobile robot with servo brakes in cooperation with a human," *Advanced Robotics*, vol. 23, pp. 387–404, 2009.

[24] S. P. Buerger, "Stable, high-force, low-impedance robotic actuators for human-interactive machines," Ph.D. dissertation, MIT, Department of Mechanical Engineering, 2005.

[25] D. A. Lawrence, M. Marietta, and C. O. Denver, "Impedance control stability properties in common implementations," *Proceedings of the 1988 IEEE International Conference on Robotics and Automation*, pp. 1185–1190, 1998.

[26] I. Bonilla, F. Reyes, M. Mendoza, and E. J. Gonzalez-Galvan, "A dynamic-compensation approach to impedance control of robot manipulators," *Journal of Intelligent and Robotic Systems*, vol. 63, pp. 51–73, 2011.

[27] Z. M. Sotirov and R. G. Botev, "A model reference approach to adaptive impedance control of robot manipulators," *Proceedings of the 1993 IEEE/RSJ International Conference on Intelligent Robots and Systems*, pp. 727–733, 1993.

[28] J. J. E. Slotine and W. Li, "On the adaptive control of robotic manipulators," *The International Journal of Robotics Research*, vol. 6, no. 3, 1987.

[29] W.-S. Lu and Q.-H. Meng, "Impedance control with adaptation for robotic

manipulations," *IEEE Transactions on Robotics and Automation*, vol. 7, no. 3, pp. 408–415, 1991.

[30] D. Dawson and Z. Qu, "Comments on 'Impedance control with adaptation for robotic manipulations'," *IEEE Transactions on Robotics and Automation*, vol. 7, no. 6, pp. 879–881, 1991.

[31] W.-S. Lu and Q.-H. Meng, "Reply to "Comments on 'Impedance control with adaptation for robotic manipulations'"," *IEEE Transactions on Robotics and Automation*, vol. 7, no. 6, p. 881, 1991.

[32] Z. H. Jiang, "Impedance control of flexible robot arms with parametric uncertainties," *Journal of Intelligent and Robotic Systems*, vol. 42, pp. 113–133, 2005.

[33] M. C. Chien and A. C. Huang, "Adaptive impedance control of robot manipulators based on function approximation technique," *Robotica*, vol. 22, pp. 395–403, 2004.

[34] R. Colbaugh, H. Seraji, and K. Glass, "Direct adaptive impedance control of manipulators," *Proceedings of the 30th Conference on Decision and Control*, pp. 2410–2415, 1991.

[35] K. Wedeward and R. Colbaugh, "New stability results for direct adaptive impedance control," *Proceedings of the 1995 IEEE International Symposium on Intelligent Control*, pp. 281–287, 1995.

[36] S. S. Ge, C. C. Hang, L. C. Woon, and X. Q. Chen, "Impedance control of robot manipulators using adaptive neural networks," *International Journal of Intelligent Control and Systems*, vol. 2, no. 3, pp. 433–452, 1998.

[37] L. Huang, S. S. Ge, and T. H. Lee, "Neural network based adaptive impedance control of constrained robots," *International Journal of Robotics and Automation*, vol. 19, no. 3, pp. 117–124, 2004.

[38] M. Sun and S. S. Ge, "Adaptive repetitive control for a class of nonlinearly parametrized systems," *IEEE Transactions on automatic control*, vol. 51, no. 10, pp. 1684–1688, 2006.

[39] T. Kuc and J. S. Lee, "An adaptive learning control of uncertain robotic systems," *Proceedings of the 30th Conference on Decision and Control*, no. 9, pp. 1206–1211, 1991.

[40] D. Wang and C. C. Cheah, "An iterative learning-control scheme for impedance control of robotic manipulators," *The International Journal of Robotics Research*, vol. 17, no. 10, pp. 1091–1099, 1998.

[41] C. C. Cheah and D. Wang, "Learning impedance control for robotic manipulators," *IEEE Transactions on Robotics and Automation*, vol. 14, no. 3, pp. 452–465, 1998.

[42] R. Ikeura and H. Inooka, "Variable impedance control of a robot for cooperation with a human," *Proceedings of the 1995 IEEE International Conference on Robotics and Automation*, pp. 3097–3102, 1995.

[43] T. Tsumugiwa, R. Yokogawa, and K. Hara, "Variable impedance control with regard to working process for man-machine cooperation-work system," *Proceedings of IEEE/RSJ International Conference on Intelligent Robots and Systems*, pp. 1564–1569, 2001.

[44] R. Ikeura, T. Moriguchi, and K. Mizutani, "Optimal variable impedance control

for a robot and its application to lifting an object with a human," *Proceedings of the International Workshop on Robot and Huamn Interactive Communication*, pp. 500–505, 2002.

[45] M. M. Rahman, R. Ikeura, and K. Mizutani, "Investigation of the impedance characteristic of human arm for development of robots to cooperate with humans," *JSME International Journal Series C*, vol. 45, no. 2, pp. 510–518, 2002.

[46] T. Tsumugiwa, R. Yokogawa, and K. Hara, "Variable impedance control based on estimation of human arm stiffness for human-robot cooperative calligraphic task," *Proceedings of the 2002 IEEE International Conference on Robotics and Automation*, pp. 644–650, 2002.

[47] S. P. Buerger and N. Hogan, "Complementary stability and loop shaping for improved human-robot interaction," *IEEE Transactions on Robotics*, vol. 23, no. 2, pp. 232–244, 2007.

[48] B. Siciliano, L. Sciavicco, L. Villani, and G. Oriolo, *Robotics: Modelling, Planning and Control*. Springer Verlag, 2009.

[49] J. de Gea and F. Kirchner, "Contact impedance adaptation via environment identification," *Proceedings of IEEE International Symposium on Industrial Electronics*, pp. 1365–1370, 2008.

[50] T. Yamamoto, M. Bernhardt, A. Peer, M. Buss, and A. M. Okamura, "Techniques for environment parameter estimation during telemanipulation," *The 2nd IEEE RAS and EMBS International Conference on Biomedical Robotics and Biomechatronics*, pp. 217–223, 2008.

[51] D. Mitrovic, S. Klanke, and S. Vijayakumar, "Learning impedance control of

antagonistic systems based on stochastic optimization principles," *The International Journal of Robotics Research*, vol. 30, no. 5, pp. 556–573, 2011.

[52] J. Buchli, F. Stulp, E. Theodorou, and S. Schaal, "Learning variable impedance control," *International Journal of Robotics Research*, vol. 30, pp. 820–833, 2011.

[53] C. Yang, G. Ganesh, S. Haddadin, S. Parusel, A. Albu-Schaeffer, and E. Burdet, "Human-like adaptation of force and impedance in stable and unstable interactions," *IEEE Transactions on Robotics*, vol. 27, no. 5, pp. 918–936, 2011.

[54] M. Cohen and T. Flash, "Learning impedance parameters for robot control using an associative search network," *IEEE Transactions on Robotics and Automation*, vol. 7, no. 3, pp. 382–390, June 1991.

[55] T. Tsuji and P. G. Morasso, "Neural network learning of robot arm impedance in operational space," *IEEE Transactions on Systems, Man and Cybernetics-Part B: Cybernetics*, vol. 26, no. 2, pp. 290–298, 1996.

[56] D. S. M. F. A. Albers, S. Schillo and P. Meckl, "A new two-layer reinforcement learning approach the control of a 2DOF manipulator," *2010 8th IEEE International Conference on Control and Automation (ICCA)*, pp. 546–551, 2010.

[57] R. S. Sutton and A. G. Barto, *Reinforcement Learning: An Introduction*. Cambridge, MA, USA: MIT Press, 1998.

[58] B. Kim, J. Park, S. Park, and S. Kang, "Impedance learning for robotic contact tasks using natural actor-critic algorithm," *IEEE Transactions on Systems, Man and Cybernetics-Part B: Cybernetics*, vol. 40, no. 2, pp. 433–443, 2010.

[59] B. H. Yang and H. Asada, "Progressive learning and its application to robot

impedance learning," *IEEE Transactions on Neural Networks*, pp. 941–952, 1996.

[60] K. Kosuge, Y. Fujisawa, and T. Fukuda, "Mechanical system control with man-machine-environment interactions," *Proceedings of the 1993 IEEE International Conference on Robotics and Automation*, pp. 239–244, 1993.

[61] K. Kosuge, H. Yoshida, and T. Fukuda, "Dynamic control for robot-human collaboration," *Proceedings of the 2nd IEEE International Workshop on Robot and Human Communication*, pp. 398–401, 1993.

[62] K. Kosuge, M. Sato, and N. Kazamura, "Mobile robot helper," *Proceedings of the 2000 IEEE International Conference on Robotics and Automation*, pp. 583–588, 2000.

[63] K. Iqbal and Y. F. Zheng, "Arm-manipulator coordination for load sharing using predictive control," *Proceedings of IEEE International Conference on Robotics and Automation*, pp. 2539–2544, 1999.

[64] N. Jarrasse, V. Pasqui, and G. Morel, "How can human motion prediction increase transparency?" *Proceedings of the 2008 IEEE International Conference on Robotics and Automation*, pp. 2134–2139, 2008.

[65] R. O. Saber, "Flexible cooperation between human and robot by interpreting human intention from gaze information," *Proceedings of 2004 IEEE/RSJ International Conference on Intelligent Robots and Systems*, pp. 846–851, 2004.

[66] K. B. Reed and M. A. Peshkin, "Physical collaboration of human-human and human-robot teams," *IEEE Transactions on Haptics*, vol. 1, no. 2, pp. 108–120, 2008.

[67] V. Duchaine and C. Gosselin, "Safe, stable and intuitive control for physical human-robot interaction," *Proceedings of the 2009 IEEE International Conference on Robotics and Automation*, pp. 3676–3681, 2009.

[68] ——, "Stable and intuitive control of an intelligent assist device," *IEEE Transactions on Haptics*, vol. 5, no. 2, pp. 148–159, 2012.

[69] E. Burdet and T. E. Milner, "Quantization of human motions and learning of accurate movements," *Biological Cybernetics*, no. 78, pp. 307–318, 1998.

[70] B. Corteville, E. Aertbelien, H. Bruyninckx, J. D. Schutter, and H. V. Brussel, "Human-inspired robot assistant for fast point-to-point movements," *Proceedings of the 2007 IEEE International Conference on Robotics and Automation*, pp. 3639–3644, 2007.

[71] M. S. Erden and T. Tomiyama, "Human-intent detection and physically interactive control of a robot without force sensors," *IEEE Transactions on Robotics*, vol. 26, no. 2, pp. 370–382, 2010.

[72] Z. Wang, A. Peer, and M. Buss, "An hmm approach to realistic haptic human-robot interaction," *Proceedings of the Third Joint Eurohaptics Conference and Symposium on Haptic Interfaces for Virtual Environment and Teleoperator Systems*, pp. 374–379, 2009.

[73] K. Wakita, J. Huang, P. Di, K. Sekiyama, and T. Fukuda, "Human-walking-intention-based motion control of an omnidirectional-type cane robot," *IEEE/ASME Transactions on Mechatronics*, 2011.

[74] Y. Chua, K. P. Tee, and R. Yan, "Human-robot motion synchronization using

reactive and predictive controllers," *Proceedings of the 2010 IEEE International Conference on Robotics and Biomimetics*, pp. 223–228, 2010.

[75] F. L. Lewis, S. Jagannathan, and A. Yesildirek, *Neural Network Control of Robot Manipulators and Nonlinear Systems*. London : Taylor & Francis, 1999.

[76] J. H. Chung, "Control of an operator-assisted mobile robotic system," *Robotica*, vol. 20, pp. 439–446, 2002.

[77] R. Z. Stanisic and A. V. Fernandez, "Simultaneous velocity, impact and force control," *Robotica*, vol. 27, pp. 1039–1048, 2009.

[78] H. Seraji and R. Colbaugh, "Force tracking in impedanc control," *International Journal of Robotics Research*, vol. 16, no. 1, pp. 97–117, 1997.

[79] S. Jung and T. C. Hsia, "Robust neural force control scheme under uncertainties in robot dynamics and unknown environment," *IEEE Transactions on Industrial Electronics*, vol. 47, no. 2, pp. 403–412, 2000.

[80] S. Jung, T. C. Hsia, and R. G. Bonitz, "Force tracking impedance control of robot manipulators under unknown environment," *IEEE Transactions on Control Systems Technology*, vol. 12, no. 3, pp. 474–483, 2004.

[81] K. Lee and M. Buss, "Force tracking impedance control with variable target stiffness," *Proceedings of the 17th IFAC World Congress*, vol. 17, pp. 6751–6756, 2008.

[82] R. Z. Stanisic and A. V. Fernandez, "Adjusting the parameters of the mechanical impedance for velocity, impact and force control," *Robotica*, vol. 30, pp. 583–597, 2012.

[83] S. S. Ge, T. H. Lee, and C. J. Harris, *Adaptive Neural Network Control of Robotic Manipulators*. London: World Scientific, 1998.

[84] L. L. Whitcomb, A. A. Rizzi, and D. E. Koditschek, "Comparative experiments with a new adaptive controller for robot arms," *IEEE Transactions on Robotics and Automation*, vol. 9, no. 1, pp. 59–70, 1993.

[85] S. Arimoto, "Fundamental problems of robot control: part I, innovations in the realm of robot servo-loops," *Robotica*, vol. 13, pp. 19–27, 1995.

[86] ——, "Fundamental problems of robot control: part II, nonlinear circuit theory towards an understanding of dexterous motions," *Robotica*, vol. 13, pp. 111–122, 1995.

[87] A. Tayebi, "Adaptive iterative learning control for robot manipulators," *Automatica*, vol. 40, no. 7, pp. 1195–1203, 2004.

[88] F. Ghorbel1, B. Srinivasan, and M. W. Spong, "On the uniform boundedness of the inertia matrix of serial robot manipulators," *Journal of Robotic Systems*, vol. 15, no. 1, pp. 17–28, 1998.

[89] J. X. Xu, V. Badrinath, and Z. Qu, "Robust learning control for robotic manipulators with an extension to a class of nonlinear systems," *International Journal of Control*, vol. 73, no. 10, pp. 858–870, 2000.

[90] P. I. Corke, "A robotics toolbox for MATLAB," *IEEE Robotics and Automation Magazine*, vol. 3, no. 1, pp. 24–32, Mar. 1996.

[91] A. R. Barron, "Universal approximation bounds for superposition for a sigmoidal function," *IEEE Transactions on Information Theory*, vol. 39, no. 3, pp. 930–945, 1993.

[92] T. P. Chen and H. Chen, "Approximation capability to functions of several variables, nonlinear functionals, and operators by radial basis function neural networks," *IEEE Transactions on Neural Networks*, vol. 6, no. 4, pp. 904–910, 1995.

[93] V. Cherkassky, D. Ghering, and F. Mulier, "Comparison of adaptive methods for function estimation from samples," *IEEE Transactions on Neural Networks*, vol. 7, no. 4, pp. 969–984, 1996.

[94] S. S. Ge, C. C. Hang, and L. C. Woon, "Adaptive neural network control of robot manipulators in task space," *IEEE Transactions on Industrial Electronics*, vol. 44, no. 6, pp. 746–752, 1997.

[95] S. C. Tong, Y. M. Li, and P. Shi, "Fuzzy adaptive backstepping robust control for siso nonlinear system with dynamic uncertainties," *Information Sciences*, vol. 179, pp. 1319–1332, 2009.

[96] S. Arimoto, S. Kawamura, and F. Miyazaki, "Bettering operation of robots by learning," *Journal of Robotic Systems*, vol. 1, no. 2, pp. 123–140, 1984.

[97] S. Arimoto, "Equivalence of learnability to output-dissipativity and application for control of nonlinear mechanical systems," *Proceedings of the 1999 IEEE International Conference on Systems, Man, and Cybernetics*, vol. 5, pp. 39–44, 1995.

[98] S. Arimoto, P. T. A. Nguyen, and T. Naniwa, "Learning of robot tasks on the basis of passivity and impedance concepts," *Robotics and Autonomous Systems*, vol. 32, pp. 79–87, 2000.

[99] S. Arimoto, "Passivity-based control," *Proceedings of the 1999 IEEE International Conference on Robotics and Automation*, pp. 227–232, 2000.

[100] R. Johansson and M. W. Spong, "Quadratic optimization of impedance control," *Proceedings of IEEE International Conference of Robotics and Automation*, vol. 1, pp. 616–621, 1994.

[101] D. J. Braun, M. Howard, and S. Vijayakumar, "Optimal variable stiffness control: formulation and application to explosive movement tasks," *Autonomous Robots*, vol. 33, pp. 237–253, 2012.

[102] S. S. Ge, J. J. Cabibihan, Z. Zhang, Y. Li, C. Meng, H. He, M. R. Safizadeh, Y. B. Li, and J. Yang, "Design and development of Nancy, a social robot," *Proceedings of the International Conference on Ubiquitous Robots and Ambient Intelligence*, pp. 568–573, 2011.

[103] T. Flash, "The control of hand equilibrium trajectories in multi-jioint arm movement," *Biological Cybernetics*, vol. 57, no. 4-5, pp. 257–274, 1987.

[104] K. K. Tan, S. Zhao, and S. Huang, "Iterative reference adjustment for high-precision and repetitive motion control applications," *IEEE Transactions on Control Systems Technology*, vol. 13, no. 1, pp. 85–97, 2005.

[105] D. Gorinevsky, "On the persistency of excitation in radial basis function network identification of nonlinear systems," *IEEE Transactions on Neural Networks*, vol. 6, no. 5, pp. 1237–1244, 1995.

[106] V. D. Sapio, J. Warren, O. Khatib, and S. Delp, "Simulating the task-level control of human motion: a methodology and framework for implementation," *The Visual Computer*, vol. 21, pp. 289–302, 2005.

[107] R. Colbaugh and K. Glass, "Cartesian control of redundant robots," *Journal of Robotic Systems*, vol. 6, no. 4, pp. 427–459, 1989.

[108] H. Seraji and R. Colbaugh, "Singularity-robustness and task-prioritization in configuration control of redudant robots," *Proceedings of the 1990 IEEE Conference on Decision and Control*, pp. 3089–3095, December 1990.

[109] O. Khatib, "Inertial properties in robotic manipulation: an object-level framework," *The International Journal of Robotics Research*, vol. 13, no. 1, pp. 19–36, February 1995.

[110] O. Khatib, J. Warren, V. D. Sapio, and L. Sentis, "Human-like motion from physiologically-based potential energies," *On Advances in Robot Kinematics*, pp. 149–163, 2004.

[111] A. Spiers, G. Herrmann, C. Melhuish, T. Pipe, and A. Lenz, "Robotic implementation of realistic reaching motion using a sliding mode/operational space controller," *Lecture Notes in Computer Science*, pp. 230–238, 2009.

[112] T. Tsumugiwa, R. Yokogawa, and K. Hara, "Variable impedance control with virtual stiffness for human-robot cooperative peg-in-hole task," *Proceedings of IEEE/RSJ International Conference on Intelligent Robots and Systems*, pp. 1075–1081, 2002.

[113] S. Arimoto, "Learning control theory for robotic motion," *International Journal of Adaptive Control and Signal Processing*, vol. 4, no. 6, pp. 543–564, 1990.

[114] M. Sun, S. S. Ge, and I. M. Y. Mareels, "Adaptive repetitive learning control of robotic manipulators without the requirement for initial repositioning," *IEEE Transactions on Robotics*, vol. 22, no. 3, pp. 563–568, 2006.

[115] R. Yan, K. P. Tee, and H. Li, "Adaptive learning tracking control of robotic manipulators with uncertainties," *Journal of Control Theory and Applications*, vol. 8, no. 2, pp. 160–165, 2010.

[116] J. Roy and L. L. Whitcomb, "Adaptive force control of position/velocity controlled robots: theory and experiment," *IEEE Transactions on Robotics and Automation*, vol. 18, no. 2, pp. 121–137, 2002.

[117] T. Nef, M. Mihelj, and R. Riener, "ARMin: a robot for patient-cooperative arm therapy," *Medical and Biological Engineering and Computing*, vol. 45, pp. 887–900, 2007.

[118] F. Janabi-Sharifi and I. Hassanzadeh, "Experimental analysis of mobile-robot teleoperation via shared impedance control," *IEEE Transactions on Systems, Man, and Cybernetics, Part B: Cybernetics*, vol. 41, no. 2, pp. 591–606, 2011.

[119] L. Biagiotti, H. Liu, G. Hirzinger, and C. Melchiorri, "Cartesian impedance control for dexterous manipulation," *Proceedings of the IEEE/RSJ International Conference on Intelligent Robots and Systems*, pp. 3270–3275, 2003.

[120] C. C. Cheah, S. P. Hou, Y. Zhao, and J. J. E. Slotine, "Adaptive vision and force tracking control for robots with constraint uncertainty," *IEEE/ASME Transactions on Mechatronics*, vol. 15, no. 3, pp. 389–399, 2010.

[121] M. Matinfar and K. Hashtrudi-Zaad, "Optimization-based robot compliance control: Geometric and linear quadratic approaches," *The International Journal of Robotics Research*, vol. 24, no. 8, pp. 645–656, 2005.

[122] C. Yang and E. Burdet, "A model of reference trajectory adaptation for interaction with objects of arbitrary shape and impedance," *Proceedings of the*

2011 IEEE/RSJ International Conference on Intelligent Robots and Systems, pp. 4121–4126, 2011.

Author's Publications

Journal papers:

1. **Y. Li** and S. S. Ge, "Human-Robot Collaboration Based on Motion Intention Estimation," *IEEE Transactions on Mechatronics*, accepted, 2013.

2. S. S. Ge and **Y. Li**, "Force Tracking Control for Motion Synchronization in Human-Robot Collaboration," *Robotica*, in revision, 2013.

3. S. S. Ge and **Y. Li**, "Impedance Learning for Robot Interacting with Unknown Environments," *IEEE Transactions on Control Systems Technology*, in minor revision, 2013.

4. **Y. Li**, S. S. Ge, Q. Zhang and T. H. Lee, "NN Learning Impedance Control for Robots Interacting with Environments," *IET Control Theory & Applications*, in major revision, 2013.

5. **Y. Li**, S. S. Ge and C. Yang, "Learning Impedance Control for Physical Robot-Environment Interaction," *International Journal of Control*, 85(2), pp. 182-193, 2012.

6. **Y. Li**, C. Yang, S. S. Ge and T. H. Lee, "Adaptive Output Feedback NN Control of a Class of Discrete-Time MIMO Nonlinear Systems with Unknown Control Directions," *IEEE Transactions on System, Man and Cybernetics, Part B*, 41(2), pp. 507-517, 2011.

7. C. Yang, **Y. Li**, S. S. Ge and T. H. Lee, "Adaptive Control of a Class of Discrete-Time MIMO Nonlinear Systems with Uncertain Couplings," *International Journal of Control*, 83(10), pp. 2120-2133, 2010.

Conference papers:

1. **Y. Li**, S. S. Ge and K. P. Tee, "Adaptive Impedance Control for Natural Human-Robot Collaboration," *Workshop at SIGGRAPH ASIA 2012*, Singapore, pp.91-96, 2012.

2. S. S. Ge and **Y. Li**, "Motion Synchronization for Human-Robot Collaboration," *Lecture Notes in Computer Science Series*, vol. 7621, pp. 248-257, 2012.

3. Y. Zeng, **Y. Li**, S. S. Ge and P. Xu, "Human-Robot Handshaking: A Hybrid Deliberate/Reactive Model," *Lecture Notes in Computer Science Series*, vol. 7621, pp. 258-267, 2012.

4. W. He, S. S. Ge, **Y. Li**, E. Chew and Y. S. Ng, "Impedance Control of a Rehabilitation Robot for Interactive Training," *Lecture Notes in Computer Science Series*, vol. 7621, pp. 526-535, 2012.

5. Y. S. Liau, Q. Zhang, **Y. Li** and S. S. Ge "Non-Metric Navigation for Mobile Robot Using Optical Flow," In *Proceedings of IEEE/RSJ International Conference on Intelligent Robots and Systems*, Vilamoura, Algarve, Portugal, pp. 4953-4958, 2012.

6. J. Ma, **Y. Li** and S. S. Ge, "Adaptive Control for a Cable Driven Robot Arm," In *Proceedings of IEEE International Conference on Mechatronics and Automation*, Chengdu, China, pp. 1074-1079, 2012.

7. S. S. Ge, M. R. Safizadeh and **Y. Li**, "Mechanical Design of Social Robot Nancy," In *Proceedings of IEEE/SICE International Symposium on System Integration*, Kyoto, Japan, pp. 324-329, 2011.

8. S. S. Ge, C. F. Liew, **Y. Li** and J. Yang, "System Design and Hardware Integration of Social Robot Nancy," In *Proceedings of IEEE/SICE International Symposium on System Integration*, Kyoto, Japan, pp. 336-341, 2011.

9. S. S. Ge, **Y. Li** and H. He, "Neural-Network-Based Human Intention Estimation for Physical Human-Robot Interaction," In *Proceedings of International Conference on Ubiquitous Robots and Ambient Intelligence*, Incheon, Korea, pp. 390-395, 2011.

10. S. S. Ge, J. J. Cabibihan, Z. Zhang, **Y. Li**, C. Meng, H. He, M. R. Safizadeh, Y. B. Li and J. Yang, "Design and Development of Nancy, a Social Robot," In *Proceedings of International Conference on Ubiquitous Robots and Ambient Intelligence*, Incheon, Korea, pp. 568-573, 2011.

11. S. S. Ge, C. F. Liew and **Y. Li**, "System Design and Implementation of Social Interactive Robot Nancy," In *Proceedings of International Conference on Interaction Sciences: Information Technology, Human and Digital Content*, Busan, Korea, pp. 41-46, 2011.

12. **Y. Li**, S. S. Ge, X. Li and K. P. Tee, "Model-Free Impedance Control for Safe Human-Robot Interaction," In *Proceedings of IEEE International Conference on Robotics and Automation*, Shanghai, China, pp. 6021-6026, 2011.

13. **Y. Li**, S. S. Ge and C. Yang, "Impedance Control for Multi-Point Human-Robot Interaction," In *Proceedings of Asian Control Conference*, Kaohsiung, Taiwan, pp. 1187-1192, 2011.

14. C. Chin, **Y. Li**, S. S. Ge and J. J Cabibihan, "Adaptive Compliance Control for Collision-Tolerant Robot Arm with Viscoelastic Trunk," In *Proceedings of International Conference on Intelligent Robotics and Applications*, Shanghai, China, pp. 683-694, 2011.

15. **Y. Li**, C. Yang and S. S. Ge, "Learning Compliance Control of Robot Manipulators in Contact with the Unknown Environment," In *Proceedings of IEEE Conference on Automation Science and Engineering*, Toronto, Canada, pp. 644-649, 2010.

16. C. Yang, **Y. Li**, S. S. Ge and T. H. Lee, "Adaptive Predictive Control of a Class of Discrete-Time MIMO Nonlinear Systems with Uncertain Couplings," In *Proceedings of American Control Conference*, Baltimore, Maryland, USA, pp. 2428-2433, 2010.

17. S. S. Ge, C. Yang, **Y. Li** and T. H. Lee, "Decentralized Adaptive Control of a Class of Discrete-Time Multi-Agent Systems for Hidden Leader Following Problem," In *Proceedings of IEEE/RSJ International Conference on Intelligent Robots and Systems*, St. Louis, Missouri, USA, pp. 5065-5070, 2009.

18. **Y. Li**, C. Yang, S. S. Ge and T. H. Lee, "Adaptive Output Feedback NN Control of a Class of Discrete-Time MIMO Nonlinear Systems with Unknown Control Directions," In *Proceedings of Asian Control Conference*, Hong Kong, China, pp. 1239-1244, 2009.

19. B. Ren, S. S. Ge, **Y. Li**, Z. Jiao, J. Liu and T. H. Lee, "Target Region Tracking for Multi-Agent Systems," In *Proceedings of Asian Control Conference*, Hong Kong, China, pp. 123-128, 2009.